

PhD PROCEEDINGS

ANNUAL ISSUES OF THE DOCTORAL SCHOOL

FACULTY OF INFORMATION TECHNOLOGY & BIONICS

2021

PhD PROCEEDINGS

ANNUAL ISSUES OF THE DOCTORAL SCHOOL

FACULTY OF INFORMATION TECHNOLOGY & BIONICS
PÁZMÁNY PÉTER CATHOLIC UNIVERSITY

PhD PROCEEDINGS

ANNUAL ISSUES OF THE DOCTORAL SCHOOL
FACULTY OF INFORMATION TECHNOLOGY & BIONICS
2021



PÁZMÁNY *1635*
— s i n c e

PÁZMÁNY UNIVERSITY *e*PRESS
BUDAPEST, 2021

© PPKE Információs Technológiai és Bionikai Kar, 2021

HU ISSN 2064-7271

Kiadja a Pázmány Egyetem eKiadó
Budapest, 2021

Felelős kiadó
Rev. Mons. Dr. Kuminetz Géza
a Pázmány Péter Katolikus Egyetem rektora

The publication of this volume was supported by the European Union,
co-financed by the European Social Fund (EFOP-3.6.3-VEKOP-16-2017-00002)
and by the New National Excellence Program of the Ministry for Innovation and Technology

Cover image by Nawar Al-Hemeary: *Hexacopter components*

Contents

| | |
|--|-----------|
| Introduction | 9 |
| PROGRAM 1: BIONICS, BIO-INSPIRED WAVE COMPUTERS, NEUROMORPHIC MODELS | 10 |
| Imaginary movement detection in EEG Signals, using 2D and 3D Convolutional Neural Networks | 11 |
| <i>András ADOLF</i> | |
| Coupling between the cell cycle, the circadian clock and DNA damage in <i>Neurospora crassa</i> | 12 |
| <i>Zsófia BUJTÁR</i> | |
| Studying the robustness of biological oscillators | 13 |
| <i>Suchana CHAKRAVARTY</i> | |
| IGF-1 regulates GnRH neurons in prepubertal and pubertal male mice | 14 |
| <i>Veronika CSILLAG</i> | |
| Multiclass classification of motor imagery EEG signals using image-based deep neural networks | 15 |
| <i>Ward FADEL</i> | |
| Effect of F508 deletion on the CFTR NBD1 nanomechanics | 16 |
| <i>Bianka Vivien FARKAS</i> | |
| Expression, functional characterization and initial NMR analysis of the PSD-95 GK domain | 17 |
| <i>Fanni FARKAS</i> | |
| Cytotoxic activity of stimulated $\gamma\delta$ T cells | 18 |
| <i>Anna HAJDARA</i> | |
| Benchmarking microbiome sequencing dataset using statistically equivalent signatures | 19 |
| <i>Regina KALCSEVSZKI</i> | |
| Large-scale analysis of postsynaptic protein:protein interactions | 20 |
| <i>Zsófia Etelka KÁLMÁN</i> | |
| Separation of micron-sized particles with pinched flow fractionation | 21 |
| <i>Máté KÁLOVICS</i> | |
| Agent-based models in biological simulation | 22 |
| <i>Bence Márk KEÖMLEY-HORVÁTH</i> | |
| Optogenetic identification of rhythmic neurons in the medial septum | 23 |
| <i>Barnabás KOCSIS</i> | |

| | |
|--|-----------|
| Parameter space investigation of multi-class SVM problem for brain-computer interfaces | 24 |
| <i>Csaba Márton KÖLLŐD</i> | |
| Electrochemical impedance spectroscopy (EIS) for microfluidic qualitative and quantitative cell separation | 25 |
| <i>Dániel Zoltán KOLPASZKY</i> | |
| An overview of the MSLA 3D printing-based manufacturing process of a split-ring resonator-based microfluidic sensor | 26 |
| <i>Adrienn Lilla MÁRTON</i> | |
| Distribution and structure of postsynaptic protein complexes assessed by simulations | 27 |
| <i>Marcell MISKI</i> | |
| Benchmarking state-of-the-art algorithms with a neural optimization user interface | 28 |
| <i>Máté MOHÁCSI</i> | |
| Differentiating the overlapping neural action potentials using deep learning | 29 |
| <i>Obada MUHAMMAD</i> | |
| Cellular interactions between yeast strains | 30 |
| <i>Biborka PILLÉR</i> | |
| Dynamic behaviour of the Shank1 PDZ domain during interaction | 31 |
| <i>Anna SÁNTA</i> | |
| Which optical characteristics make a transparent micro-ECoG suitable for multimodal measurements? | 32 |
| <i>Ágnes SZABÓ</i> | |
| Investigation of the role of specific sequence motifs in protein phase separation | 33 |
| <i>András László SZABÓ</i> | |
| Multimodal prediction of Alzheimer’s disease | 34 |
| <i>János SZALMA</i> | |
| Modelling calcium channels in hippocampal pyramidal neurons | 35 |
| <i>Luca TAR</i> | |
| Fetal breathing movements and fetal heart sounds in single channel phonocardiographic signals | 36 |
| <i>Bálint Áron ÜVEGES</i> | |
| Characterization of age-related neurodegenerative disease models in transgenic animals | 37 |
| <i>Zsófia VARGA-MEDVE CZKY</i> | |
| Investigating the use of deep learning for EEG motor imagery signals classification | 38 |
| <i>Moutz WAHDOW</i> | |
| PROGRAM 2: COMPUTER TECHNOLOGY BASED ON MANY-CORE PROCESSOR CHIPS, VIRTUAL CELLULAR COMPUTERS, SENSORY AND MOTORIC ANALOG COMPUTERS | 39 |
| Construction of unmanned aerial vehicles applying INS/GPS navigation | 40 |
| <i>Nawar AL-HEMEARY</i> | |
| Survey of motion analysis in neuroscience mouse experiments | 41 |
| <i>Boldizsár Zsolt BALOG</i> | |

| | |
|--|-----------|
| Automatic parallelisation of structured mesh computations with SYCL | 42 |
| <i>Gábor Dániel BALOGH</i> | |
| Progress report on estimation and control of COVID-19 epidemics in Hungary using the theory of nonlinear dynamic systems | 43 |
| <i>Balázs CSUTAK</i> | |
| Heterogenous architecture for visual servoing a prosthetic arm | 44 |
| <i>Attila FEJÉR</i> | |
| Cognitive complexity of data manipulation languages | 45 |
| <i>Árpád GORETITY</i> | |
| A theater presentation model to test the different interaction methods for light field displays | 46 |
| <i>Mary GUINDY</i> | |
| Developing a measurement environment for the Memristor Cellular Neural Network architecture | 47 |
| <i>Dániel HAJTÓ</i> | |
| Study the effect of the risk factors in the estimation of the breast cancer risk score using machine learning | 48 |
| <i>Sam KHOZAMA</i> | |
| Non-contact monitoring of adults' respiration by computer vision algorithms | 49 |
| <i>Ádám NAGY</i> | |
| Bitwise reproducible execution of unstructured mesh applications | 50 |
| <i>Bálint SIKLÓSI</i> | |
| Investigation of cell motility | 51 |
| <i>Gergely SZABÓ</i> | |
| Computing different realizations of linear dynamical systems with embedding Eigenvalue assignment | 52 |
| <i>Gergely SZLOBODNYIK</i> | |
| PROGRAM 3: FEASIBILITY OF ELECTRONIC AND OPTICAL DEVICES, MOLECULAR AND NANOTECHNOLOGIES, NANO-ARCHITECTURES, NANOBIONIC DIAGNOSTIC AND THERAPEUTIC TOOLS | 53 |
| Optimal design of a Van Atta array for reflector applications | 54 |
| <i>András ESZES</i> | |
| Optimizations in neural network architectures | 55 |
| <i>András FÜLÖP</i> | |
| Review of style transfer methods on ultrasound images | 56 |
| <i>Péter MAROSÁN-VILIMSZKY</i> | |
| Stochastic micromagnetic simulations of invertible logic gates | 57 |
| <i>Tamás RUDNER</i> | |
| PROGRAM 4: HUMAN LANGUAGE TECHNOLOGIES, ARTIFICIAL UNDERSTANDING, TELEPRESENCE, COMMUNICATION | 58 |
| Improving the effectiveness of open-set recognition with generated negative inputs | 59 |
| <i>András Pál HALÁSZ</i> | |

| | |
|--|-----------|
| Applying Deep Learning Algorithms for Azerbaijani Named Entity Recognition Dataset | 60 |
| <i>Kamran IBIYEV</i> | |
| Using linguistic transfer to improve abstractive Arabic text summarization | 61 |
| <i>Mram KAHLA</i> | |
| State space reconstruction with generative models in POMDPs | 62 |
| <i>András Attila SULYOK</i> | |
| PROGRAM 5: ON-BOARD ADVANCED DRIVER ASSISTANCE SYSTEMS | 63 |
| What to do after adversarial attacks detection? | 64 |
| <i>Jalal ALAFANDI</i> | |
| Deep learning for the segmentation of masonry wall images | 65 |
| <i>Yahya IBRAHIM</i> | |
| Automatic selection of difficult input images for neural network based denoising algorithms | 66 |
| <i>Ákos KOVÁCS</i> | |
| Change detection in unregistered 3D point clouds | 67 |
| <i>Lóránt KOVÁCS</i> | |
| Echocardiogram evaluation using Spatiotemporal Convolutional Neural Networks | 68 |
| <i>Bálint MAGYAR</i> | |
| Application of the Mask R-CNN architecture in synaptic cleft detection | 69 |
| <i>Franciska Sára RAJKI</i> | |
| Multimodal change detection between LiDAR point clouds | 70 |
| <i>Örkény Ádám H. ZOVÁTHI</i> | |
| Appendix | 71 |

Introduction

It is our pleasure to publish this Annual Proceedings again to demonstrate the genuine multidisciplinary research done at the Jedlik Laboratories by young talents working in the Roska Tamás Doctoral School of Sciences and Technology of the Faculty of Information Technology and Bionics at Pázmány Péter Catholic University. The scientific results of our PhD students outline the main recent research directions in which our faculty is engaged. We also appreciate the support of the supervisors and consultants, as well as that of the five collaborating National Research Laboratories of the Loránd Eötvös Research Network, Semmelweis University and the University of Pannonia. The collaborative work with the partner universities, especially Katolieke Universiteit Leuven, Politecnico di Torino, Technische Universität München, University of California at Berkeley, University of Notre Dame, Universidad de Sevilla, Università di Catania, Université de Bordeaux and Universidad Autónoma de Madrid is gratefully acknowledged.

We acknowledge the support of numerous institutes, organizations and companies:

- Loránd Eötvös Research Network (ELKH),
- National Research, Development and Innovation Office (NKFIH),
- Hungarian Academy of Sciences (MTA),
- UNKP Programme, Ministry for Innovation and Technology, Hungarian Government,
- KDP Programme, Ministry for Innovation, and Technology, Hungarian Government,
- Gedeon Richter Co.,
- Office of Naval Research (ONR) of the US,
- NVIDIA Ltd.,
- Verizon Computer Vision Group (Eutecus Inc.), Berkeley, CA,
- MorphoLogic Ltd., Budapest,
- Analogic Computers Ltd., Budapest,
- AnaFocus Ltd., Seville,

and several other companies and individuals.

Needless to say, the resources and support of the Pázmány Péter Catholic University are gratefully acknowledged.

Budapest, June 2021.

GÁBOR PRÓSZÉKY

Chairman of the Board of the Doctoral School

GÁBOR SZEDERKÉNYI

Head of the Doctoral School

PROGRAM 1

BIONICS, BIO-INSPIRED WAVE COMPUTERS, NEUROMORPHIC MODELS

Heads: Tamás FREUND, György KARMOS, Zsolt LIPOSITS, Sándor PONGOR

Imaginary movement detection in EEG Signals, using 2D and 3D Convolutional Neural Networks

András ADOLF

(Supervisor: István ULBERT)

Pázmány Péter Catholic University, Faculty of Information Technology and Bionics

50/a Práter street, 1083 Budapest, Hungary

adolof.andras@itk.ppke.hu

Abstract—As one of the most essential parts of brain-computer interfaces (BCI) is the classification of EEG signals, the goal of my research is to develop a system capable of recognizing different imaginary movements. In this paper, I present my implemented structures of Convolutional Neural Networks: using 2D and 3D convolutions over the 3 Dimensional EEG data. To overcome the problem of the small number of signals to train on, I have implemented a Transfer Learning method and compared the results obtained by using it or training only on the data of a given subject. The dataset I have tested my networks on is the Physionet database, which consists of the data of 109 subjects.

Keywords—brain-computer interfaces; neural networks; transfer learning; 2D convolution, 3D convolution

I. SUMMARY

Brain-computer interfaces represent a rapidly evolving research field nowadays. However these devices could mean essential help to people with different serious disabilities, a reliable classification accuracy is essential to be applicable in real life. [1]

In this work, I have implemented convolutional neural network structures and tested them on the data of the Physionet database. This is a movement intention EEG database, collected by Schalk et al., in 2004. The measurements were done with 64 electrode channels and with a sampling rate of 160 Hz. This database is one of the largest EEG-based human movement intention datasets which has been ever made: it has 109 subjects and 14 measurements for each sequence. The database has 5 different labeled tasks: baseline activity, open and close the left hand, the right hand, both hands, and both legs. During my work I focused on the classification of two different classes: I have separated the REST data into a single class, and every other performed imaginary task got an ACTIVE label. [2]

To perform the classification, I have implemented two types of networks, one with 2D and the second with 3D convolution, both of them have an input of a 3D structured EEG time window. In this representation, 2 dimensions correspond to the spatial arrangement of the electrodes, while the third one is the time. The implemented structures can be observed in Figure 1

In cases, where a limited number of input data is available, Transfer Learning (TL) is a generally used method to improve performance. Because it is especially true for EEG signals, I have implemented a TL method to be able to reach higher accuracy. The weights were initialized by pre-training the neural networks on data of different subjects, namely over subjects 51-100 when testing the first 50 subjects, and pre-trained on 1-50 for the second half. Both networks was able to achieve an accuracy of around 75%, and TL increases accuracy

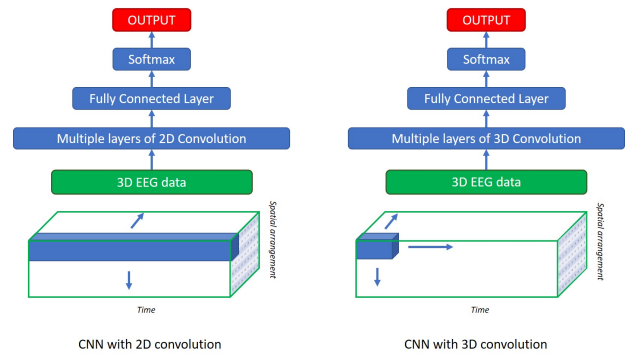


Fig. 1. The structure of the implemented neural networks

in both cases. The highest results were achieved by using the 3D convolutional network with pre-trained weights over the data of different subjects: 79.9%. Without TL the network with the 2D Convolution performed a better accuracy, which can be the result of that 3D convolution requires more diverse data to generalize the features of the 3D EEG data.

ACKNOWLEDGEMENTS

I would like to express my sincere gratitude to my consultant, István ULBERT, who supported me during my work. I would also like to say thank you to the research group working on EEG classification with me, in particular, Csaba KÖLLŐD and Gergely MÁRTON.

REFERENCES

- [1] J. R. Wolpaw, N. Birbaumer, W. J. Heetderks, D. J. McFarland, P. H. Peckham, G. Schalk, E. Donchin, L. A. Quatrano, C. J. Robinson, and T. M. Vaughan, "Brain-computer interface technology: a review of the first international meeting," *IEEE transactions on rehabilitation engineering*, vol. 8, no. 2, pp. 164–173, 2000.
- [2] A. L. Goldberger, L. A. N. Amaral, L. Glass, J. M. Hausdorff, P. C. Ivanov, R. G. Mark, J. E. Mietus, G. B. Moody, C.-K. Peng, and H. E. Stanley, "PhysioBank, PhysioToolkit, and PhysioNet: Components of a new research resource for complex physiologic signals," *Circulation*, vol. 101, no. 23, pp. e215–e220, 2000 (June 13). Circulation Electronic Pages: <http://circ.ahajournals.org/content/101/23/e215.full> PMID:1085218; doi: 10.1161/01.CIR.101.23.e215.

Coupling between the cell cycle, the circadian clock and DNA damage in *Neurospora crassa*

Zsófia BUJTÁR

(Supervisor: Attila CSIKÁSZ-NAGY)

Pázmány Péter Catholic University, Faculty of Information Technology and Bionics

50/a Práter street, 1083 Budapest, Hungary

bujtar.zsofia@itk.ppke.hu

I. INTRODUCTION

Radiation and chemotherapy are often applied treatments for cancer patients. DNA damage is induced to eliminate the cancer cells (with high proliferation). Unfortunately DNA damage also affects healthy cells as a side effect of the treatment. The reaction of cells depends on their internal state, namely the circadian clock-regulated cell cycle. For this purpose, I studied the molecular regulations of the circadian rhythm and cell cycle (for which discovery, Nobel Prizes were awarded) and the coupling between them. Furthermore, I examined how the DNA damage response affects this complex processes in systems level, especially in *Neurospora crassa*.

II. CIRCADIAN RHYTHM AND CELL CYCLE

Circadian clock is an intrinsic molecular mechanism in many organisms, which works as a metronome that temporally controls key aspects of physiology. Many biochemical, behavioural processes like cell cycle are regulated by this endogenous clock in a day-time dependent (circadian) manner. The disruption of the circadian cycles can cause many diseases. The main regulatory mechanism of the circadian rhythm is a simple delayed, negative, regulatory feedback loop. The cell division cycle is another important periodic, molecular mechanism, which has well known phases.

Neurospora crassa is a model organism with its well-established chrono-genetics to study the coupling between the circadian rhythm and the cell cycle [1]. A circadian regulation of the cell cycle was described by a computational model [2]. FRQ molecule is the core circadian component in *Neurospora crassa*. CLB-1 is its key cell cycle component, which concentration rises only after G2 phase. By inactivating CLB-1, STK-29 protein - another important cell cycle regulator - can prevent entry into mitosis. Furthermore, it is known that STK-29 protein shows circadian pattern: its expression is regulated by a circadian component, so it works as a clock-dependent cell cycle gate (Figure 1). This circadian regulation of cell cycle is so important, that the dysfunction of the circadian clock can lead to the development of cancer.

III. DNA DAMAGE RESPONSE

DNA damage must normally be artificially induced during cancer therapies to eliminate the highly proliferative cells. DNA damage (double-strand DNA breaks) activates the ATM serine/threonine kinase, which activates the PRD-4 (period-4) kinase (which is homologous with the human Checkpoint kinase 2 [3]). The active PRD-4 kinase delays the cell cycle by a direct effect. Furthermore it phosphorylates, degrades the circadian proteins, the FRQ monomer, homo-dimer (like Chk2 molecule), so it has an important role controlling the circadian

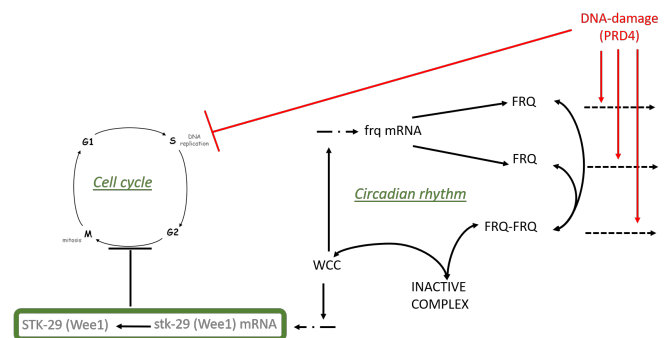


Fig. 1. Molecular connections between cell cycle, circadian rhythm and DNA damage response pathway. The main mechanism in the circadian rhythm is a delayed negative regulatory feedback loop at FRQ clock molecule. The circadian rhythm influences the cell cycle through STK-29 cell cycle component. The DNA damage response (namely its PRD-4 molecular component) can affect directly the cell cycle and the circadian rhythm.

rhythm at DNA damage. Besides this, it is known that the expression of PRD-4 is regulated by the circadian clock [3]. (Figure 1)

IV. CHRONOTHERAPY

Chronotherapy is such a potential treatment of cancer patients (especially at DNA damage induction), which is based on a rhythmic cycle [4]. The efficiency of the treatment can be increased by fitting it to the patient's circadian clock. The patient gets the treatment at optimal time of the day, when it is the most effective, the side effect is minimal. For this purpose, it is important to take into consideration the effect of DNA damage response on the cell cycle through the circadian rhythm: the coupling between the circadian clock and cell cycle and the circadian rhythm-dependency of the DNA damage response have a key role in this regulatory system.

REFERENCES

- [1] J. Zámorszky, A. Csikász-Nagy, and C. I. Hong, "Neurospora crassa as a model organism to explore the interconnected network of the cell cycle and the circadian clock," *Fungal Genetics and Biology*, vol. 71, pp. 52–57, 2014.
- [2] C. I. Hong, J. Zámorszky, M. Baek, L. Labiscsak, K. Ju, H. Lee, L. F. Larrondo, A. Goity, H. S. Chong, W. J. Belden, and A. Csikász-Nagy, "Circadian rhythms synchronize mitosis in neurospora crassa," *Proceedings of the National Academy of Sciences*, vol. 111, no. 4, pp. 1397–1402, 2014.
- [3] A. M. Pregelero, Q. Liu, C. L. Baker, J. C. Dunlap, and J. J. Loros, "The neurospora checkpoint kinase 2: a regulatory link between the circadian and cell cycles," *Science*, vol. 313, no. 5787, pp. 644–649, 2006.
- [4] F. Lévi, E. Filipinski, I. Jurisci, X. Li, and P. Innominato, "Cross-talks between circadian timing system and cell division cycle determine cancer biology and therapeutics," *Cold Spring Harbor symposia on quantitative biology*, vol. 72, pp. 465–75, 02 2007.

Studying the robustness of biological oscillators

Suchana CHAKRAVARTY

(Supervisor: Attila CSIKÁSZ-NAGY)

Pázmány Péter Catholic University, Faculty of Information Technology and Bionics

50/a Práter street, 1083 Budapest, Hungary

chakravarty.suchana@itk.ppke.hu

Abstract—One of the unique behavior of a circadian clock is temperature compensation. This property allows the circadian pacemaker to keep the period of oscillation stable, in order to respond towards any biological fluctuations. The oscillations can occur due to the presence of a negative feedback exerted by a nuclear period protein (PER) on the synthesis of mRNA. Goodwin's study inspired many computational biologists to identify the minimal network, that can be responsible for the generation of oscillation. Furthermore, negative auto-regulation of gene expression can also generate oscillations. Here we would like to demonstrate the temperature compensation property and robustness of three different kinds of oscillatory systems- cyanobacterial model, substrate depletion model and simple negative feedback loop model.

Keywords-biological oscillator; negative feedback; cyanobacterial oscillator; substrate depletion model; temperature compensation.

DISCUSSION

Living organisms accrue oscillatory networks. These biological oscillations are one of the unique features that provide the organism to cope up with any kind of environmental fluctuations. Calcium oscillations, circadian rhythms are the examples of oscillatory networks among many others. Previous study reveals that, for generating an oscillatory behaviour, the system must possess a negative feedback loop. Furthermore, the presence of both positive and negative feedback loops can enhance chances for obtaining oscillations without compromising the amplitude of oscillation.

One of the classic examples of an oscillatory network is Goodwin's model [1]. Nowadays many theoreticians are interested to find out the minimal network motif, that can be responsible for oscillation. Rosa D. Hernansaiz-Ballesteros et al., propose a minimal network topology required for oscillation [2] in prokaryotic cyanobacteria. On the other hand, substrate depletion model with a positive auto-catalytic feedback is known to exhibit sustained oscillation.

Our aim is to find out the most robust oscillatory network. For that purpose, we would like to focus on three different kinds of network motifs – negative feedback oscillator, cyanobacterial oscillator, substrate depletion oscillator. In order to identify a temperature compensated [3] biological clock, we have introduced the temperature sensitivity co-efficient Q_{10} to the dynamical equations of the networks. Through out the analysis, we have considered the mass-action kinetics instead of non-linear Hill equations. Without any perturbation to the temperature (Fig1.), these systems show similar length of period of oscillation (Fig1.). Studying the robustness of the oscillatory system would help in constructing a synthetic oscillator.

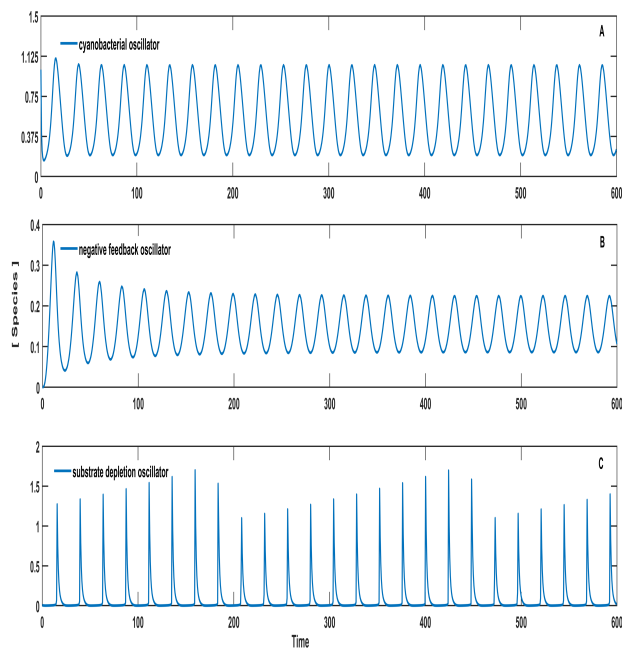


Fig. 1. The oscillation behavior with three different cases - cyanobacteria (Top Panel), simple negative feedback loop (Middle Panel), and substrate depletion model (Bottom Panel) has been shown here.

REFERENCES

- [1] D. Gonze and P. Ruoff, "The Goodwin Oscillator and its Legacy," Acta Biotheor., 2020.
- [2] R. D. Hernansaiz-Ballesteros, L. Cardelli, and A. Csikász-Nagy, "Single molecules can operate as primitive biological sensors, switches and oscillators." BMC Syst. Biol., vol. 12, no. 1, pp. 1-14, 2018.
- [3] C. H. Johnson and Martin Egly, "Metabolic Compensation and Circadian Resilience in Prokaryotic Cyanobacteria." Annu Rev Biochem., vol. 83, pp. 221-247, 2014.

IGF-1 regulates GnRH neurons in prepubertal and pubertal male mice

Veronika CSILLAG

(Supervisors: Imre FARKAS, Zsolt LIPOSITS)

Pázmány Péter Catholic University, Faculty of Information Technology and Bionics

50/a Práter street, 1083 Budapest, Hungary

csillag.veronika@itk.ppke.hu

Mammalian reproduction requires numerous precisely orchestrated events, for successful fertilization, and initiation of embryonic development. These processes can be readily modulated by the energy state of the body. Since reproduction is a highly energy consuming process, it is therefore vital for the body to be prepared for optimal circumstances when energy can be consumed for reproduction without any high risk. Availability of food, thus nutritional state can cause fluctuations in the level of metabolic hormones having major effects upon reproduction. One of these substances, the insulin-like growth factor-1 (IGF-1) originating both from peripheral and central sources, is abundant in the hypothalamus at the time of puberty. Earlier data have shown that IGF-1 administration during this developmental period can act centrally by inducing GnRH secretion and accelerating the onset of puberty in female rats [1]. These data suggest that IGF-1 may regulate the HPG axis by modulating the function of GnRH neurons directly.

Therefore, responsiveness of GnRH neurons to IGF-1 and the molecular pathways acting downstream to IGF-1 receptor were investigated. In vitro electrophysiological experiments were carried out on GnRH-GFP neurons of acute brain slices from prepubertal (23-29 days) male mice. We found that application of IGF-1 (13 nM) significantly increased the frequency of the action potentials (APs) spontaneous postsynaptic currents (sPSCs) compared to the control in 42% of the neurons, and that of the excitatory GABAergic miniature postsynaptic currents (mPSCs) in 40% of the measured neurons. This effect was also demonstrated in pubertal male mice. The increase in the mPSC frequency was prevented by the usage of the IGF-1 receptor antagonist, JB1 showing the involvement of IGF-1 receptor in the mechanism. Literature data suggest that binding of IGF-1 to its receptor activates a phosphoinositide-3 kinase (PI3K)-dependent pathway and the intracellularly applied PI3K blocker (LY294002) indeed inhibited the effect of IGF-1. Changes in the mPSC frequency, but not in the amplitude indicated that IGF-1 acts through various retrograde pathways we described earlier in GnRH neurons [2,3,4]. The elevation of the frequency suggested the involvement of retrograde nitric oxide (NO) signaling pathway, but the NO synthase blocker NPLA failed to abolish the effect of IGF-1 demonstrating that the NO retrograde machinery was not involved in this process. Therefore, we examined the retrograde endocannabinoid pathway which has a tonic inhibition on GnRH neurons via reducing frequency of excitatory GABAergic mPSCs, and blockade of this tonic endocannabinoid pathway can lead to excitation. The transient receptor potential vanilloid 1 (TRPV1) is one of the components of this endocannabinoid pathway and the TRPV1 receptor blocker (AMG9810) abolished the frequency elevat-

ing effect of IGF-1 on GnRH neurons. To further examine the involvement of the retrograde endocannabinoid pathway, we applied a cannabinoid receptor type-1 (CB1) blocker (AM251) in the ACSF, which also prevented the IGF-1-related frequency elevation of the mPSCs. Our results, therefore, show that IGF-1 can block the tonic retrograde endocannabinoid pathway in GnRH neurons and this disinhibition increases the release of excitatory GABA from the presynaptic terminals. We also demonstrated the effect of IGF-1 in pubertal mice.

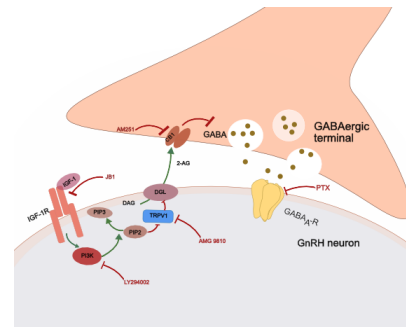


Fig. 1. Schematic illustration of the IGF-1 receptor signaling in GnRH neurons. IGF-1 activates PI3K which leads to the phosphorylation of PIP2 to PIP3. In cells, TRPV1 is inactivated by its binding to PIP2, and after the activation of PI3K, TRPV1 receptor will be released from the PIP2 blockade. Activation of TRPV1 leads to the blockade of DGL and decreases the postsynaptic production and release of 2-AG resulting in the suppression of inhibition of the presynaptic excitatory GABA release. Abbreviations: IGF-1R: Insulin-like growth factor 1 receptor; JB1: IGF-1R antagonist; PI3K: Phosphoinositide-3 kinase; LY294002: PI3K blocker; PIP2: Phosphatidylinositol 4,5-bisphosphate; PIP3: phosphatidylinositol 3,4,5 trisphosphate; DAG: Diacylglycerol; DGL: Diacylglycerol lipase; TRPV1: transient receptor potential cation channel subfamily V member 1; AMG9810: TRPV1 antagonist; 2-AG: 2-Arachidonoylglycerol; CB1: Cannabinoid receptor type 1; AM251: CB1 receptor antagonist; GABA-A-R: GABA-A receptor; PTX: picrotoxin.

ACKNOWLEDGEMENT

This paper was co-authored by Flóra Bálint.

REFERENCES

- [1] Hiney JK, Srivastava VK, Pine MD, Les Dees W: Insulin-like growth factor-I activates KiSS-1 gene expression in the brain of the prepubertal female rat. *Endocrinology* 2009;150:376-384.
- [2] Farkas I, Vastagh C, Sarvari M, Liposits Z: Ghrelin decreases firing activity of gonadotropin-releasing hormone (GnRH) neurons in an estrous cycle and endocannabinoid signaling dependent manner. *PloS one* 2013;8:e78178.
- [3] Farkas, I., et al., Glucagon-Like Peptide-1 Excites Firing and Increases GABAergic Miniature Postsynaptic Currents (mPSCs) in Gonadotropin-Releasing Hormone (GnRH) Neurons of the Male Mice via Activation of Nitric Oxide (NO) and Suppression of Endocannabinoid Signaling Pathways. *Front Cell Neurosci*, 2016. 10: p. 214.
- [4] Csillag V, Vastagh C, Liposits Z, Farkas I: Secretin Regulates Excitatory GABAergic Neurotransmission to GnRH Neurons via Retrograde NO Signaling Pathway in Mice. *Frontiers in cellular neuroscience* 2019;13

Multiclass classification of motor imagery EEG signals using image-based deep neural networks

Ward FADEL

(Supervisors: István ULBERT, Lucia WITTNER)

Pázmány Péter Catholic University, Faculty of Information Technology and Bionics

50/a Práter street, 1083 Budapest, Hungary

fadel.ward@itk.ppke.hu

Abstract—Motor Imagery (MI) based Brain-Computer Interface (BCI) systems are widely used recently. Designing a general EEG classification model is not an easy mission as EEG signals are noisy and differ for the same subjects and among different subjects. To overcome such limitations, relatively large datasets should be used with a deep learning model, and new approaches have to be investigated. In this work, the EEG signals were preprocessed and filtered to Delta, Mu, and Beta bands, and then transformed into 3 channel images using Clough-Tocher interpolation and Azimuthal projection, and after that, the images are plugged into the Deep Learning model which consists of Convolutional Neural Network (CNN) to extract spatial and frequency dependencies, followed by Long Short Term Memory (LSTM) to extract time dependencies between the EEG frames. 4 motor imagery classes are then classified with highly promising results with 70.64 % average accuracy (5% better than Support Vector Machine (SVM)). Adding Delta band increased the classification accuracy by 2.51%.

Keywords-Brain-Computer Interface (BCI); Classification; Motor Imagery; Deep Learning.

I. SUMMARY

The EEG signals are noisy and differ from subject to subject, and this makes the feature extraction and classification a challenging task. To overcome such limitations, relatively large datasets need to be used with choosing the appropriate deep learning model. In this work, LSTM following CNN was used to extract frequency, space, and time information of the consecutive frames that represent the EEG images that have been projected into 2-d plane using azimuthal projection and interpolated into 32*32 images using Clough-Tocher interpolation. In [1], memory workload signals have been classified using CNN followed by LSTM, and we used a similar approach but for motor imagery tasks, and this model proved to be robust with Physionet motor imagery dataset which consists of 109 subjects motor imagery data (imagining moving right fist, left fist, both fists, and both feet). The data was filtered into Delta, Mu, and Beta bands before applying FFT to estimate power spectral density for each band and represent it on a color intensity basis to have 3 channel images after projection and interpolation. The normalization played an important role, each band features were normalized between 0 and 1 after the relative power normalization was applied, and later the images were normalized between -1 and 1 before being fed to the network. The logic behind transforming EEG signals into image frames is to use deep learning which is, generally speaking, the best approach for video classification problems, and following so, we were able to obtain competitive results. The results for multiclass motor imagery EEG signals classification are promising with 70.64 % average

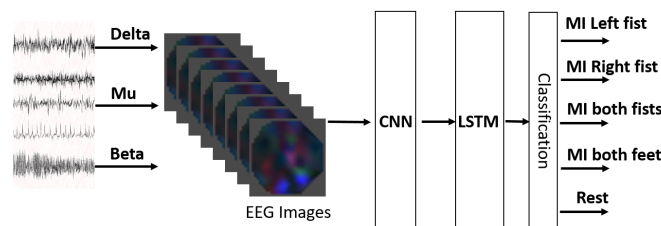


Fig. 1. The proposed approach for MI-EEG signals classification.

accuracy (5% better than Support Vector Machine (SVM)). Adding Delta band increased the classification accuracy by 2.51%. We are planning to use the different signal to image transformation methods and to test different models, and our progress in this direction showed interesting results.

REFERENCES

- [1] Pouya Bashivan, Irina Rish, Mohammed Yeasin, Noel Codella, *Learning Representations from EEG with Deep Recurrent-Convolutional Neural Networks*, ICLR Conference, 2016.
- [2] Reza Abiri et al, *A comprehensive review of EEG-based brain-computer interface paradigms*, *J. Neural Eng.* 2019, 16, 011001.
- [3] F Lotte, L Bougrain, A Cichocki, M Clerc, M Congedo, A Rakotomamonjy and F Yger, *A review of classification algorithms for EEG-based brain-computer interfaces: a 10 year update*, *J. Neural Eng.* 2018, 15, 031005.

Effect of F508 deletion on the CFTR NBD1 nanomechanics

Bianka Vivien FARKAS

(Supervisors: Tamás HEGEDŰS, Zoltán GÁSPÁRI)

Pázmány Péter Catholic University, Faculty of Information Technology and Bionics

50/a Práter street, 1083 Budapest, Hungary

farkas.bianka.vivien@itk.ppke.hu

SUMMARY

The ATP-Binding Cassette (ABC) superfamily is one of the largest and oldest protein families. Most of these proteins are active transporters. They transport molecules through the plasma membrane using ATP molecules as energy source. The CFTR/ABCC7 is an exception, since this protein functions as a channel of negatively charged small molecules, most importantly chloride ions. Binding and hydrolysis of ATP molecules are still required for channel gating. Additionally, the phosphorylation of the disordered regulatory domain (RD) is required as well, which is unique to CFTR among ABC proteins. [1]

Several mutations in the gene of CFTR results in cystic fibrosis (CF), a monogenic disease with high morbidity and mortality. CFTR is an important chloride channel in the apical membrane of epithelial cells. Mutations with impaired expression of functional plasma membrane CFTR cause imbalanced salt and water homeostasis leading to CF symptoms. The most frequent mutation, the deletion of phenylalanine 508 ($\Delta F508$) is localized in the first nucleotide binding domain (NBD1) of CFTR. This single amino acid deletion results in CFTR misfolding and degradation. [2]

Most of the currently used CF drugs stabilize the mature protein. However, correcting folding during the early steps of maturation may result in more efficient therapies. For this purpose, precise knowledge of the folding-unfolding pathways at the atomic resolution is required.

To investigate whether the $\Delta F508$ influences the mechanical unfolding of NBD1 we performed steered pulling molecular dynamics simulations with the CFTR NBD1 structure (PDBID:2BBO) in the presence and absence of F508, using all-atom $G\ddot{o}$ model. To validate our simulation results, we performed atomic force microscopy experiments with the wild type (WT) and $\Delta F508$ NBD1 constructs. We characterized the NBD1 unfolding by identifying unfolding pathways. Our results suggested that the S6- α -S8 core region of NBD1 (residues 487 to 604), where the F508 is localized, may have a central role in the unfolding-folding process. We performed additional simulations with the S6- α -S8 core using GROMACS with the CHARMM36m force field. These all-atom pulling simulations enabled us to describe the unfolding steps more accurately and to study the formation of non-native interactions and intermediate structures. The comparison showed that the F508 deletion changed the detachment timing of certain secondary structural elements and the frequencies of alternative pathways. Detachment of S6 β -strand occurred earlier in time and by smaller forces in a significant population of pulling simulations suggesting a weaker binding

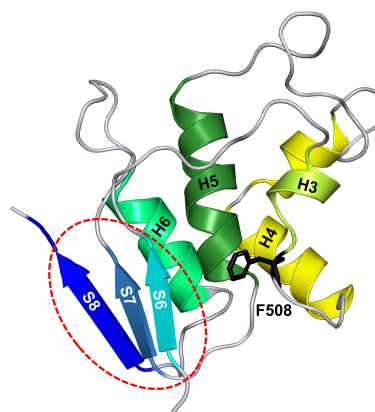


Fig. 1. Structural organization of the CFTR NBD1 S6- α -S8 core region is shown by cartoon representation. Dashed red circle marks the β -strands forming the interface between the NBD1 S6- α -S8 core and NBD1 β -subdomain (not represented here). The residue phenylalanine 508 is highlighted (stick representation in black).

in the mutant S6- α -S8 core. Besides, we observed that the deletion of F508 disturbed the formation of a non-native intermediate at the last stage of unfolding. Comparing the separation-force curves derived from the simulations and the experiments enabled us to accurately evaluate and correctly interpret our experimental results. The comparison of rupture event distributions calculated with simulations and the ones measured by *in vitro* experiments show a similar pattern.

In summary, our study showed that the S6 β -strand is the most sensitive region to mechanical unfolding and that the F508 deletion affects the interface between the β -subdomain and the S6- α -S8 core. Targeting this interface may lead to more efficient drug molecules for future CF therapies.

ACKNOWLEDGEMENTS

The support of NKFIH K127961, Cystic Fibrosis Foundation (CFF HEGEDU18I0, HEGEDU20I0), Grubmüller laboratory at Max Planck Institute, NIIF/KIFŰ HPC, MTA Wigner GPU Laboratory, Semmelweis Infrastructure Funding is greatly acknowledged.

REFERENCES

- [1] S. H. Cheng, D. P. Rich, J. Marshall, R. J. Gregory, M. J. Welsh, and A. E. Smith, "Phosphorylation of the R domain by cAMP-dependent protein kinase regulates the CFTR chloride channel," *Cell*, vol. 66, pp. 1027–1036, Sept. 1991.
- [2] J. R. Riordan, J. M. Rommens, B. Kerem, N. Alon, R. Rozmahel, Z. Grzelczak, J. Zielenski, S. Lok, N. Plavsic, and J. L. Chou, "Identification of the cystic fibrosis gene: cloning and characterization of complementary DNA," *Science (New York, N.Y.)*, vol. 245, pp. 1066–1073, Sept. 1989.

Expression, functional characterization and initial NMR analysis of the PSD-95 GK domain

Fanni FARKAS

(Supervisor: Zoltán GÁSPÁRI)

Pázmány Péter Catholic University, Faculty of Information Technology and Bionics

50/a Práter street, 1083 Budapest, Hungary

farkas.fanni@itk.ppke.hu

Abstract—PSD-95 is one of the most abundant scaffold proteins in the postsynaptic density (PSD) of glutamatergic synapses. With its GK domain, it can interact with GKAP, another scaffold protein, and form an important part of the core structure of PSD. Mutations in these proteins can be associated with serious neurodegenerative diseases, therefore their detailed structural and functional characterization is of high importance. Our aim is to characterize these proteins by NMR spectroscopy, as the only suitable method to detect subtle changes in structure and function at the atomic level upon partner binding.

Keywords—PSD, PSD-95, GKAP, protein interaction, NMR

I. INTRODUCTION

In excitatory glutamatergic synapses, the postsynaptic density (PSD) plays an important role in memory formation and learning processes. PSD is a functional and morphological unit, it is a complex, dynamically changing structure with a huge number of different types of proteins (scaffolds, ion channels, chaperons, motor proteins) [1]. Scaffold proteins, like PSD-95 and GKAP, are two of the most abundant PSD proteins, they participate in the maintenance of the structure, form the core complex of PSD, but also participate in the information transfer. These two proteins are interacting with each other. This interaction occurs between the GK domain of PSD-95 and the GBR region of GKAP protein [2]. According to the literature, the requirement of the interaction is the phosphorylated state of the GBR region [3]. However, detailed atomic-level structural investigations about their interaction are not yet available. Three-dimensional structures and dynamics can be detected with the help of Nuclear Magnetic Resonance (NMR) spectroscopy. And with its help, we can do a binding test at an atomic level also. Therefore, we can get closer to understanding the function of proteins and the whole structure of PSD [4].

II. METHODS

Recombinant PSD-95 and GKAP proteins were produced by using competent *E. coli* bacteria cells (BL21). After ultrasonic homogenization, also called sonication (to extract proteins), the protein samples were purified with immobilized metal affinity- (IMAC) and ion-exchange chromatography (IEC). SDS-polyacrylamide gel electrophoresis (SDS-PAGE) was used to check the results of sonication, IMAC, and IEC. GBR region was phosphorylated by CAMKII β . Phosphorylation was checked by mass spectrometry (MS). Using the double-labeled GK domain, multidimensional NMR spectra were obtained at 700 MHz using TROSY-based techniques. Initial analysis of the obtained spectra have been performed using CARRA.

III. RESULTS

All protein production and purification steps were successfully accomplished. The proteins obtained were suitable for interaction investigation and for performing the phosphorylation step before that. MS measurement was conducted to check the success of phosphorylation, unfortunately, it was not conclusive because of the high NaCl content of the protein sample. Therefore, new sample with optimized conditions are prepared. Initial analysis of the NMR spectra confirmed the presence of a well-folded globular domain. The number of peaks obtained were less than expected the reason for which can only be determined after resonance assignment. Unfortunately, the quality of the high-dimension spectra recorder for this step is not sufficient, raising the need to optimize sample and measurement conditions before we can proceed.

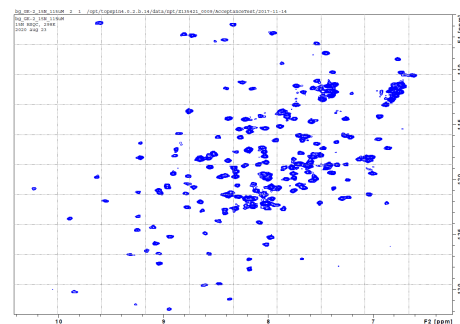


Fig. 1. HSQC NMR spectrum of GK-2 protein indicate a well folded globular protein.

ACKNOWLEDGEMENTS

I would like to thank my supervisor Dr. Zoltán Gáspári for his guidance and to Dr. Bálint Ferenc Péterfia for his help during my laboratory work and to Dr. András Czajlik for helping in the resonance assignment process and to Dr. Gyula Batta for performing the NMR measurement.

REFERENCES

- [1] M. Sheng and E. Kim, "The postsynaptic organization of synapses," *Cold Spring Harbor perspectives in biology*, vol. 3, no. 12, p. a005678, 2011.
- [2] J. Zhu, Y. Shang, and M. Zhang, "Mechanistic basis of maguk-organized complexes in synaptic development and signalling," *Nature Reviews Neuroscience*, vol. 17, no. 4, p. 209, 2016.
- [3] J. Zhu, Q. Zhou, Y. Shang, H. Li, M. Peng, X. Ke, Z. Weng, R. Zhang, X. Huang, S. S. Li, *et al.*, "Synaptic targeting and function of sapaps mediated by phosphorylation-dependent binding to psd-95 maguks," *Cell reports*, vol. 21, no. 13, pp. 3781–3793, 2017.
- [4] A. Bax and G. M. Clore, "Protein nmr: boundless opportunities," *Journal of Magnetic Resonance*, vol. 306, pp. 187–191, 2019.

Cytotoxic activity of stimulated $\gamma\delta$ T cells

Anna HAJDARA

(Supervisors: Balázs MAYER, Miklós GYÖNGY)

Pázmány Péter Catholic University, Faculty of Information Technology and Bionics

50/a Práter street, 1083 Budapest, Hungary

hajdara.anna@itk.ppke.hu

Abstract— $\gamma\delta$ T cells, a subpopulation of unconventional lymphocytes can infiltrate solid tumors and enhance the anti-tumor immune response. The role of $\gamma\delta$ T cells has been studied in bacterial infections and in various types of carcinomas, but not yet thoroughly examined in melanoma or in other types of malignant skin diseases. $\gamma\delta$ T cells can be expanded from peripheral blood mononuclear cells (PBMC) with zoledronic acid and interleukin-2. Zoledronic acid inhibits the farnesyl-pyrophosphate synthase enzyme in cells leading to the enhanced accumulation and release of isopentenyl-pyrophosphate (IPP), an intermediate of the mevalonate pathway [1]. Increased IPP release from cells is responsible for the activation and proliferation of $\gamma\delta$ T cells. Tumors release high amount of IPP that could be further enhanced by zoledronic acid which makes this stimulating agent potential candidate of cancer treatment. In this manuscript we investigate the *in vitro* cytotoxic activity of $\gamma\delta$ T cells against melanoma associated fibroblasts.

I. RESULTS

Apoptotic melanoma associated fibroblast populations

MAFs were gated based on the presence of CD73 on their cell surface and on the absence of CD45. Although the Annexin V and 7AAD double positive late apoptotic population was below 5%, the Annexin V positive early apoptotic population increased gradually with the zoledronic acid concentration. Annexin V is able to bind phosphatidyl serine, an apoptotic marker on the outer leaflet of the plasma membrane. There is a significant difference between the unstimulated and zoledronic acid stimulated $\gamma\delta$ T cell samples. Without $\gamma\delta$ T cells the early apoptotic population was approximately above 22% of the total fibroblast population, which did not change by the presence of unstimulated $\gamma\delta$ T cells.

Apoptotic $\gamma\delta$ T cell populations

$\gamma\delta$ T cell population was gated by their positivity of the leukocyte marker CD45 and by the absence of CD73 marker. Compared to the fibroblasts the early apoptotic populations were below 10%, except in the 50 μ M zoledronic acid stimulated sample, which resulted in 42,8%. This concentration exceeds the clinical dosage of zoledronic acid and the higher ratio of apoptotic population among the T cells can be explained by their excessive activation and their interaction with the fibroblast cells, which resulted in their own apoptosis.

Expression of butyrophilin 2A1 and 3A1 mRNA on melanoma associated fibroblasts

The BTN2A1 and BTN3A1 mRNA was detectable on each type of cells, which makes them recognizable to the

gamma-delta T cell receptors.

Expression of MICA and MICB proteins on melanoma associated fibroblasts

MICA and MICB were also present in both MAF donors, in normal dermal fibroblasts and in SKMEL-28 cells. The expression of MICA/B may seem higher, than that of the butyrophilin molecules

II. CONCLUSION

Our findings suggest that cytotoxic activity of $\gamma\delta$ T cells can be measured by detecting the early and late apoptotic populations of fibroblast cells in $\gamma\delta$ T cell –fibroblast co-culture assays. The expression of butyrophilin molecules and unconventional MHC molecules on melanoma associated fibroblasts indicates, that these molecules may be the molecular targets of stimulated $\gamma\delta$ T cells.

Melanoma-associated fibroblasts (MAFs) and melanoma tumor cells were isolated from either primary or metastatic tumors of melanoma patients. Normal dermal fibroblasts were isolated from naevus excisions of healthy individuals.

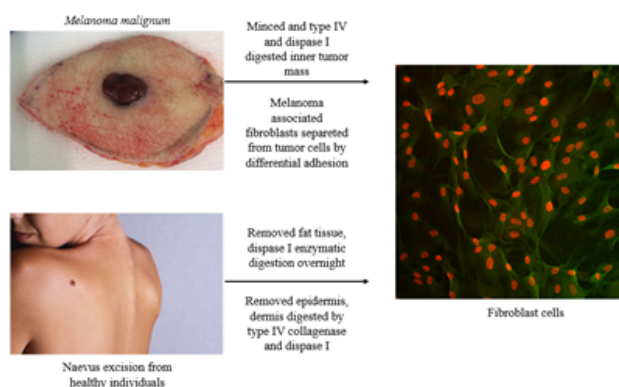


Fig. 1. Isolation of melanoma associated fibroblasts and normal dermal fibroblasts

REFERENCES

- [1] H. Mönkkönen, P. D. Ottewill, J. Kuokkanen, J. Mönkkönen, S. Auriola, and I. Holen, "Zoledronic acid-induced IPP/AppPI production in vivo," *Life Sci.*, vol. 81, no. 13, pp. 1066–1070, Sep. 2007, doi: 10.1016/j.lfs.2007.08.007.

Benchmarking microbiome sequencing dataset using statistically equivalent signatures

Regina KALCSEVSZKI

(Supervisor: Sándor PONGOR)

Pázmány Péter Catholic University, Faculty of Information Technology and Bionics

50/a Práter street, 1083 Budapest, Hungary

kalcsevszki.regina@itk.ppke.hu

Abstract—In recent years more and more scientific study is written about the connection of human microbiome and diseases. The human microbiome contains the organisms which are living inside and on human. While the human genome contains about 20,000 genes, in the human microbiome this number is larger by a factor of ten. To investigate the connections we have to sequence and analyse the sequences. Microbiome sequencing results tremendous amount of data that bioinformatics has to process, understand, and draw conclusions from them.

Implementing new bioinformatics algorithm calls for benchmarking datasets, sets where we know the ground truth of the data. However, in the case of real-world microbiome abundance data we never know the ground truth, because until this day none of the tools can determine the ratios perfectly.

In this study I implemented a benchmarking-dataset generation pipeline and generated two datasets in different sequencing depth and I tested whether SES algorithm is applicable on microbiome abundance data to find statistically equivalent signatures on the generated benchmarking datasets. SES algorithm found the correlated pair on the ratios and on the generated dataset, that's abundances were the closest to the original ratios.

Keywords-metagenome; benchmarking

I generated two simulated datasets based on bacterial genomes of RefSeq database and artificial ratios. The ratios was chosen in a way that two of the bacteria was differently abundant in diseased and control phenotypes, while all other bacteria had the same ratios on every sample. One of the dataset was a smaller, less deep sequencing dataset, while the other represents a more deep sequencing dataset.

I ran two taxonomic classifier on the datasets *MetaPhlan3* and *Kraken2* to find the abundances of the bacteria of the samples. I was able to compare the found abundances of the benchmarking dataset to the original ratio. Based on Bray-Curtis dissimilarity the best results was achieved by *MetaPhlan3* on the larger dataset.

As it was expected, SES algorithm reached the best result on the abundances that approximated best the original ratios. Here SES found both bacteria. The results found on the datasets classified by *Kraken2* fell way behind.

With the new pipeline of benchmarking dataset generation, shown in Figure 1, we will be able to monitor our results in a controlled way.

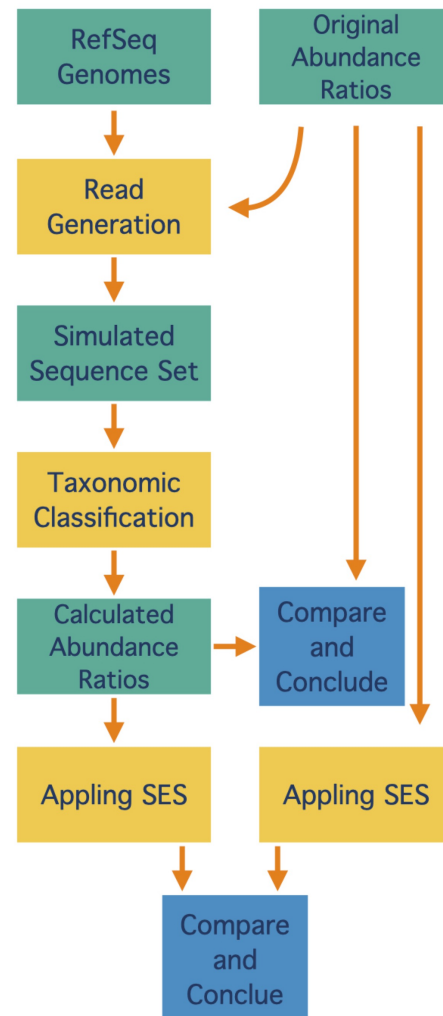


Fig. 1. Benchmarking pipeline for microbiome abundance data. First, we generate a simulated microbiome sequencing dataset based on reference genomes and predefined abundance ratios. We use taxonomic classifiers to find the abundance ratios based on generated sequences, then we compare the original ratios with the calculated abundances. We apply SES algorithm to find statistically equivalent signatures on both of the abundance ratios, then we compare the results.

REFERENCES

- [1] Pruitt, K. D. et al., *NCBI reference sequences (RefSeq): A curated non-redundant sequence database of genomes, transcripts and proteins*, Nucleic Acids Research, 2007
- [2] Nicholas A. Bokulich et al., *Measuring the microbiome: Best practices for developing and benchmarking microbiomics methods* ELSEVIER, 2020
- [3] Simon H. Ye et al., *Benchmarking Metagenomics Tools for Taxonomic Classification* Cell, 2019
- [4] Derrick E. Wood et al., *Improved metagenomic analysis with Kraken 2*, bioRxiv, 2019
- [5] Francesco Beghini et al., *Integrating taxonomic, functional, and strain-level profiling of diverse microbial communities with bioBakery 3*, bioRxiv, 2020
- [6] Vincenzo Lagani et al., *Journal of Statistical Software Feature Selection with the R Package MXM: Discovering Statistically-Equivalent Feature Subsets*, ResearchGate, 2016

R. KALCSEVSZKI, "Benchmarking microbiome sequencing dataset using statistically equivalent signatures" in *PhD Proceedings – Annual Issues of the Doctoral School, Faculty of Information Technology and Bionics, Pázmány Péter Catholic University – 2021*. G. Prószéky, G. Szederkényi Eds. Budapest: Pázmány University ePress, 2021, p. 19. This research has been partially supported by the European Union, co-financed by the European Social Fund (EFOP-3.6.3-VEKOP-16-2017-00002).

Large-scale analysis of postsynaptic protein:protein interactions

Zsófia KÁLMÁN

(Supervisor: Zoltán GÁSPÁRI)

Pázmány Péter Catholic University, Faculty of Information Technology and Bionics
50/a Práter street, 1083 Budapest, Hungary
kalman.zsofia.etelka@itk.ppke.hu

I. INTRODUCTION

In the past several years proteomic approaches helped the identification of nearly 2000 synaptic proteins, which approximately takes 10% of the whole human proteome. The synaptic proteins can be divided into two basic groups to pre- and postsynaptic, based on their localization in the synaptic cell. Proteins harboring different localization fulfill entirely different functions. The postsynaptic site of the synapse is responsible for receiving neurotransmitters released from the presynaptic neuron. The postsynaptic site consists of membrane proteins, ion channels, scaffolding proteins, and cytoskeletal proteins mainly, exhibiting major differences depending on the type of the synapse, (i.e. excitatory and inhibitory) (Figure 1). Proteins in both systems interact with each other to form a constantly changing highly dynamic network. The high number of proteins and their constant reorganization still challenge scientists to describe the whole network. Our research group's main aim is to describe postsynaptic density from various aspects from structure determination of individual synaptic proteins to large-scale bioinformatics analysis. However, a missing piece of the puzzle is the comprehensive description of various protein:protein interactions (PPIs) governing the organization of the postsynaptic site [1] [2].

Advancements in experimental techniques yielded ten thousand PPIs in recent decades. Despite the effort, most information is scattered in the literature and losing visibility, and one can find this data with only laborious work. Another problem is the diversity of experimental techniques, where there is no common ground to unify information from fundamentally different techniques and research fields. To overcome these limitations there is a growing interest in the scientific community to I) collect PPI data from the literature II) Deposit this information in publicly available repositories with definitions established by the research community. The HUPO - Proteomics Standards Initiative works on developing and maintaining such standards to describe molecular interactions. In the past semester, I participated in several courses and learned how to collect data from the literature and translate it to a common language accessible for researchers from different fields.

II. MATERIALS AND METHODS

MIMIX format [3] was used to store the interactions and Molecular Interaction controlled vocabulary to describe the terms [4]. Publications were collected from Pubmed.

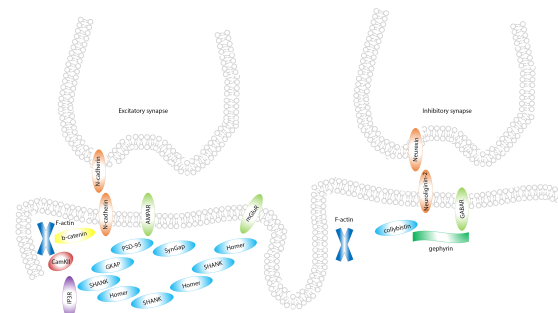


Fig. 1. Postsynaptic organization of the synapses - simplified picture about some of the typical protein and their network

III. SUMMARY

During the previous semester, I prepared an interaction data set that fulfilled all the requirements set by HUPO-PSI. For the description of the interaction, I choose the MIMIX format which contains the minimum necessary information required for interaction. In most of the cases, I also collected additional information besides the minimum requirements, such as the interacting region of the partners. To describe the interactions we use the controlled vocabulary, which contains all the terms for a proper and detailed description of the interactions. I already collected over 1000 interaction data from hundreds of articles. I also prepared a protocol to guide the curation by other research group members. These uniformized and highly reliable data will be used in in-depth investigations of PPIs in the postsynapse and aid a range of computational approaches to understand the organization and dynamics of the postsynaptic protein network.

REFERENCES

- [1] M. Sheng and E. Kim, "The postsynaptic organization of synapses," *Cold Spring Harbor perspectives in biology*, vol. 3, no. 12, p. a005678, 2011.
- [2] M. Gonzalez-Lozano, F. Koopmans, P. Sullivan, J. Protze, G. Krause, M. Verhage, K. Li, F. Liu, and A. Smit, "Stitching the synapse: Cross-linking mass spectrometry into resolving synaptic protein interactions," *Science advances*, vol. 6, no. 8, p. eaax5783, 2020.
- [3] S. Orchard, L. Salwinski, S. Kerrien, L. Montecchi-Palazzi, M. Oesterheld, V. Stümpflen, A. Ceol, A. Chatr-Aryamontri, J. Armstrong, P. Woolford *et al.*, "The minimum information required for reporting a molecular interaction experiment (mimix)," *Nature biotechnology*, vol. 25, no. 8, pp. 894–898, 2007.
- [4] R. G. Côté, P. Jones, L. Martens, R. Apweiler, and H. Hermjakob, "The ontology lookup service: more data and better tools for controlled vocabulary queries," *Nucleic acids research*, vol. 36, no. suppl_2, pp. W372–W376, 2008.

Separation of micron-sized particles with pinched flow fractionation

Máté KÁLOVICS

(Supervisor: Kristóf IVÁN)

Pázmány Péter Catholic University, Faculty of Information Technology and Bionics

50/a Práter street, 1083 Budapest, Hungary

kalovics.mate@itk.ppke.hu

Abstract—The miniaturized, low-cost, portable devices with reduced sample volumes and analysis time, reduced contamination chance and high sensitivity makes microfluidic particle separation and manipulation techniques are in demand both industry and research.

The aim of this PhD research is to highlight and understand the effects that influence particle separation in pinched flow fractionation. There will be a device presented which is eligible for separation of micron sized particles. I will cover the device parameters, the experimental settings and the results of the measurements. To establish study these kind of devices in operation, computational fluid dynamics simulations were done with COMSOL Multiphysics 5.2a (COMSOL, Inc., PaloAlto, CA, USA). Channels were designed with AutoCAD 2019. (Autodesk Inc., San Rafael, CA, USA).

Keywords—pinched flow fractionation, microfluidics, particle separation, CFD

I. SUMMARY

Pinched flow fractionation (PFF) was first introduced by Yamada *et. al* [1] in 2004 by separating micrometer sized particles by size. The very first equation was based on the laminar flow properties and the phenomenon that the particles are following the streamlines was [1]:

$$y = \frac{(W_p - \frac{d_p}{2})W_b}{W_p}, \quad (1)$$

where W_p and W_b are the width of the pinched and the broadened segments, respectively, and d_p is the particle diameter. This equation is about the position of the particles in the outlets based on a relation between the pinched and the broadened segment with completely pinched round shaped and same sized particles. This equation does not take into consideration internal forces, particle rotation, attraction to the wall.

Since this invention many groups were working on this topic to improve and achieve the best separation resolution. Jain *et. al* [2] defined an equation which describes how to set the flow ratios the reach perfect alignment of the particles. Sai *et. al* [3] suggested an ideal channel width depending on particle sizes you want to separate. Maenaka *et. al* [4] realised that the particles are migrating away from the channel wall on its length. Shardt *et. al* [5] determined the reason for attraction to the channel wall and suggested why specific geometries are better.

In this project I will present the design, manufacturing and the separation efficiency of a PFF device.

REFERENCES

- [1] M. Yamada, M. Nakashima, and M. Seki, "Pinched flow fractionation: continuous size separation of particles utilizing a laminar flow profile in a pinched microchannel," *Analytical chemistry*, vol. 76, no. 18, pp. 5465–5471, 2004.

M. KÁLOVICS, "Separation of micron-sized particles with pinched flow fractionation" in *PhD Proceedings – Annual Issues of the Doctoral School, Faculty of Information Technology and Bionics, Pázmány Péter Catholic University – 2021*. G. Prószéky, G. Szederkényi Eds. Budapest: Pázmány University ePress, 2021, p. 21. This research has been partially supported by the European Union, co-financed by the European Social Fund (EFOP-3.6.3-VEKOP-16-2017-00002).

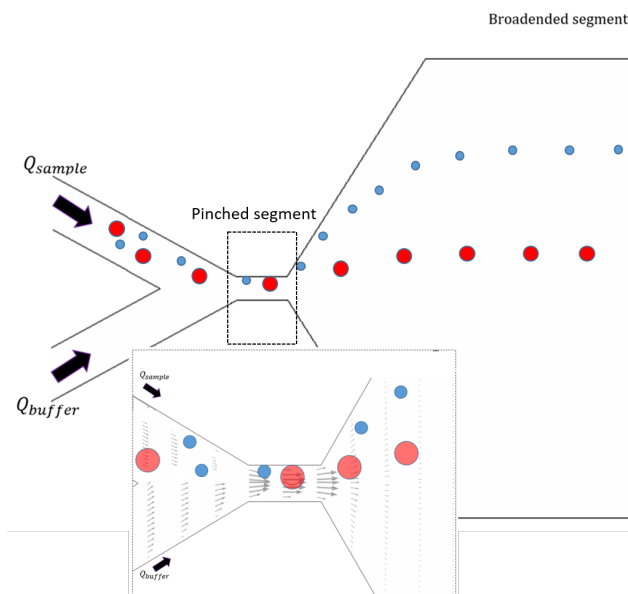


Fig. 1. Working principle of basic pinched flow fractionation devices. The sample (particle containing liquid) enters the device in the first inlet with a flow rate of Q_{sample} and a buffer solution on the second inlet with a flow rate of Q_{buffer} where $Q_{sample} \ll Q_{buffer}$. In the pinched segment the particles are pushed to the channel wall by the buffer liquid independent to size. The opening angle rapidly spreads the streamlines and significantly increases the differences in particle positions in the broadened segment. Separates particles perpendicular to flow direction based on size [1].

- [2] A. Jain and J. D. Posner, "Particle dispersion and separation resolution of pinched flow fractionation," *Analytical chemistry*, vol. 80, no. 5, pp. 1641–1648, 2008.
- [3] Y. Sai, M. Yamada, M. Yasuda, and M. Seki, "Continuous separation of particles using a microfluidic device equipped with flow rate control valves," *Journal of chromatography A*, vol. 1127, no. 1-2, pp. 214–220, 2006.
- [4] H. Maenaka, M. Yamada, M. Yasuda, and M. Seki, "Continuous and size-dependent sorting of emulsion droplets using hydrodynamics in pinched microchannels," *Langmuir*, vol. 24, no. 8, pp. 4405–4410, 2008.
- [5] O. Shardt, S. K. Mitra, and J. Derksen, "Lattice boltzmann simulations of pinched flow fractionation," *Chemical engineering science*, vol. 75, pp. 106–119, 2012.

Agent-based models in biological simulation

Bence Márk KEÖMLEY-HORVÁTH

(Supervisors: Attila CSIKÁSZ-NAGY, István Zoltán REGULY)

Pázmány Péter Catholic University, Faculty of Information Technology and Bionics

50/a Práter street, 1083 Budapest, Hungary

keomley-horvath.bence.mark@itk.ppke.hu

I. INTRODUCTION

COVID-19 became a global pandemic in this year. Controlling the spread of the virus is not a trivial task. The decision-makers have to weigh the health risk and the economic impact of the lockdowns. Multiple epidemic models exist which can model the possible outcomes of the given scenarios. In most of the models, the effect of the different measures can be simulated by changing some parameters in a differential equation.

Much of the available literature applied a deterministic model for the current COVID pandemic. In Röst et al., they proposed a system control model that can modify the constants in runtime in the differential equations to archive different goals. [1]

There are many agent-based models created for this pandemic, with different level of accuracies and runtime performance.

A much more detailed and, therefore, a more computational heavy approach is proposed in Alexiadis et al. [2]. Their work started from a molecular dynamics model with detailed spatial information of real cities (Bogotá and Birmingham). The agent has a detailed behaviour pattern, including daily movement routines and mask-wearing customs. With 16 Xeon E5-2680v4 processor, each with 28 cores took 80 hours for Bogotá.

Epidemics simulations are not a new challenge. It just became more important due to the current COVID pandemic. There has already been an existing agent-based model, which they used to specialise for this pandemic. For Australia there is a pre-existing model [3], where agents have a specific schedule and corresponding movement pattern on a highly detailed location graph. They improved and specialised that model for the COVID-19 pandemic [4]. Using the HPC cluster (Artemis at the University of Sydney), with 4264 computing cores to simulate entire Australia for 180 days, it takes 42 minutes.

II. OUR GOALS

Our goal is to simulate every person directly, considering every aspect of life relevant to the virus's spreading with agent-based modelling. We have to follow their movements because this defines where they can be infected and transmit the virus. Another important aspect are those data that can affect their response to the virus; therefore, we have to consider the agent's age and precondition.

The purpose of this simulation is to predict the effect of different scenarios. These can be governmental regulations like obligatory mask-wearing, closing various institutions and lockdowns. Different testing policies define when an agent gets tested and the effect of a positive test. We have to be able to handle all these events in a way that some can dynamically change throughout the simulation.

III. IMPLEMENTATION

A. Thrust

A detailed simulation like this has a high computational cost. We used the Thrust Parallel Algorithm Library to implement most algorithms in our simulation. There are multiple advantages to this library. It makes the application more portable because it is possible to define at compile time what type of parallelisation it should use, like CPU+OpenMP or GPU+CUDA.

B. Algorithms

There are three big large section of the algorithm. During the movement we have to move the agents between their locations based on their schedule and the agent's well-being state. As the code improved and we added new features, like testing, quarantines, and hospitalisation, the movement became complicated. The actual location ID is stored for every agent in an array the same way as the agents' other attributes. Updating this vector is simple because we only have to rewrite one value in that array.

During infection we have to calculate the infected agents on the same locations and infect randomly the susceptible agents.

During midnight we update the state of the agents to simulate the progression of the disease. There are many possible events during a simulation to model different scenarios, such as lockdowns, mask regulations, vaccination strategies.

ACKNOWLEDGEMENTS

This research was supported by the ÚNKP-20-3-II New National Excellence Program of the Ministry for Innovation and Technology From the source of the National Research,

Development and Innovation Fund.



REFERENCES

- [1] T. Péni, B. Csutak, G. Szederkényi, and G. Röst, "Nonlinear model predictive control with logic constraints for COVID-19 management," *Nonlinear Dynamics*, vol. 102, p. 1965–1986, Dec 2020.
- [2] A. Alexiadis, A. Albano, A. Rahmat, M. Yildiz, A. Kefal, M. Ozbulut, N. Bakirci, D. A. Garzón-Alvarado, C. A. Duque-Daza, and J. H. Eslava-Schmalbach, "Simulation of pandemics in real cities: enhanced and accurate digital laboratories," *Proceedings of the Royal Society A: Mathematical, Physical and Engineering Sciences*, vol. 477, p. 20200653, Jan 2021.
- [3] O. M. Cliff, N. Harding, M. Piraveenan, E. Y. Erten, M. Gambhir, and M. Prokopenko, "Investigating spatiotemporal dynamics and synchrony of influenza epidemics in Australia: an agent-based modelling approach," *Simulation Modelling Practice and Theory*, vol. 87, p. 412–431, Sep 2018.
- [4] S. L. Chang, N. Harding, C. Zachreson, O. M. Cliff, and M. Prokopenko, "Modelling transmission and control of the COVID-19 pandemic in Australia," *Nature Communications*, vol. 11, Nov 2020.

Optogenetic identification of rhythmic neurons in the medial septum

Barnabás KOCSIS

(Supervisor: István ULBERT)

Pázmány Péter Catholic University, Faculty of Information Technology and Bionics

50/a Práter street, 1083 Budapest, Hungary

kocsis.barnabas@itk.ppke.hu

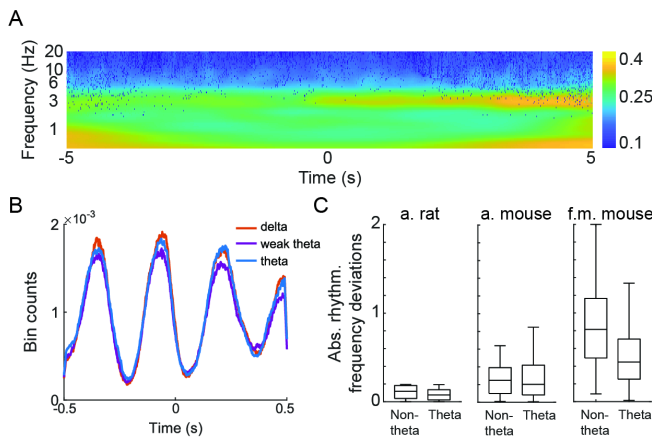


Fig. 1. Synchronization of pacemaker units. A: Population mean cross-coherence for all pacemaker pairs recorded in parallel and for all delta-theta transitions ($t = 0$) (a. mouse). Around hippocampal theta initiation pacemakers increase power in the 3 Hz band. B: Example cross-correlation change for a representative pacemaker pair during delta (red), theta initiation (blue) and theta termination (purple) (a. mouse). Relative rhythmic firing is reduced during the end of theta dominant segments (purple). C: Rhythmicity differences between pacemakers recorded together. Significantly smaller absolute deviations (Wilcoxon signed-rank test) were characteristic to rat ($p = 0.0037$) and f. m. mouse ($p = 0.0025$), but not for a. mouse ($p = 0.4608$) (outliers removed from plot).

from theta rhythmic cells, whereas GABAergic and glutamatergic neurons are mainly non-rhythmic cells.

The synchronization of PV+ pacemaker neurons promoted the notion of frequency synchronization, that was described previously [1].

Keywords-neuronal oscillations, theta rhythm, hippocampus, medial septum, pacemaker, synchronization, optogenetic tagging

REFERENCES

- [1] B. Kocsis and B. Hangya, "Huygens synchronization of medial septal pacemaker neurons generates hippocampal theta oscillation." submitted.
- [2] H. Inokawa, H. Yamada, N. Matsumoto, M. Muranishi, and M. Kimura, "Juxtacellular labeling of tonically active neurons and phasically active neurons in the rat striatum," *Neuroscience*, vol. 168, no. 2, pp. 395–404, 2010.
- [3] I. Gritti, P. Henny, F. Galloni, L. Mainville, M. Mariotti, and B. Jones, "Stereological estimates of the basal forebrain cell population in the rat, including neurons containing choline acetyltransferase, glutamic acid decarboxylase or phosphate-activated glutaminase and colocalizing vesicular glutamate transporters," *Neuroscience*, vol. 143, no. 4, pp. 1051–1064, 2006.
- [4] F. Sotty, M. Danik, F. Manseau, F. Laplante, R. Quirion, and S. Williams, "Distinct electrophysiological properties of glutamatergic, cholinergic and gabaergic rat septohippocampal neurons: novel implications for hippocampal rhythmicity," *The Journal of physiology*, vol. 551, no. 3, pp. 927–943, 2003.

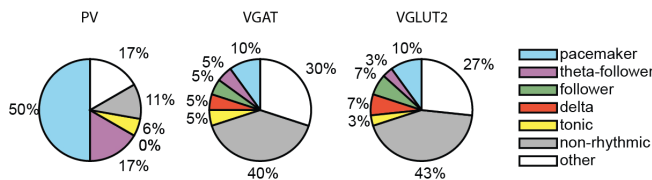


Fig. 2. Rhythmicity group distributions in the three different tagged cell groups (PV $n = 18$; VGAT, $n = 20$; VGLUT2, $n = 30$). PV+ cells are comprised the highest ratio of pacemakers, whereas the GABAergic and glutamatergic cell groups had similar proportions for all rhythmicity components.

Abstract—In this article we further analyzed the network mechanisms of MS synchronization resulting in hippocampal theta oscillation in rodents. Starting from our previous work [1] we demonstrated that tonic cells spatially differentiate from slower theta rhythmic cells (pacemakers, theta-followers) strengthening the idea of their different neurochemical nature, that is also reflected in their fast theta rhythmicity and single spiking behavior [2].

Further analysis of rhythmicity network and pacemaker synchronization supported our previous conclusions on the 'synchronizing role' of pacemakers and the frequency synchronization mechanism underlying it.

With the help of optogenetic tools we managed to tag PV+, GABAergic and glutamatergic cells in anaesthetized mice [3], [4]. The proportions of rhythmicity groups in the labeled neurons unambiguously demonstrated that PV+ neurons are comprised

Parameter space investigation of multi-class SVM problem for brain-computer interfaces

Csaba Márton KÖLLŐD

(Supervisor: István ULBERT)

Pázmány Péter Catholic University, Faculty of Information Technology and Bionics

50/a Práter street, 1083 Budapest, Hungary

kollod.csaba@itk.ppke.hu

Abstract—This report present the results of a Multi-class SVM problem, focusing on the parameter space investigation, which was done on the HPC server of ITK. The result are supporting a Brain-Computer Interface development.

I. INTRODUCTION

Brain-Computer Interfaces (BCI) are integrated software and hardware systems which record the bio-electrical signals of the brain. And by classifying the signals it controls an external device. (Fig. 1.)

Our research team, lead by István ULBERT, aims to create a BCI system, which will be challenged by other BCI devices of other research groups, in 2024 at the international Cybathlon competition. <https://cybathlon.ethz.ch/>

II. DATASET

The parameter investigation were run on two databases. The first is the Physionet database, created by Schalk et. al. [1], which is available on <https://physionet.org/> [2]. The second is our own database created similarly as the Physionet database. For signal recording, 64 channeled ActiChamp+ EEG system were used, which is produced by Brain Products. In our initial paradigm, four motor movements and the resting activity were imagined by the subjects, which concluded overall five imaginary classes. However, during the resting phase, subjects were allowed to blink, swallow and do many different short movements in purpose to avoid artefact appearance under motor movement imagination. Therefore later on the resting activity were avoid in EEG signal classification.

III. METHODS

For searching the parameter space the High Performance Cluster (HPC) machine were used. The original BCI code were uploaded to the server with the databases. Many different preprocessing configurations were created and submitted as jobs to calculate the Accuracy results on the whole databases.

Raw EEG data is recorded and send to the Signal Processing part of the BCI System. With a given window length data is cut and for each window the Power Spectral Density (PSD) is calculated. Two different methods are created for feature extraction and classification. One of them is the FFT POWER method, where the average FFT of a well known EEG band is calculated for each channel. This resulted a *number of channel x 1* feature vector which is used as train and test data for a Support Vector Machine (SVM). The other is the FFT RANGE method, which further utilizes the FFT Power method, by creating feature vectors form distinct 2 Hz wide parts of the PSD. These features are fed to separate SVMs

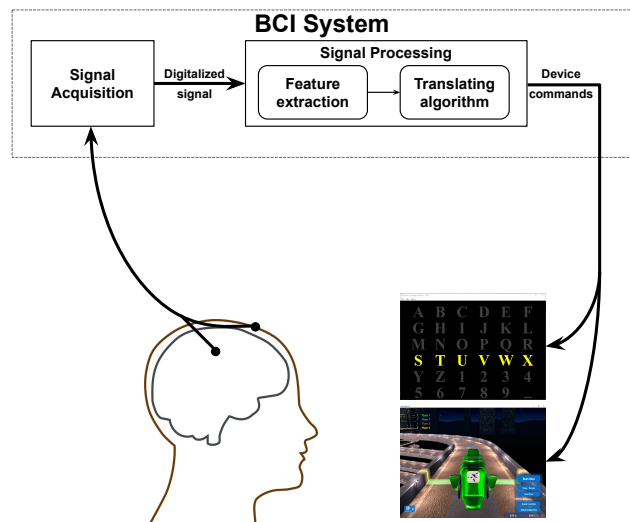


Fig. 1. BCI System workflow, based on J. R. Wolpaw et al. [3]

with respect to the frequency range. The final classification result is calculated as the max vote of the individual SVMs.

The parameter space investigation included different frequency analysis techniques eg. pure FFT method versus PSD, window length investigation and different normalization and scaling techniques.

IV. RESULTS

The FFT Range method clearly outperformed the FFT Power methods. The 2 second long window with PSD increased additionally the accuracy of both databases. These results are contributes to the development of the BCISystem.

REFERENCES

- [1] G. Schalk, D. J. McFarland, T. Hinterberger, N. Birbaumer, and J. R. Wolpaw, “BCI2000: A general-purpose brain-computer interface (BCI) system,” *eng, IEEE transactions on bio-medical engineering*, vol. 51, no. 6, pp. 1034–1043, 2004.
- [2] Goldberger Ary L., Amaral Luis A. N., Glass Leon, *et al.*, “PhysioBank, PhysioToolkit, and PhysioNet,” *Circulation*, vol. 101, no. 23, e215–e220, 2000.
- [3] J. R. Wolpaw, N. Birbaumer, D. J. McFarland, G. Pfurtscheller, and T. M. Vaughan, “Brain–computer interfaces for communication and control,” *Clinical Neurophysiology*, vol. 113, no. 6, pp. 767–791, 2002.

Electrochemical impedance spectroscopy (EIS) for microfluidic qualitative and quantitative cell separation

Dániel KOLPASZKY

(Supervisor: Kristóf IVÁN)

Pázmány Péter Catholic University, Faculty of Information Technology and Bionics
50/a Práter street, 1083 Budapest, Hungary
kolpaszky.daniel@itk.ppke.hu

Abstract—An increasing research field today is the cells and particles separation and focusing in microfluidics. These processes are useful in biomedical applications and basic cell biology research as they offer cost-effective and miniaturized point-of-care (POC) diagnostic tools and replication of rare cells.

The aim of this PhD research is to implement an EIS sensor in microfluidic environment as cost-effective as possible, modeling the microchannel and the sensor geometries were made by AutoCAD 2018 (Autodesk Inc., San Rafael, CA, USA) vector-graphing program and simulating their hydrodynamic and electrochemical properties with finite element method analysis FEM, COMSOL Multiphysics 5.2a (COMSOL, Inc., PaloAlto, CA, USA).

Keywords-microfluidics; electrochemical impedance spectroscopy; particle separation; MEMS;

I. SUMMARY

Microfluidics deals with the behaviour, control and manipulation of liquids and particles, in and under the micro scale; where the fluid viscosity, resistance and energy dissipation differ from commonly described hydrodynamics. This is a multidisciplinary field of engineering, physics, chemistry, microtechnology and biology. Beside many application what microfluidics is capable, particle separation and sorting is an essential pretreatment procedure in diagnostics, chemical and biological analyzes, food and chemical processing, and environmental testing. A continuous, easily analysable, high-performance microsize particle sorting device with lower manufacturing cost is required for wide variety of application within the mentioned areas. [1] Electrochemical impedance spectroscopy allows the quantitative and qualitative study of cells or other biological samples by creating an alternating electric field (by changing the frequency), with which a specific impedance spectrum can be generated. The main advantages of EIS sensors are that they allow real-time non-invasive detection, and that the electromagnetic waves don't damage the sample. In order to reduce the noise received by the sensor, the system should be miniaturized and as integrated as possible with the microfluidic environment. [2], [3], [4] The aim of this research topic is to create an impedance cytometer in a microfluidic environment that can measure the dielectric properties of biological samples in the mega-, gigahertz frequency range. The dielectric properties of biological cells provide information on cell size, cell membrane resistance and capacity, cytoplasmic conductivity. The electroanalysis can provide information of diagnostic and / or prognostic significance for cancer, and can be used to study neurodegenerative diseases and capture complex cellular responses through drug

or chemical interactions. [5], [6], [7]

II. FIGURES

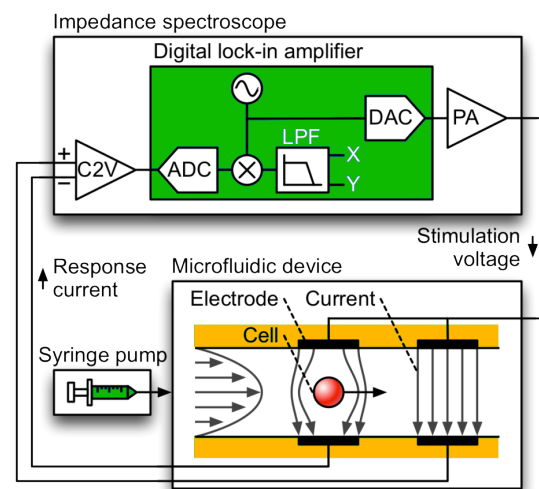


Fig. 1. Impedance Signal Generation: Passage of a particle between two pairs of facing electrodes and resulting differential impedance signal.

REFERENCES

- [1] H. Amini, W. Lee, and D. Di Carlo, "Inertial microfluidic physics," *Lab on a Chip*, vol. 14, no. 15, pp. 2739–2761, 2014.
- [2] A. Manickam, A. Chevalier, M. McDermott, A. D. Ellington, and A. Hasibi, "A cmos electrochemical impedance spectroscopy (eis) biosensor array," *IEEE Transactions on Biomedical Circuits and Systems*, vol. 4, no. 6, pp. 379–390, 2010.
- [3] J. S. Daniels and N. Pourmand, "Label-free impedance biosensors: Opportunities and challenges," *Electroanalysis: An International Journal Devoted to Fundamental and Practical Aspects of Electroanalysis*, vol. 19, no. 12, pp. 1239–1257, 2007.
- [4] Y. Chen, C. C. Wong, T. S. Pui, R. Nadipalli, R. Weerasekera, J. Chandran, H. Yu, and A. R. Rahman, "Cmos high density electrical impedance biosensor array for tumor cell detection," *Sensors and Actuators B: Chemical*, vol. 173, pp. 903–907, 2012.
- [5] R. Elshafey, C. Tlili, A. Abulrob, A. C. Tavares, and M. Zourob, "Label-free impedimetric immunosensor for ultrasensitive detection of cancer marker murine double minute 2 in brain tissue," *Biosensors and Bioelectronics*, vol. 39, no. 1, pp. 220–225, 2013.
- [6] T. Chi, J. S. Park, J. C. Butts, T. A. Hookway, A. Su, C. Zhu, M. P. Styczynski, T. C. McDevitt, and H. Wang, "A multi-modality cmos sensor array for cell-based assay and drug screening," *IEEE transactions on biomedical circuits and systems*, vol. 9, no. 6, pp. 801–814, 2015.
- [7] F. Gozzini, G. Ferrari, and M. Sampietro, "An instrument-on-chip for impedance measurements on nanobiosensors with attofarad resolution," in *2009 IEEE International Solid-State Circuits Conference-Digest of Technical Papers*, pp. 346–347, IEEE, 2009.

An overview of the MSLA 3D printing-based manufacturing process of a split-ring resonator-based microfluidic sensor

Adrienn Lilla MÁRTON
(Supervisor: Kristóf IVÁN)

Pázmány Péter Catholic University, Faculty of Information Technology and Bionics
50/a Práter street, 1083 Budapest, Hungary
marton.adrienn.lilla@itk.ppke.hu

Additive manufacturing technology is one of the most developing industries today. It has many advantages over the traditional technologies including cost and time effectivity, production with less waste, and significantly higher complexity of the geometry can be achieved. As a result, it is widely used in both the industry and the research areas to create various device components and MEMS devices. In addition, 3D printers are already famous in everyday usage due to its ever-cheaper price. The most common printers are the Fused Deposition Modeling (FDM) printer [1], the Stereolithography (SLA) 3D printer [2] and Inkjet 3D printer [3]. Masked Stereolithography (MSLA) as a type of SLA printing has fast prototyping feature and proven high resolution can be achieved with it [4]. Its light source is a UV LED array shining through an LCD screen functioning as a mask for a single layer slice to harden each one after another. Its key feature that most determines the granularity of a print is the pixel size of its LCD photomask. The goal of our research team is to make a sensor utilizing electromagnetic field interactions combined with microfluidics using MSLA 3D printer supplemented with other techniques. We are testing a cheap 3D-printer usability for research studies. First, a microfluidic mold was fabricated using an epoxy-based UV-curable resin and Elegoo Mars Pro printer (Elegoo Indsutry, China). Then the microfluidic chip prepared from polydimethylsiloxane (PDMS) using the printed mold and baked for 1 hours at 65°C. To test its application, it was applied on a microwave filter which composed of a microstrip waveguide and a double complementary split ring resonator (CSRR) etched to the ground plate. The CSRR is sensitive to the changes within its near field making it well-applicable as a sensor. Based on that, if the channel of the microfluidic chip is placed onto the CSRR the fluid and even its components inside the microfluidic tunnel can be detected effectively. The procedure of the placing started with spin coating a very thin PDMS layer onto the ground plate which hardened for 15 min at 65°C. Then the microfluidic chip was placed carefully onto it and baked for 45 min at 65°C. The fabrication was successful. The error of the accuracy was within 5%. The mold surface was almost perfectly smooth, only micro bubbles obtained due to the bubble formation in the resin. The resulted fluidic sensor then tested using two-port vector network analyzer. At microwave frequency, resonant shift was observed due to the change in the electric permittivity in the sensing region of the sensor. That means our attempt to use one of the cheapest commercially available 3D printer to create a CSRR sensor was completed successfully.

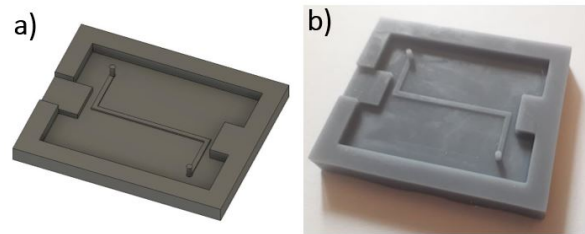


Fig. 1. (a) The image shows the design of the microfluidic mold created in AutoCad Fusion 360. (Autodesk Inventor, USA) (b) The photo shows the printed mold using Elegoo Mars Pro Masked Stereolithography (MSLA) 3D printer and Anycubic standard UV-curable grey resin.

ACKNOWLEDGMENT

I would like to thank you to Zsolt Szabó and my supervisor Kristóf Iván for their guidance and many advices which are helping me to cope with the arising problems and achieve our goals. This work was supported by the National Research, Development and Innovation Office of Hungary under Project K-132050.

REFERENCES

- [1] F.Kotz et al. "Fused Deposition Modeling of Microfluidic Chips in Polymethylmethacrylate" *Micromachines (Basel)* vol. 11, no. 9, pp. 873. 19 Sept 2020.
- [2] R. Zhang and N.B.Larsen "Stereolithographic hydrogel printing of 3D culture chips with biofunctionalized complex 3D perfusion networks" *Lab on a Chip* vol. 17, pp. 4273-4282. 3. Nov 2017.
- [3] R. Walczak, B. Kawa and K. Adamski "Inkjet 3D printed microfluidic device for growing seed root and stalk mechanical characterization" *Sensors and Actuators A: Physics* vol. 297, no. 1, pp. 111557. 12. August 2019.
- [4] T. Tamura and T. Suzuki, "Seamless fabrication technique for micro to millimeter structures by combining 3D printing and photolithography" *Japanese Journal Applied Physics* vol. 58, SDDL10 10. June 2019.

Distribution and structure of postsynaptic protein complexes assessed by simulations

Marcell MISKI

(Supervisor: Attila CSIKÁSZ-NAGY)

Pázmány Péter Catholic University, Faculty of Information Technology and Bionics

50/a Práter street, 1083 Budapest, Hungary

miski.marcell@itk.ppke.hu

Abstract—Understanding the structure and dynamics of postsynaptic protein complexes is key to get insight into the molecular mechanisms behind learning and memory, as well as several neurological conditions like autism. I am using computer simulations and modeling to decipher the composition and 3D structure of complexes arising in the postsynaptic density (PSD) as a function of the abundance of individual proteins.

Methods: Simulations to estimate complex formation using different input protein abundance data were performed with CytoCast. Structural data for the individual proteins were obtained from the PDB database and complemented by specialized predictions to identify functionally disordered and fibrillar segments.

Results: I have made significant steps for the modeling of actual 3D structures of several proteins and their complexes, but these have to be refined further to obtain realistic geometry and interaction surfaces.

Keywords—keyword;postsynaptic density; CytoCast; Synaptic Theory; PeProb; disordered regions; protein models

I. INTRODUCTION

My research is focusing on the Synaptic Theory [1]. According to the Theory the protein abundances in the postsynaptic density largely determine the neuron's behaviour. From the protein abundances I am trying to predict the possible complexes formed. The disadvantages of the simulations made were that the complexes were considered only a graph - three dimensional orientation of the binding sites and the protein structures were not included. In order to incorporate these aspects into the model I initiated the building of 3D structural models of each protein.

II. METHODS AND VALIDATION

I provided the experimentally determined protein abundance data as input for the agent-based Gillespie simulation program CytoCast where I obtained the resulting complexes as a graph (nodes are the proteins, edges are the bindings). I performed around a thousand different simulations but still further ones, with parameters reflecting the actual cellular conditions better. are needed to be able to draw robust conclusions. To obtain a more detailed picture, it is necessary to establish a method for the quantitative comparison of all the complexes formed, a task getting rather difficult for complexes with more than 10 constituent proteins, termed supercomplexes. Supercomplexes are formed in the majority of the simulations and are usually present in low copy numbers.

To assess the biological relevance of the complexes predicted by CytoCast, a full 3D model of these has to be built to assess the feasibility of it including steric constraints. Our approach is to prepare models of individual proteins and then build their structure using the software IMP (Integrative

Modeling Platform ([2]) that can build the complexes by satisfying the provided domain-domain interaction constraints while treating the flexibility of the proteins according to predefined settings.

III. DISCUSSION

I conclude that the protein models joining together known parts of the protein by modeled disordered regions can be used to create complexes by the software IMP because the IMP can manage the different domain orientations by flexible regions. However the models of the proteins are not creditable alone due to the artificial orientation of the domains. In each case, consider what the model of the protein is to be used for and decide how much the reliability for that purpose.



Fig. 1. The structure of a constructed PSD-95

ACKNOWLEDGEMENTS

The authors acknowledge the support of the National Research, Development and Innovation Office – NKFIH through grant no. NN124363. The research was funded by the European Union and co-financed by the European Social Fund under grant number EFOP-3.6.2-162017-00013. Molecular graphics and analyses performed with UCSF Chimera, developed by the Resource for Biocomputing, Visualization, and Informatics at the University of California, San Francisco, with support from NIH P41-GM103311.

REFERENCES

- [1] S. G. Grant, "The synaptic theory of behavior and brain disease," *Cold Spring Harbor Symposia on Quantitative Biology*, vol. 83, pp. 45–56, 2018.
- [2] B. W. J. V.-M. E. T. D. S.-D. B. P. Daniel Russel, Keren Lasker and A. Sali, "Putting the pieces together: Integrative modeling platform software for structure determination of macromolecular assemblies," *PLoS Biol*, vol. 10, no. 1, p. e1001244, 2012.

Benchmarking state-of-the-art algorithms with a neural optimization user interface

Máté MOHÁCSI

(Supervisor: Szabolcs KÁLI, Tamás FREUND)

Pázmány Péter Catholic University, Faculty of Information Technology and Bionics

50/a Práter street, 1083 Budapest, Hungary

mohacsi.mate@itk.ppke.hu

Keywords-computational neuroscience; algorithm;

I. INTRODUCTION

Finding optimal parameters for detailed neuronal models is a persistent challenge in neuroscientific research. A standard method is to manually tune the unconstrained parameters of the model until it provides a suitable approximation of the behavior of the real cell. Some more recent studies have examined the feasibility of utilizing automated parameter search [1], [2], [3]. Nevertheless, finding the most efficient algorithm for a specific problem is a nontrivial task, especially for more complex models that require time-consuming simulations.

II. METHODS

We implemented a unique software tool (Neuroptimus) for optimizing the parameters of neural models. Neuroptimus offers various search methods; the majority of these are global optimization algorithms, along with some popular local search methods. Neuroptimus also implements methods to configure, run, and evaluate simulations using the Neuron tool, or using an arbitrary black-box simulator. The software provides a graphical user interface that navigates less experienced users through the steps of setting up the optimization task, while there is also a command line interface that allows experts to rapidly restart a modified optimization and also forms the basis of batch evaluation.

III. RESULTS

We defined a benchmark suite of six different neuronal optimization problems of varying complexity. We then used our evaluation framework to compare the performance of different optimization algorithms on these benchmarks, visualized their progress on each problem, and ranked them by final results and convergence speed. This is demonstrated through the use case of fitting the conductance parameters of an active compartmental neuronal model in Fig. 1. Across the whole benchmark suite, evolution strategy-related and swarm intelligence-based algorithms delivered consistently good results. Therefore, we recommend using these algorithms for similar problems and also trying them first in future optimization problems.

ACKNOWLEDGEMENTS

Our research was funded by the Széchenyi 2020 Program of the Human Resource Development Operational Program, and from the Program of Integrated Territorial Investments in Central-Hungary (EFOP3.6.2-16-2017-00013 and 3.6.3-VEKOP- 16-2017- 00002).

M. MOHÁCSI, "Benchmarking state-of-the-art algorithms with a neural optimization user interface" in *PhD Proceedings – Annual Issues of the Doctoral School, Faculty of Information Technology and Bionics, Pázmány Péter Catholic University – 2021*. G. Prószéky, G. Szederkényi Eds. Budapest: Pázmány University ePress, 2021, p. 28. This research has been partially supported by the European Union, co-financed by the European Social Fund (EFOP-3.6.3-VEKOP-16-2017-00002).

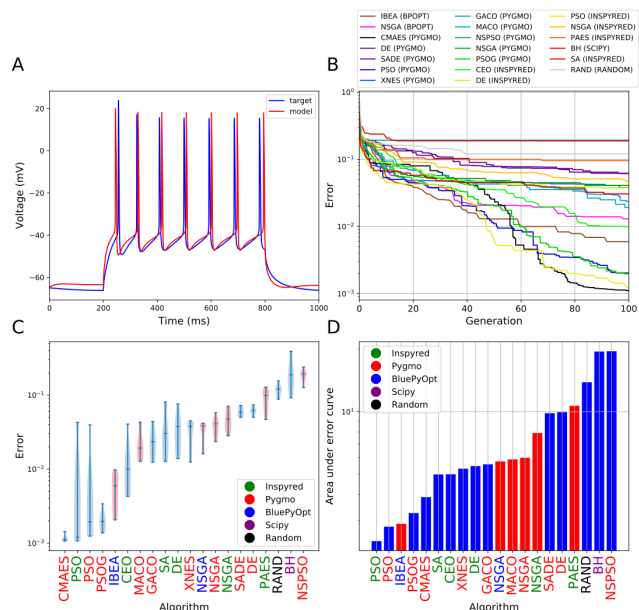


Fig. 1. The results of fitting the conductance parameters of a simple model to voltage traces from a more detailed compartmental model. (A) Comparison of the original (simulated) data (blue) and the trace of the best model found by the algorithm (red). (B) Generation plot showing the median over 10 consecutive runs of the cumulative minimum error for each relevant algorithm. The total number of model runs was 10,000 in each case. Algorithm names are represented in the legend. (C) Violin plot representing the distribution of the best error scores over 10 independent runs of the algorithms. The algorithms are represented on the horizontal axis, and error rates on the vertical axis. The legend shows the color code applied to the algorithm names based on the implementing packages. (D) Comparison of convergence speed based on the area under the median curve of the generation plot. The algorithms are represented on the horizontal axis, and the area under the curves on the vertical axis. The single-objective algorithms are represented by blue bars and the multi-objective ones by red bars.

REFERENCES

- [1] B. J. Vanier M.C., "A comparative survey of automated parameter-search methods for compartmental neural models," 1999.
- [2] D. et al., "Evaluating automated parameter constraining procedures of neuron models by experimental and surrogate data," 2008.
- [3] A. P. Van Geit W. and D. S. E., "Neurofitter: a parameter tuning package for a wide range of electrophysiological neuron models," 2007.

Differentiating the overlapping neural action potentials using deep learning

Obada MUHAMMAD

(Supervisor: István ULBERT)

Pázmány Péter Catholic University, Faculty of Information Technology and Bionics

50/a Práter street, 1083 Budapest, Hungary

muhammad.obada@itk.ppke.hu

Abstract—Recently, techniques for recording extracellular neural activity with High-density neural probes have developed widely allowing to record neural action potentials (spikes) from hundreds of neurons simultaneously. classifying neural spikes of different neurons is problematic, one of the reasons is the overlapping happening among different neurons firing near the electrodes at once. In this research, a new approach is introduced using speech separation techniques with deep learning called permutation invariant training (PIT) in order to solve the overlapping problem.

Keywords-neural activity; action potential; spike sorting; deep learning

I. DISCUSSION

Extracellular neural activity is measured by implementing high-density neural probes with a large number of channels into the brain to record dense data from the neural space. usually, the recorded data of one neuron has huge background noise due to the interference from local neurons in the periphery area of the electrode where they have similar amplitude and shape [1]. In such cases, simple methods such as threshold detection do not work because the overlapped signals have the same amplitude where the neural spikes interfere with each other in the form of a distorted action potential [2], as shown in the Fig. 1. According to [2] the number of neurons detected from the extracellular recordings differs from that which would be expected to be observed based on spatial and anatomical considerations which can lead to recording different neuronal activity in response to different things [2]. One way to understand the firing patterns of neurons is based on detecting and clustering neural action potentials which can be improved using spike sorting algorithms. Spike sorting algorithms face various challenges, such as silent neurons with a low firing rate, electrode drifts during the recording process, which causes changes in the shape of the neuron spike, neuron bursts with rapid succession of action potentials, and overlapping between neural action potentials fired by two neighboring neurons close to the recording electrode [2]. This research aims to find a solution to the problem of overlapping neural spikes, by proposing the idea of using a deep learning algorithm called permutation invariant training (PIT) which is used in the field of speech recognition for multi-speaker separation [3] and adapting it to separate the interference between neural action potentials. to evaluate the model results, a ground truth data and two steps of spike detection algorithm is used before and after the PIT model.

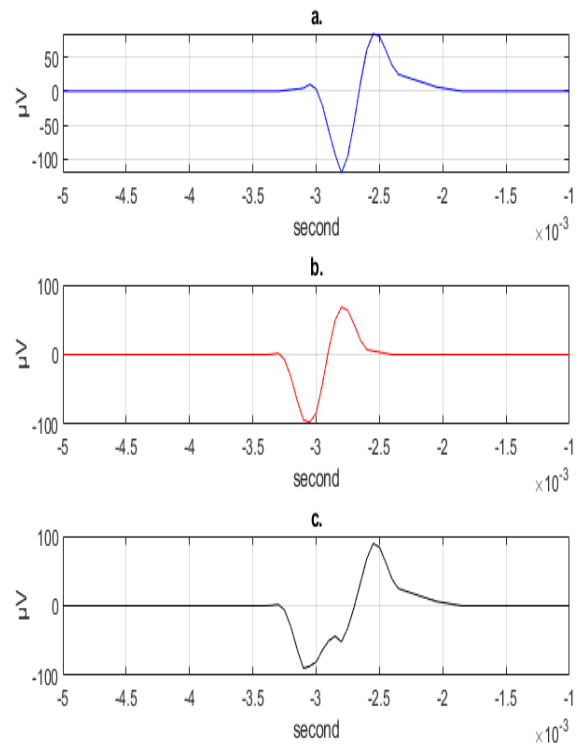


Fig. 1. simulation of two extracellular action potentials. (a) represents a typical action potential of a neuron. (b) represents a neighboring neuron firing an action potential shortly after the last. (c) the overlapping between the two neuron's signals

REFERENCES

- [1] M. S. Lewicki, "A review of methods for spike sorting: the detection and classification of neural action potentials," *Network: Computation in Neural Systems*, vol. 9, no. 4, pp. R53–R78, 1998.
- [2] H. G. Rey, C. Pedreira, and R. Q. Quiroga, "Past, present and future of spike sorting techniques," *Brain research bulletin*, vol. 119, pp. 106–117, 2015.
- [3] D. Yu, M. Kolbæk, Z.-H. Tan, and J. Jensen, "Permutation invariant training of deep models for speaker-independent multi-talker speech separation," in *2017 IEEE International Conference on Acoustics, Speech and Signal Processing (ICASSP)*, pp. 241–245, IEEE, 2017.

Cellular interactions between yeast strains

Bíborka PILLÉR

(Supervisor: Attila CSIKÁSZ-NAGY)

Pázmány Péter Catholic University, Faculty of Information Technology and Bionics

50/a Práter street, 1083 Budapest, Hungary

pillér.biborka@itk.ppke.hu

Abstract—While most laboratory experiments of microbial colony growth are focusing on individual strains, in nature microbial communities consist of many different strains. They grow together in mixed colonies affecting each other, and these arising interactions can influence the fate and the future of a colony. Our goal is to study the interactions between different strains of *Saccharomyces cerevisiae* and to gain a better understanding of the importance of coexisting strains for example in a vineyard.

Keywords—wine yeast strains; yeast growth; fluorescence;

I. INTRODUCTION

Saccharomyces cerevisiae, commonly known as Baker's yeast is an important research and industrial microorganism [1]. It played a role in many discoveries regarding cellular and evolutionary processes.

Interactions between natural strains have been examined previously [2]. The most common interaction that occurs in every microbial colony is the competition for nutrients, but besides these microbes can develop various strategies to survive, like cooperating with each other or producing toxins against each other [3]. Some interactions have already been observed between yeast strains in the 1970s. These experiments mainly included the investigation of the effect of mixed colonies on the fermentation process [4]. They were curious about how the mixture of most strains will improve the flavour of the wine and the yield [4]. They found that some of these strains are able to produce killer toxins against other strains or different microorganisms [5]. This toxin production was proved to be important in fermentation of food and beverages and even in medical research [4]. We would like to extend this knowledge by examining wine yeast strains in a laboratory environment. With the help of a fluorescence based approach we were able to measure the growth of these strains in co-cultures.

II. DISCUSSION

Although growth experiments usually rely on optical density measurements, in our case to differentiate the strains in a co-culture, fluorescence measurements were also required. That is why it was important to label our strains with different fluorescent proteins before starting the co-culture experiments. The transformation of the four wine yeast strains (UVA DA, UVA 228, UVA PM, UVA CM) was successful, which means that we were able to label them with the mCherry and GFP fluorescent proteins.

After the labeling, the initial co-culture experiments could be carried out. To evaluate the results properly non-fluorescent strains were used as controls. The control co-cultures were composed of the non-fluorescent and the fluorescent variants of the same strain. This way in these co-cultures the initial ratio of the strains is maintained so if a competition arises in other co-cultures it can be observed compared to these.

Firstly to test how these wine yeast strains interact with each other in a laboratory setting in a growth medium with 2% glucose concentration, two of them (UVA DA, UVA CM) was chosen for a co-culture experiment, one of them (UVA DA) being a killer toxin producer. The results can be seen on Figure 1.

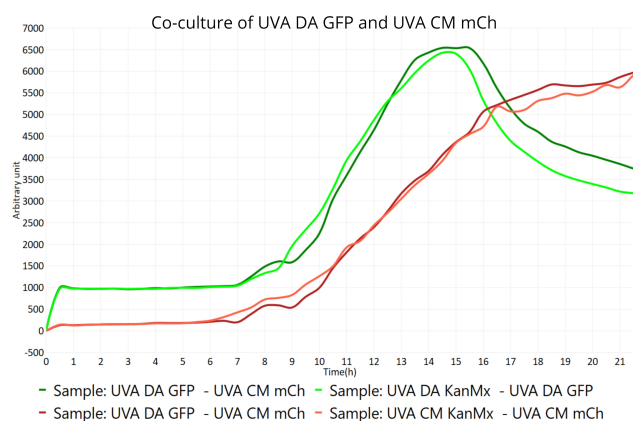


Fig. 1. The growth curves of UVA DA and UVA CM in the mixed cultures. The green curves indicate GFP and the red curves mCherry fluorescence.

Between UVA DA and UVA CM there was no observable interaction, UVA DA did not affect the growth of UVA CM, despite the fact that it is a known toxin producer. However it is not so surprising, because the laboratory environment is very different from the environment during fermentation.

ACKNOWLEDGEMENTS

Experimental work described were carried out together with Nóra Görög

REFERENCES

- [1] M. Cavaliere, S. Feng, O. S. Soyer, and J. I. Jiménez, "Cooperation in microbial communities and their biotechnological applications," *Environmental microbiology*, vol. 19, no. 8, pp. 2949–2963, 2017.
- [2] D. Rivero, L. Berná, I. Stefanini, E. Baruffini, A. Bergerat, A. Csikász-Nagy, C. De Filippo, and D. Cavalieri, "Hsp12p and pau genes are involved in ecological interactions between natural yeast strains," *Environmental microbiology*, vol. 17, no. 8, pp. 3069–3081, 2015.
- [3] J. Friedman and J. Gore, "Ecological systems biology: The dynamics of interacting populations," *Current Opinion in Systems Biology*, vol. 1, pp. 114–121, 2017.
- [4] B. C. Viljoen, "Yeast ecological interactions. yeast'yeast, yeast'bacteria, yeast'fungi interactions and yeasts as biocontrol agents," in *Yeasts in food and beverages*, pp. 83–110, Springer, 2006.
- [5] V. Palpacelli, M. Ciani, and G. Rosini, "Activity of different 'killer' yeasts on strains of yeast species undesirable in the food industry," *FEMS microbiology letters*, vol. 84, no. 1, pp. 75–78, 1991.

Dynamic behaviour of the Shank1 PDZ domain during interaction

Anna SÁNTA

(Supervisor: Zoltán GÁSPÁRI)

Pázmány Péter Catholic University, Faculty of Information Technology and Bionics

50/a Práter street, 1083 Budapest, Hungary

santa.anna@itk.ppke.hu

Abstract—Shank proteins are an important part of the scaffold in the postsynaptic density of glutamatergic synapses, bridging the membrane embedded ion channels with the cytoskeleton through interaction with GKAP. In this study, the PDZ domain of Shank1 was produced in isotope-labelled forms to characterize structural dynamics during binding.

Keywords—postsynaptic density; protein interaction; NMR; PDZ

I. INTRODUCTION

The postsynaptic density (PSD) is a signal processing complex found in glutamatergic synapses. The PSD transduces signals via dynamic rearrangements that affect the morphology of the dendritic spine, with internal mechanisms that are not fully understood to this day. Scaffolding proteins that create the connection between the glutamate receptors and the cytoskeleton have a significant role in ensuring proper functionality of the synapse. [1] [2]

One such scaffold protein is Shank, short for “SH3 and multiple ankyrin repeats domains protein” a family of three proteins possessing the same characteristic domain composition. All of these domains act as protein-protein interaction domains, that allow for elaborate regulation and tethering of other PSD proteins, and the formation of a higher order scaffolding network. [3] Out of these interaction domains, the highly conserved Shank PDZ is remarkable in its promiscuity and the structural flexibility that is allowing it. The C-terminal GH1 domain of GKAP is the main interaction partner of Shank PDZ domains that they bind with much higher affinity, and disordered extradomain segments could play a regulatory role in the interaction. [4]

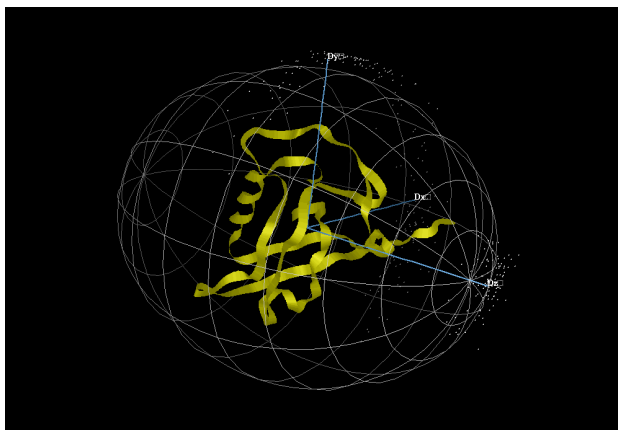


Fig. 1. Visualization of the diffusion tensor of the Shank PDZ as shown in the program Tensor2 [5]

II. MATERIALS AND METHODS

Recombinant protein constructs corresponding to *R. norvegicus* Shank1 PDZ, and GKAP GH1 were produced in *E. coli* and purified using a protocol of subsequent chromatography steps (immobilized metal ion, ion exchange and gel filtration). NMR spectroscopy measurements were carried out on ^{15}N and ^{13}C isotope labelled samples. An NMR titration experiment was carried out utilizing GH1 as ligand.

III. RESULTS

Shank1 PDZ 3D NMR spectra were assigned and based on that, the titration spectra were analyzed. Perturbations in the spectra were noted and compared to those observed in other PDZ domains in literature. The results create the prospects for further experiments on new PDZ constructs.

ACKNOWLEDGEMENTS

The author thanks Gyula Batta for performing the NMR measurements, András Czajlik for NMR spectra expertise, and Zoltán Gáspári and Bálint Péterfia for their guidance and contributions.

REFERENCES

- [1] C. Verpelli, C. Heise, and C. Sala, “Structural and functional organization of the postsynaptic density,” *The Synapse: Structure and Function*, pp. 129–153, 12 2013.
- [2] C. M. Durand, J. Perroy, F. Loll, D. Perrais, L. Fagni, T. Bourgeron, M. Montcouquiol, and N. Sans, “SHANK3 mutations identified in autism lead to modification of dendritic spine morphology via an actin-dependent mechanism,” *Mol. Psychiatry*, vol. 17, pp. 71–84, Jan 2012.
- [3] M. Sheng and E. Kim, “The Shank family of scaffold proteins,” *J. Cell. Sci.*, vol. 113 (Pt 11), pp. 1851–1856, Jun 2000.
- [4] S. K. Ponna, S. Ruskamo, M. Myllykoski, C. Keller, T. M. Boeckers, and P. Kursula, “Structural basis for PDZ domain interactions in the postsynaptic density scaffolding protein Shank3,” *J. Neurochem.*, vol. 145, pp. 449–463, 06 2018.
- [5] P. Dosset, J. C. Hus, M. Blackledge, and D. Marion, “Efficient analysis of macromolecular rotational diffusion from heteronuclear relaxation data,” *Journal of biomolecular NMR*, vol. 16, pp. 23–28, Jan. 2000.

Which optical characteristics make a transparent micro-ECoG suitable for multimodal measurements?

Ágnes SZABÓ

(Supervisor: Zoltán FEKETE)

Pázmány Péter Catholic University, Faculty of Information Technology and Bionics

50/a Práter street, 1083 Budapest, Hungary

szabo.agnes@itk.ppke.hu

Abstract—To understand brain functionality in detail, the usage of multimodal neuroimaging techniques is advantageous. While combining electrophysiological measurement with two-photon microscopy high spatial and temporal resolution can be achieved, the material choice of the used device is crucial. Our research investigates the optical characteristics of a suitable candidate.

Keywords-microECoG; two-photon microscopy; optical characterization

I. INTRODUCTION

Electrocorticogram (ECoG) can record cortical activities with high temporal resolution while the non-invasive two-photon microscopy can detect the Ca^{2+} signals of the neurons with high spatial resolution. Combining the two imaging techniques can make it possible to find the anatomical and functional connectivity of the neurons. The material of the ECoG device is crucial not only in view of transparency but also to mitigate the immune response and provide long-term stability. A previous study presented the material combination and the detailed micromachining scheme of the recommended electrode array [1]. The multimodal measurement's experimental design used in our design was also tested and presented previously [2].

II. MATERIALS AND METHODS

The multimodal measurements are performed by a soft, thiolene-acrylate based transparent microECoG device that allows cortical signal recording and a two-photon microscope that records Ca^{2+} signals. To investigate the optical characteristics of our microECoG in vitro and in vivo experiments were performed. The long-term measurements originate from head-fixed mice. Ca^{2+} signal imaging was repeated after 9 weeks or for the other subject 8 and further 13 weeks. The image processing was performed by a custom-made Matlab program. The investigated information from the two-photon microscope images is the observed object sizes with and without our device in the light path. This size measurement was repeated in the presence of fluorescent microbead, cell body and neurites, originated from brain slices.

III. DISCUSSION

During this project, our goal is to investigate the optical distortion of Ca^{2+} signal images in the presence of a thiolene-acrylate based transparent microECoG device. Multiple images were captured from fluorescent microbeads and in vitro brain slices. The long-term stability of imaging was also examined, and we found that our proposed device makes possible two-photon imaging even after 21 weeks of implantation.

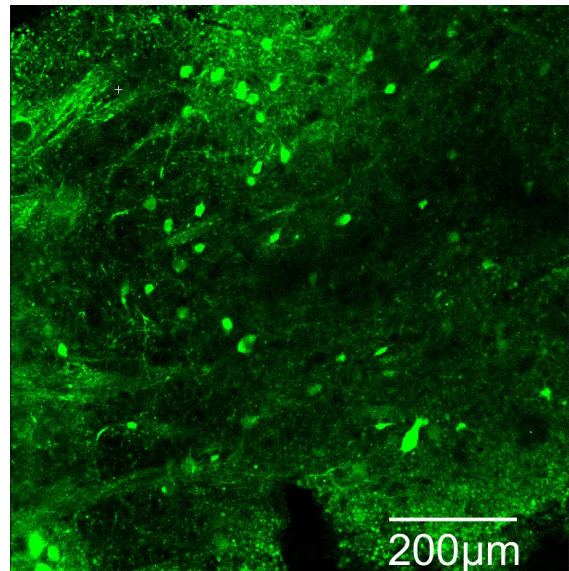


Fig. 1. Representative in vitro Ca^{2+} image captured with the microECoG in the light path.

ACKNOWLEDGEMENTS

This research was supported by the ÚNKP-20-3 New National Excellence Program Of The Ministry For Innovation And Technology From The Source Of The National Research, Development And Innovation Fund.

REFERENCES

- [1] Zátónyi, A., Orbán, G., Modi, R., Márton, G., Meszéna, D., Ulbert, I., Pongrácz, A., Ecker, M., Voit, W.E., Joshi-Imre, A., Fekete, Z., *A softening laminar electrode for recording single unit activity from the rat hippocampus.*, Scientific reports, 9(1), 1-13, 2019.
- [2] Zátónyi, A., Madarász, M., Szabó, Á., Lőrincz, T., Hodován, R., Rózsa, B., Fekete, Z., *Transparent, low-autofluorescence microECoG device for simultaneous Ca^{2+} imaging and cortical electrophysiology in vivo.*, Journal of neural engineering, 17(1), 016062. 2020.

Investigation of the role of specific sequence motifs in protein phase separation

András SZABÓ

(Supervisor: Zoltán GÁSPÁRI)

Pázmány Péter Catholic University, Faculty of Information Technology and Bionics

50/a Práter street, 1083 Budapest, Hungary

szabo.andras.laszlo@itk.ppke.hu

Abstract—Protein phase separation is a major governing factor in various cellular processes, contributing to the formation of membrane-less organelles and is pivotal in the proper function of postsynaptic densities. This study aims to examine the possible correlations between the phenomenon of phase separation and certain protein sequence motifs such as single α -helices.

Keywords—protein phase separation; single α -helices; charge-dense regions

I. INTRODUCTION

Advancements in our knowledge of the central nervous system constitutes one of the most intensely researched fields of science today. However, further steps require a profound understanding of the mechanism of synaptic plasticity, for which the postsynaptic density (PSD) provides a stage, thus contributing to the molecular processes of learning and memory. In recent years, an ever-increasing number of experiments showed that protein phase separation plays a major role in various cellular processes such as the organisation of the PSD. Multivalent interactions between PSD proteins are crucial for the dynamic changes that take place within this network, primarily influencing them through the formation of membrane-less organelles (MLOs). [1] Since RNA-binding proteins exhibit an above average affinity towards phase separation, specifically liquid-liquid phase separation (LLPS), as well as an abundance of special regions with repetitive patterns of charged residues such as single α -helices (SAHs), it seems plausible that the two traits correlate.

II. METHODS

The FT-CHARGE algorithm of the CSAH webserver proved to be a useful tool for the recognition of SAHs, while several online databases provided insight into the LLPS-relation of human proteins. Correlation between the above-mentioned attributes were examined via Fisher's exact test of independence. [2], [3]

III. RESULTS

A high through-put approach was developed for the recognition of specific sequence motifs, and together with the FT-CHARGE algorithm their plausible contribution to LLPS was analysed.

REFERENCES

- [1] Z. Feng, X. Chen, M. Zeng, and M. Zhang, "Phase separation as a mechanism for assembling dynamic postsynaptic density signalling complexes," *Current Opinion in Neurobiology*, vol. 57, pp. 1–8, Aug. 2019.
- [2] Z. Gáspári, D. Süveges, A. Perczel, L. Nyitray, and G. Tóth, "Charged single alpha-helices in proteomes revealed by a consensus prediction approach," *Biochimica Et Biophysica Acta*, vol. 1824, pp. 637–646, Apr. 2012.

A. SZABÓ, "Investigation of the role of specific sequence motifs in protein phase separation" in *PhD Proceedings – Annual Issues of the Doctoral School, Faculty of Information Technology and Bionics, Pázmány Péter Catholic University – 2021*. G. Prószéky, G. Szederkényi Eds. Budapest: Pázmány University ePress, 2021, p. 33. This research has been partially supported by the European Union, co-financed by the European Social Fund (EFOP-3.6.3-VEKOP-16-2017-00002).

```
magvsvfsghrlellaayeevireesa  
adwalytyedgssddlklaasgegglq  
elsghfenqkvmygfcsvkdsqaalp  
kyvlinwvgedvdpdarkcacashvak  
vaeffqgvdivvnassvedidagaig  
qrlsnglarlsspvhlrlrlredena  
epvgttyqktdaavemKRINREQFWE  
QAKKEEELRKEEERKKALDERLRFEQ  
ERMEQERQEQEERERRREREQQIEE  
HRRKQQTLEAEEAKRRLkeqsifgdh  
rdeeeethmkkseveveeaaiaaqr  
pdnpreffkqgervasasagscdvps  
pfnhrpgshldshrrmaptptpitrsp  
sdsstastpvaeqieraldevtssqp  
pplppppppaquetqepspildseetr  
aaapqawagpmeppqaqapprgpgs  
paedlmfmesaeqavlaapvepatad  
ateihdaadtietdtatadtvtannv  
ppaatslidlwpnggegastlqgepr  
aptppsgtevtlaevplldevapepl  
lpagegcatllnfdelpeppatfcdp  
eevegeslaapqtptlpsaleelege  
qepephlltngettqkegtqasegyf  
sqsqeeefaqseelcakappvvfyнк  
ppeiditc wdadpvpeeeegfeggd
```

Fig. 1. Predicted SAH in the human actin cytoskeleton-organising protein Drebrin.

- [3] K. You, Q. Huang, C. Yu, B. Shen, C. Sevilla, M. Shi, H. Hermjakob, Y. Chen, and T. Li, "PhaSepDB: a database of liquid-liquid phase separation related proteins," *Nucleic Acids Research*, vol. 48, pp. D354–D359, Jan. 2020.

Multimodal prediction of Alzheimer’s disease

János SZALMA

(Supervisor: Béla WEISS)

Pázmány Péter Catholic University, Faculty of Information Technology and Bionics

50/a Práter street, 1083 Budapest, Hungary

szalma.janos@itk.ppke.hu

Abstract—Alzheimer’s disease (AD), the most common form of dementia is affecting 44 million people worldwide. Early prediction and suitable intervention could delay the onset of the disease and improve the quality of life of people affected by it. We utilized the multimodal TADPOLE challenge dataset consisting of patients with normal cognition, mild cognitive impairment and AD. To assess which machine learning models would be the most suitable in predicting disease status, we considered three different classifiers. All three models were evaluated using a 10-fold stratified cross-validation with the hyperparameters optimized for each fold’s training set. While the highest classification accuracy of 80 % was achieved by the Random Forest, the features that were most important for the prediction were neurocognitive tests and the baseline diagnosis.

I. INTRODUCTION

Alzheimer’s disease (AD) is a neurodegenerative disease, the most common form of dementia, affecting 44 million people [1]. The heterogeneity of AD and related dementias makes these diseases difficult to diagnose, manage, and treat, leading to better methods to forecast and monitor disease progression and to improve the drug design and clinical trial development.

II. MATERIALS AND METHODS

We utilized the TADPOLE challenge [2] dataset (part of the ADNI database) consisting of 1667 patients, 517 with normal cognition (NC), 934 with mild cognitive impairment (MCI) and 217 with Alzheimer’s disease (AD). Only features that were available at the baseline measurement for at least 20 % of subjects were included and the missing values were imputed using the feature median. These were: basic clinical and demographic data (age, gender, education level), neurocognitive tests, APOE4 gene, amyloid and tau levels, brain region of interest (ROI) -level volume, surface and thickness measures (based on structural MRI) and also ROI based FDG-PET and amyloid PET activity. As the target variable for prediction, the diagnosis of the last available time-point was used for each subject. This meant a 3 year prediction into the future on average. The amount of time passed between the baseline and last diagnosis was also included as a feature.

To predict future diagnosis three classifiers were considered: Logistic Regression (LR), Radial Basic Function Support Vector Machine (RBF SVM) and Random Forest (RF). To avoid overfitting and make comparison fair model hyperparameters for all classifiers were optimized using a Tree-structured Parzen Estimation. The data standardization, hyperparameter optimization and classification pipeline was implemented using nested 10-fold stratified cross-validation, while the hyperparameters were evaluated with an inner 5-fold stratified cross-validation for each of the outer 10 fold’s training sets.

III. RESULTS AND DISCUSSION

In this study we have shown that Alzheimer’s prediction can be achieved with a high accuracy. Figure 1 shows that this increase was most prominent in the case of LR, where classification accuracy was improved by 5 % after hyperparameter optimization and the least prominent in the case of RF where the increase in accuracy was 1.5 %. In the case of RBF SVM the classification accuracy increased by 4 % after the optimization. Figure 1 also shows that out of the three models LR achieved the lowest accuracy (74.9 %), followed by RBF SVM (77.1 %) and the RF proved to be the most predictive classifier both with (80 %) and without (78.5 %) hyperparameter optimization.

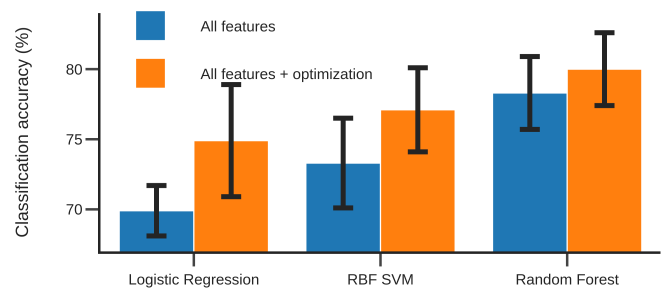


Fig. 1. Classification accuracy of all three classifiers with and without hyperparameter optimization. The error bars represent the standard deviation of the accuracy across the 10 folds

To assess what features were the most important we looked at features with the highest feature importance for the best performing RF model. While most of these were neurocognitive tests, the baseline diagnosis, time passed, average FDG-PET activity and hippocampus volume were predictive as well.

Although these results are promising as the TADPOLE challenge participants achieved similar classification accuracies [1] the prediction pipeline could be further improved by more complex imputation methods and feature selection. Also, besides the prediction of the diagnosis, neurocognitive test scores or brain atrophy could be predicted allowing disease progression modelling.

REFERENCES

- [1] Castellani, R. J., Rolston, R. K., and Smith, M. A. (2010). Alzheimer disease. *Disease-a-month*: DM, 56(9), 484.
- [2] Marinescu, R. V., Oxtoby, N. P., Young, A. L., Bron, E. E., Toga, A. W., Weiner, M. W., ... and Alexander, D. C. (2018). TADPOLE challenge: Prediction of longitudinal evolution in Alzheimer’s disease. arXiv preprint arXiv:1805.03909.

Modelling calcium channels in hippocampal pyramidal neurons

Luca TAR

(Supervisor: Szabolcs KÁLLI, Tamás FREUND)

Pázmány Péter Catholic University, Faculty of Information Technology and Bionics

50/a Práter street, 1083 Budapest, Hungary

tar.luca@itk.ppke.hu

Keywords-hippocampus; pyramidal cell; basket cell

I. SUMMARY

Getting the channel models right in an anatomically and biophysically detailed cell model is the key to get the right behavior in the soma and the dendritic arbor as well. To have a channel kinetics that fit the experimental data better. There are two different methods to describe the kinetics of ion channels. For most of our ion channel models we used the Hodgkin-Huxley equation, where the current through and ion channel model can be described as the following:

$$I = m * h * gmax * (v - e)$$

where m and h are sigmoids fitted to the activation and inactivation of the given channel as the function of voltage, $gmax$ is the maximal conductance of the channel, v is the voltage and e is the reversal potential of the ion. However for calcium channels the Goldman-Hodgkin-Katz flux equation gives better fit to the experimental results. With that equation the current takes shape as the following:

$$I = m * h * pbar * ghk(v, cai, cao)$$

where the ghk function for a calcium channel is:

$$z = (1e^{-3}) * 2 * F * v / (R * (celsius + 273.15))$$

$$ecao = cao * (z) / (\exp(z) - 1)$$

$$ecai = cai * (-z) / (\exp(-z) - 1)$$

$$ghk = (1e^{-3}) * 2 * F * (ecai - eco)$$

where F is the Faraday constant, R is the gas constant, cai is the calcium concentration inside the cell and cao is the calcium concentration outside the cell, and $pbar$ is the permeability of the channel.[1] In our parameter optimization process we tuned the $gmax$ parameter, which now changed to $pbar$, so we needed to calculate the $gmax$ - $pbar$ change to the current remains the same.

I also implemented five new ion channels to our cell model. The small-conductance calcium dependent potassium channel (SK-channel), which is present in the soma and the perisomatic dendrites. The maximum conductance of these channels are linearly decreasing if we go further from the soma on the dendritic arbor. SK channels are also present in the spineheads [2], there it is not linked to the L-type calcium channels, because it's still a debate whether they are present in the spine or not, but the current coming through the L-type calcium channel is not add to the calcium current in the spines.

The R-type calcium channels, that are exclusively present on dendritic spines and they have a huge role in shaping the EPSP and EPSC in the spine heads during synaptic stimulation.[3] One spine-head can contains 5-15 channel [4]

Last but not least, three different isoforms of the T-type calcium channel. They all have slightly different kinetics and distributed differently along the dendritic arbor, so instead of

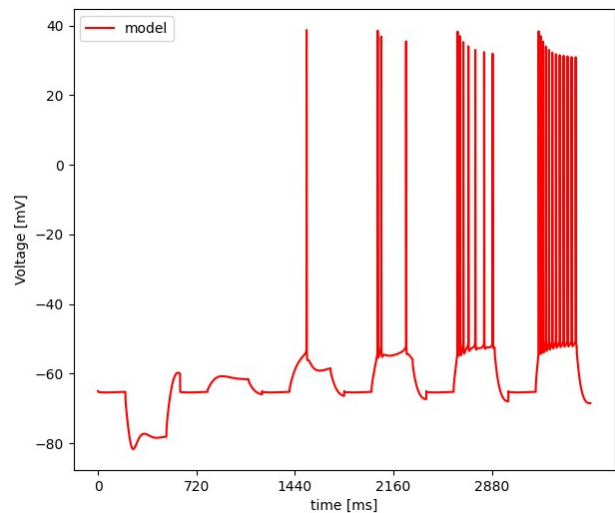


Fig. 1. The initial optimization result with all the ion-channels present in the model. Each trace are the result of a current step for -0.25, 0.05, 0.1, 0.15, 0.2 and 0.25 nA. The fitness of the result is 2.7, which is acceptable with Evolutionary Algorithm. It can be seen that the Ih, which is responsible for the sag at -0.25 nA need to be improved further.

just one T-type calcium channel model, we decided to include all three different channel models.[5] I had channel models of Cav3.2 and Cav3.3 from Lindroos et al. [6], and I created the Cav3.1 channel model based on them and the experimental data from Iftinca et al.[5]

REFERENCES

- [1] B. Hille, *Ion Channels of Excitable Membranes*. Sunderland, Massachusetts, USA: Sinauer Associates, Inc., 2001.
- [2] L. R. W. M. e. a. Lin, M., "SK2 channel plasticity contributes to ltp at schaffer collateral-cal synapses," *Nature Neuroscience*, vol. 11, pp. 170–177, 2008.
- [3] B. L. Bloodgood and B. L. Sabatini, "Nonlinear regulation of unitary synaptic signals by cav2.3 voltage-sensitive calcium channels located in dendritic spines," *Neuron*, vol. 53, no. 2, pp. 249–260, 2007. [Online]. Available: <https://www.sciencedirect.com/science/article/pii/S0896627306010221>
- [4] S. B. . S. K. Yasuda, R., "Plasticity of calcium channels in dendritic spines," *Nature Neuroscience*, vol. 6, pp. 948–955, 2003. [Online]. Available: <https://www.nature.com/articles/nn1112>
- [5] M. Iftinca, B. McKay, T. Snutch, J. McRory, R. Turner, and G. Zamponi, "Temperature dependence of t-type calcium channel gating," *Neuroscience*, vol. 142, no. 4, pp. 1031–1042, 2006. [Online]. Available: <https://www.sciencedirect.com/science/article/pii/S0306452206009821>
- [6] R. Lindroos, M. C. Dorst, K. Du, M. Filipović, D. Keller, M. Ketzef, A. K. Kozlov, A. Kumar, M. Lindahl, A. G. Nair, J. Pérez-Fernández, S. Grillner, G. Silberberg, and J. Hellgren Kotaleski, "Basal ganglia neuromodulation over multiple temporal and structural scales—simulations of direct pathway msnns investigate the fast onset of dopaminergic effects and predict the role of kv4.2," *Frontiers in Neural Circuits*, vol. 12, p. 3, 2018. [Online]. Available: <https://www.frontiersin.org/article/10.3389/fncir.2018.00003>

Fetal breathing movements and fetal heart sounds in single channel phonocardiographic signals

Bálint Áron ÜVEGES

(Supervisor: Ferenc KOVÁCS)

Pázmány Péter Catholic University, Faculty of Information Technology and Bionics

50/a Práter street, 1083 Budapest, Hungary

uveges.balint.aron@itk.ppke.hu

Abstract—Fetal phonocardiography is a non-invasive and passive measurement method to monitor the fetus’ physiological activity by collecting acoustic signals from the mother’s abdomen with a special acoustic sensor, called phonocardiograph. While the initial application of fetal phonocardiography aimed to measure the fetus’ heart rate and heart related phenomena, in recent years the application has been expanded to cover the measurement of fetal breathing movements. Based on the analysis of fetal phonocardiographic breathing movement measurements, our results suggest the feasibility of measuring fetal heart rate and fetal breathing movements from the same phonocardiographic signal within the same temporal section.

Keywords—Phonocardiography; Fetal Heart Rate, Fetal Breathing Movement; Biomedical Signal Processing; Velocity Synchronous Linear Chirplet Transform; General Parameterized Time-Frequency Transform

I. SUMMARY

In recent years research related to fetal breathing movement (FBM) in phonocardiographic signals accelerated. Goda and Kovács reported that it is possible to detect FBMs in fetal phonocardiographic signals and provided a corresponding heuristic method for FBM detection [1]. During the fourth quarter of 2017 a measurement series was implemented to collect phonocardiographic data covering fetal breathing movements. While the recordings were thoroughly investigated from FBM point of view [2], other detectable fetal physiological phenomena were not evaluated.

In our work the measurement series’ data was evaluated from fetal heart sound (FHS) and fetal heart rate (FHR) point of view. The evaluation was performed in two phases: in the first phase each phonocardiographic recording had been analysed and ranked according to the presence of FHS, while in the second phase FHR was calculated and FBM episodes were identified in the candidate recordings.

During the first phase each recording’s waveform and time-frequency representation (TFR) was evaluated. TFR was calculated with Velocity Synchronous Linear Chirplet Transform (VSLCT) [3] and General Parameterized Time-Frequency Transform’s Spline Chirplet Transform (GPTF-SCT) [4]. By analysing each signal’s waveform and TFR simultaneously, it was possible to identify both FHS and FBM in several recordings. Additionally, it was possible to retrieve S_1 and S_2 FHS components, and FBM signals from the same temporal section, as shown in Fig. 1.

During the second phase of the evaluation, for every phonocardiographic recording containing both FHS and FBM, the FHR graph and the FBM episodes were calculated. It was possible to retrieve the FHR and FBM episodes from the same temporal section of a single channel phonocardiographic signal, as shown in Fig. 2.

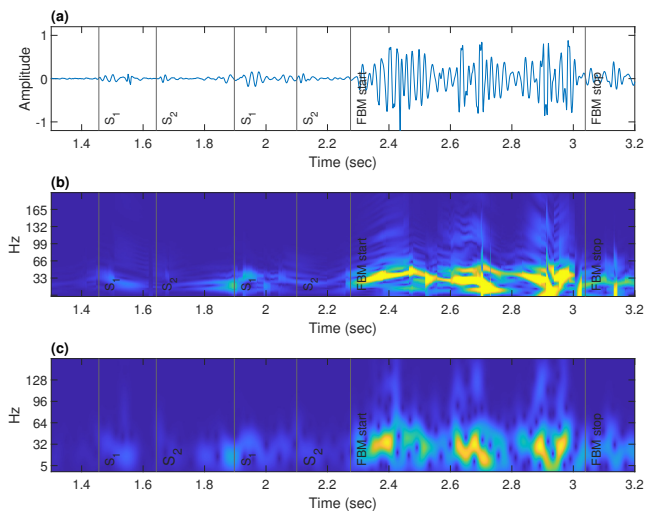


Fig. 1. FHS and FBM analysis - Filtered signal’s waveform (a), VSLCT (b) and GPTF-SCT TFR (c)

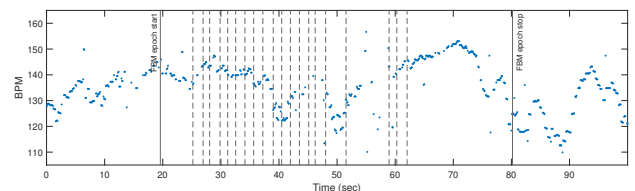


Fig. 2. FHR graph with FBMs (marked with dashed vertical line)

ACKNOWLEDGEMENTS

Bálint Áron Üveges would like to express his gratitude towards Márton Áron Goda for his support with regards to FBM, and towards Dr. Ferenc Kovács for his persevering support.

REFERENCES

- [1] F. Kovacs, M. A. Goda, G. Hosszu, and T. Telek, “A proposed phonography-based measurement of fetal breathing movement using segmented structures with frequency splitting,” in *2020 42nd Annual International Conference of the IEEE Engineering in Medicine Biology Society (EMBC)*, pp. 4483–4486, 2020.
- [2] M. A. Goda, T. Telek, and F. Kovacs, “Novel phonography-based measurement for fetal breathing movement in the third trimester,” *Sensors*, vol. 21, no. 1, 2021.
- [3] Y. Guan, M. Liang, and D. Neculescu, “Velocity synchronous linear chirplet transform,” *IEEE Transactions on Industrial Electronics*, vol. 66, pp. 6270–6280, Aug 2019.
- [4] Y. Yang, Z. K. Peng, X. J. Dong, W. M. Zhang, and G. Meng, “General parameterized time-frequency transform,” *IEEE Transactions on Signal Processing*, vol. 62, no. 11, pp. 2751–2764, 2014.

Characterization of age-related neurodegenerative disease models in transgenic animals

Zsófia VARGA-MEDVECZKY

(Supervisor: Franciska ERDŐ)

Pázmány Péter Catholic University, Faculty of Information Technology and Bionics

50/a Práter street, 1083 Budapest, Hungary

varga-medveczky.zsobia@itk.ppke.hu

Abstract—This work tries to shed light on the link between vascular problems caused by chronic hyperlipidemia and neurodegeneration using ApoB-100 transgenic mice [1]–[5]. Another transgenic mouse line, APP-PSEN1 is also investigated, which are a validated model of Alzheimer’s disease [5], [6]. The focus is on the characterization of these disease models by the investigation of the structural and functional changes of the blood-brain barrier using microdialysis, and the up- or downregulated levels of different cytokines using enzyme-linked immunosorbent assay. Besides these experiments, MRI scans were acquired to examine the anatomical changes of the affected brain areas.

Keywords—nasal delivery route, microdialysis, aging, hyperlipidemia, Alzheimer’s disease, vascular dementia, neurodegeneration

I. INTRODUCTION

There is a growing research interest in finding the relationship between vascular and neurodegenerative diseases [1]–[5], which are commonly age-related [4], [7], [8]. Based on several studies it can be concluded that impairment of the blood-brain barrier and the neurovascular unit is associated with neurodegeneration [7]–[9].

Pharmacological treatment of various neurodegenerative diseases is very difficult, as successful therapeutic treatment is hampered by the delivery of different drugs across the blood-brain barrier [7]–[10]. However, intranasal drug delivery may be a proper solution for this problem, because in contrast to oral administration, it allows rapid absorption of drugs from the nasal cavity through the trigeminal and olfactory pathways, which can successfully bypass the blood-brain barrier [10].

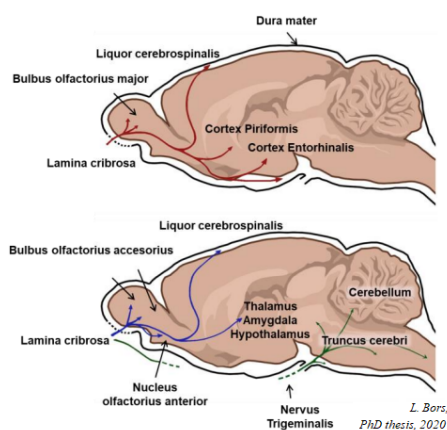


Fig. 1. Demonstration of the intranasal absorption routes

There is an increasing amount of evidence that hyperlipidemia can be associated not only with cardio- and cerebrovascular problems but also with neurodegeneration [1], [2], [4],

[5], however the relationship and the full mechanism are not yet fully understood [1], [2]. One of the main features of neurodegenerative diseases is pathological changes in the cerebrovascular network [2], [11], [12]. Several animal models are available, which were generated with elevated serum lipid levels [1]–[5]. Examining these animal models, could lead to a better understanding of the relationship between vascular diseases and neurodegeneration [1], [2], [4].

REFERENCES

- [1] Z. Hoyk, M. E. Tóth, N. Lénárt, D. Nagy, B. Dukay, A. Csefová, g. Zvara, G. Seprényi, A. Kincses, F. R. Walter, S. Veszeka, J. Vigh, B. Barabási, A. Harazin, g. Kittel, L. G. Puskás, B. Penke, L. Vigh, M. A. Deli, and M. Sántha, “Cerebrovascular Pathology in Hypertriglyceridemic APOB-100 Transgenic Mice,” *Frontiers in Cellular Neuroscience*, vol. 12, p. 380, 2018.
- [2] M. E. Tóth, B. Dukay, Z. Hoyk, and M. Sántha, “Cerebrovascular Changes and Neurodegeneration Related to Hyperlipidemia: Characteristics of the Human ApoB-100 Transgenic Mice,” *Current Pharmaceutical Design*, vol. 26, no. 13, pp. 1486–1494, 2020.
- [3] A. Bjelick, E. Bereczki, S. Gonda, A. Juhász, A. Rimanóczy, M. Zana, T. Csont, M. Pákáski, K. Boda, P. Ferdinandy, L. Dux, Z. Janka, M. Sántha, and J. Kálmán, “Human apoB overexpression and a high-cholesterol diet differently modify the brain APP metabolism in the transgenic mouse model of atherosclerosis,” *Neurochemistry International*, vol. 49, pp. 393–400, Sept. 2006.
- [4] N. Lénárt, V. Szegedi, G. Juhász, A. Kasztner, J. Horváth, E. Bereczki, M. E. Tóth, B. Penke, and M. Sántha, “Increased tau phosphorylation and impaired presynaptic function in hypertriglyceridemic ApoB-100 transgenic mice,” *PLoS One*, vol. 7, no. 9, p. e46007, 2012.
- [5] E. Bereczki, G. Bernát, T. Csont, P. Ferdinandy, H. Scheich, and M. Sántha, “Overexpression of human apolipoprotein B-100 induces severe neurodegeneration in transgenic mice,” *Journal of Proteome Research*, vol. 7, pp. 2246–2252, June 2008.
- [6] M. E. Tóth, V. Szegedi, E. Varga, G. Juhász, J. Horváth, E. Borbély, B. Csibrányi, R. Alföldi, N. Lénárt, B. Penke, and M. Sántha, “Overexpression of Hsp27 ameliorates symptoms of Alzheimer’s disease in APP/PS1 mice,” *Cell Stress & Chaperones*, vol. 18, pp. 759–771, Nov. 2013.
- [7] F. Erdő, L. Denes, and E. de Lange, “Age-associated physiological and pathological changes at the blood-brain barrier: A review,” *Journal of Cerebral Blood Flow and Metabolism: Official Journal of the International Society of Cerebral Blood Flow and Metabolism*, vol. 37, pp. 4–24, Jan. 2017.
- [8] F. Erdő and P. Krajcsi, “Age-Related Functional and Expressional Changes in Efflux Pathways at the Blood-Brain Barrier,” *Frontiers in Aging Neuroscience*, vol. 11, p. 196, 2019.
- [9] B. Obermeier, R. Daneman, and R. M. Ransohoff, “Development, maintenance and disruption of the blood-brain barrier,” *Nature Medicine*, vol. 19, pp. 1584–1596, Dec. 2013.
- [10] F. Erdő, L. A. Bors, D. Farkas, g. Bajza, and S. Gizurarson, “Evaluation of intranasal delivery route of drug administration for brain targeting,” *Brain Research Bulletin*, vol. 143, pp. 155–170, Oct. 2018.
- [11] B. V. Zlokovic, “The blood-brain barrier in health and chronic neurodegenerative disorders,” *Neuron*, vol. 57, pp. 178–201, Jan. 2008.
- [12] Z. Zhao, A. R. Nelson, C. Betsholtz, and B. V. Zlokovic, “Establishment and Dysfunction of the Blood-Brain Barrier,” *Cell*, vol. 163, pp. 1064–1078, Nov. 2015.

Investigating the use of deep learning for EEG motor imagery signals classification

Moutz WAHDOW

(Supervisor: István ULBERT)

Pázmány Péter Catholic University, Faculty of Information Technology and Bionics

50/a Práter street, 1083 Budapest, Hungary

wahdow.moutz@itk.ppke.hu

Abstract—Brain Computer Interfaces (BCIs) offer new means of communication for those with severe neuromuscular disorders or paralysis. The electroencephalogram (EEG) signal is a medium to realize BCI systems whether evoked ones like the P300 or spontaneous for Motor Imagery (MI) due to the non-invasive nature of data acquisition, low cost of fabrication, and a high degree of mobility and portability. EEG based Somatosensory (SMR) BCI Technology has bridged a direct communication pathway between the brain and computer, aiming to replace, restore, enhance, or improve the natural Central Nervous System (CNS) output to enable the disabled and improve life quality. The problem however still in the reliability and robustness of these systems due to the huge dimensionality, variability, and sensibility of the input EEG signal. Therefore, research for an optimum design for multiple applications is still ongoing and will be for a long time ahead. Deep Learning (DL) techniques, such as Convolutional Neural Networks (CNNs), have been investigated by many researchers in the field as a possible method to implement MI BCI. In this work different types of Neural Networks are applied to the datasets Physionet and BCI Competition IV-2a. The simple pipeline which converts the 1D EEG data to a 2D representation input for the Neural network, making it into a video classification problem. The average accuracy obtained is 60 percent for 5 classes which is a valid proof of concept yet it does not compete with some results obtained from literature that doesn't provide code or data sets, but the code we present is available under open source licence and can be further enhanced.

Keywords—Electroencephalogram (EEG); Brain Computer Interfaces (BCIs); Convolutional Neural Networks (CNNs).

I. INTRODUCTION

Brain-Computer Interface (BCI) is a field of research that deals with and covers a variety of advanced methods aiming to detect and decode the brain's intention and thoughts. BCI is defined as a system that measures Central Nervous System (CNS) activity and converts it into an artificial output that replaces, restores, supplements, or improves natural CNS output and thereby changes the ongoing interactions between the CNS and its external or internal environment. It is the science and technology of devices and systems responding to neural processes in the brain that generate motor movements and cognitive processes [1]. Advances in sensor technology, neuroscience, computational tools and methods, component miniaturization, and biocompatibility of materials have led to much-improved feasibility of useful BCIs that can target huge populations of which patients who suffer from stroke, paraplegia, Locked-in syndrome (LIS), amyotrophic lateral sclerosis (ALS), cerebral palsy, amputation, or trauma and more benefits may be harnessed for non-medical applications as well [2].

Electroencephalogram (EEG) is one of the most popular and promising approaches in BCI [3]. Even though it has low spatial resolution; its zero clinical risk, high temporal

resolution, increased mobility and low cost makes it favoured among researchers [4]. The two main categories of EEG based BCIs are Active and Reactive BCIs based on presenting an external stimuli or not (evoked and spontaneous). Event-related potentials (ERPs), Steady state visual evoked potentials (SSVEPs), Slow cortical potentials (SCPs) and sensorimotor rhythms (SMR). Out of these potentials, SMR based BCI which is also called Motor Imagery provides high degrees of freedom in association with both imagined and real movements of hands, arms, feet and tongue [5] [6]. The neural oscillations associated with Sensorimotor rhythms are 8–12Hz (μ) and 18–26Hz (beta) oscillations in the EEG recorded over sensorimotor cortices. When executing imagined or real movement, it causes an increase or decrease of the signal amplitude, hence the names event-related synchronization (ERS) and event-related desynchronization (ERD) [7] [8].

A BCI system design loop consists of five main processes: Signal acquisition through conductive electrodes applied at the scalp of user, Signal processing to remove noise and artifacts, Feature extraction via time/frequency analysis, Signal classification and feedback. Therefore a major challenge is for BCI systems to correctly and efficiently identify different EEG signals for different MI tasks using appropriate classification algorithms. And also one major problem has become apparent that BCIs do not work for all users [9].

REFERENCES

- [1] J. Wolpaw and E. W. Wolpaw, *Brain-computer interfaces: principles and practice*. OUP USA, 2012.
- [2] N. Shajil, S. Mohan, P. Srinivasan, J. Arivudaiyanambi, and A. A. Murguesan, "Multiclass classification of spatially filtered motor imagery eeg signals using convolutional neural network for bci based applications," *Journal of Medical and Biological Engineering*, vol. 40, no. 5, pp. 663–672, 2020.
- [3] N. Mammone, C. Ieracitano, and F. C. Morabito, "A deep cnn approach to decode motor preparation of upper limbs from time–frequency maps of eeg signals at source level," *Neural Networks*, vol. 124, pp. 357–372, 2020.
- [4] D. H. Krishna, I. Pasha, and T. S. Savithri, "Classification of eeg motor imagery multi class signals based on cross correlation," *Procedia Computer Science*, vol. 85, pp. 490–495, 2016.
- [5] X. Zhang, L. Yao, X. Wang, J. Monaghan, D. Mcalpine, and Y. Zhang, "A survey on deep learning based brain computer interface: Recent advances and new frontiers," *arXiv preprint arXiv:1905.04149*, 2019.
- [6] B. He, B. Baxter, B. J. Edelman, C. C. Cline, and W. Y. Wenjing, "Noninvasive brain-computer interfaces based on sensorimotor rhythms," *Proceedings of the IEEE*, vol. 103, no. 6, pp. 907–925, 2015.
- [7] G. Pfurtscheller and C. Neuper, "Motor imagery and direct brain-computer communication," *Proceedings of the IEEE*, vol. 89, no. 7, pp. 1123–1134, 2001.
- [8] H. Dose, J. S. Møller, S. Puthusserypady, and H. K. Iversen, "A deep learning mi-eeg classification model for bcis." in *EUSIPCO*, 2018, pp. 1676–1679.
- [9] B. Z. Allison and C. Neuper, "Could anyone use a bci?" in *Brain-computer interfaces*. Springer, 2010, pp. 35–54.

PROGRAM 2

COMPUTER TECHNOLOGY BASED ON MANY-CORE PROCESSOR CHIPS, VIRTUAL CELLULAR COMPUTERS, SENSORY AND MOTORIC ANALOG COMPUTERS

Head: Péter SZOLGAY

Construction of unmanned aerial vehicles applying INS/GPS navigation

Nawar AL-HEMEARY

(Supervisors: Gábor SZEDERKÉNYI, György CSEREY)

Pázmány Péter Catholic University, Faculty of Information Technology and Bionics

50/a Práter street, 1083 Budapest, Hungary

al.hemeary@itk.pke.hu

In the last decades, the development of studies about the usage of navigation systems autopilots for airborne in the field of geographic referenced has been noticeable. Coupling GPS and INS can provide accurate positioning and geo-referencing parameters for dynamic platforms, such as location, velocity, and attitude.

GPS provides continuous positioning and timing information anywhere in the world under any weather conditions. Due to inherent drawbacks via the possibility of dropouts or jamming and the GPS is a passive (one-way) ranging system that allows users can only receive satellite signals, it is less reliable than the Inertial Navigation System (INS) [1]. The strategy of combining specific forces and rates measured by accelerometers and rate gyros of an Inertial Measurement Unit (IMU) onboard the navigating body is so-called Inertial Navigation System (INS). While, IMU is a set of sensors such as Gyroscopes that provide information about attitude and accelerometers and thus information about the change in velocity and acceleration for a navigating body [2].

The UAV navigation is performed by the combination of GPS, INS, and vision sensors. Where GPS signals are present, the GPS data is used to calibrate the laser rangefinder LRF, optic flow modeling, and the INS sensors errors. The vertical and horizontal movements of the UAV are provided by a Charge Coupled Device video camera and laser rangefinder, fused with inertial sensors. Thus, where the GPS signals are demolished the UAV motion corresponding to the ground are maintained by the vision system [3].

The use of a tightly coupled INS/GPS integration and an augmented device state vector is taken into account when the navigating body is maneuvering with a low GPS update rate in order to handle the pseudorange errors. The anti-interference ability of the positioning system could be improved with a GNSS/INS deeply integrated positioning system, allowing for real-time positioning with much higher accuracy and reliability [4]. Because of the lock-loss as navigating body run through tunnels, high-rise structures, and forest areas, the GPS receiver is directly extracted of navigation feature. Thus, the inertial measurement unit (MPU6050), control processing unit (STM32), and GPS receiver are employed as low-cost GPS/INS integrated framework to overcome the GPS data lacking [5].

As a communication range of UAVs, our proposed integrated GPS/INS autopilots will be supposed to enable the UAVs to fly independently with relatively high accuracy to rages out of the ground station contact.

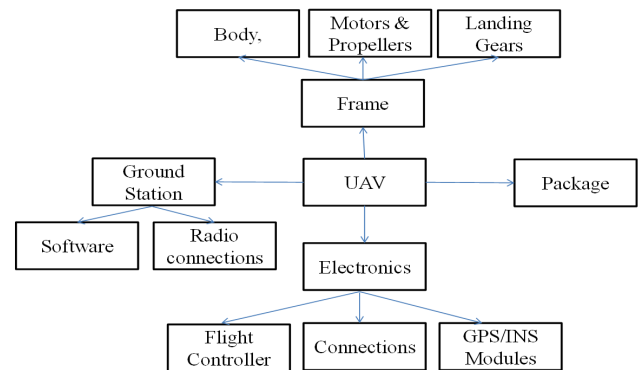


Fig. 1: Fundamental UAV structure.

REFERENCES

- [1] I. Sharp and K. Yu, *Wireless Positioning: Principles and Practice*. Springer, 2019.
- [2] W. Quan, J. Li, X. Gong, and J. Fang, *INS/CNS/GNSS integrated navigation technology*. Springer, 2015.
- [3] J. Wang, M. Garratt, A. Lambert, J. J. Wang, S. Han, and D. Sinclair, "Integration of gps/ins/vision sensors to navigate unmanned aerial vehicles," *The International Archives of the Photogrammetry, Remote Sensing and Spatial Information Sciences*, vol. 37, no. part B1, pp. 963–969, 2008.
- [4] J. Wang, X.-h. Yan, B.-g. Cai, and W. Shangguan, "Research on deeply integrated gps/ins for autonomous train positioning," in *2011 4th IEEE International Symposium on Microwave, Antenna, Propagation and EMC Technologies for Wireless Communications*. IEEE, 2011, pp. 687–690.
- [5] Y. Xu and P. Chen, "The gps/ins integrated navigation module research and design based on the stm32," in *2015 3rd International Conference on Machinery, Materials and Information Technology Applications*. Atlantis Press, 2015.

Survey of motion analysis in neuroscience mouse experiments

Boldizsár Zsolt BALOG

(Supervisors: Gábor NYÍRI, György CSEREY)

Pázmány Péter Catholic University, Faculty of Information Technology and Bionics

50/a Práter street, 1083 Budapest, Hungary

balog.boldizsar.zsolt@itk.ppke.hu

Abstract—Experimental neuroscience is essential for understanding brain functions, behavior, and brain disorders. Optogenetic mouse behavioral experiments are crucial for achieving these goals, therefore behavior needs to be measured quantitatively and objectively. This article describes the main types of approaches to quantitatively analyze animal behavior.

Keywords—behavior; analysis; survey

I. INTRODUCTION

Behavior is the collection of interactions between an organism and the environment that is evolved to ensure survival [1]. Behavioral neuroscience helps to understand and fight neuronal disorders like those related to addiction, aging, sleep, trauma, anxiety, depression, autism spectrum disorder, bipolar disorder, epilepsy, and other disorders [2]]. Behavioral neuroscience helps understanding the translation of neuronal activity into behavior [1]. To study these processes, behavior needs to be objectively quantified.

II. BEHAVIOR ANALYSING TECHNIQUES

In practical terms, the movement of the animal is behavior, thus behavioral experiments can usually be analyzed using movement-based techniques.

A. Observer-based behavior analysis

The simplest type of analysis is the human observation of the animal without video recording. Although this approach is rarely used nowadays for quantitative research, it is still common when complex animal behavior needs to be analyzed.

B. Video-based behavior analysis

New movement-based behavioral analyzing techniques emerged during the 20th century as usage of video cameras became available for investigations. Video recordings were used as basis for both manual analysis and automated detections.

C. Sensor-based behavior analysis

Researchers and engineers developed automatic tools that use sensors as data source instead of video recordings.

1) *Sensors built into the environment*: Some examples of sensors built into the environment are weight cells under the arena and infrared barriers.

2) *Sensors attached to the animal*: Ultrasonic devices and IMUs (inertial measurement units) can be attached to the animals and could be used for motion data collection. It is crucial that the attached instruments are light enough not to change the recorded movement.

Multiple approaches [3]–[6] were developed that are based on the motion of the head. Figure 1 shows some devices used for motion-based behavioral analysis in mice, bats, and rats.

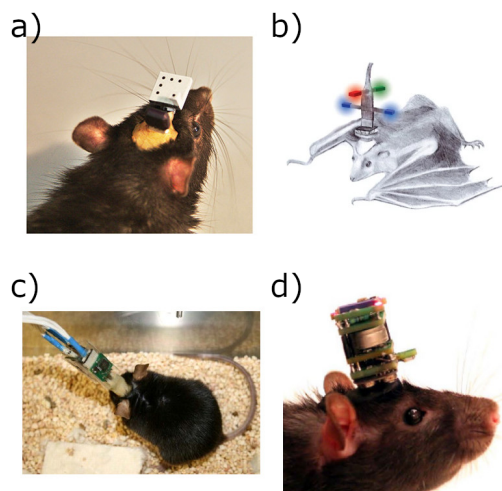


Fig. 1. Devices used for recording head movement. a) camera-based, passive approach [3], b) “tracking headstage”-based, quasi-passive approach [4], c) wired IMU-based approach [5], d) wireless IMU-based approach [6]

The passive, camera-based head-tracking system [3] seen on picture a) in Figure 1 features a pattern that is easy for an automatic video processing algorithm to track. A “tracking headstage”-based, quasi-passive approach used for recording the movement of bats [4] can be seen on Figure 1/b). The IMU-based approach [5] depicted on Figure 1/c) uses a 3D accelerometer for behavior recognition. An another IMU-based solution (Figure 1/d)) uses a 9D IMU as data source and uses custom algorithms for freezing detection [6]. None of these devices is commercially available. Supertech’s Acc-2b [7] is a commercially available 3D, analogue accelerometer developed for use in biological experiments.

REFERENCES

- [1] H. D. Schlinger, “Behavior analysis and behavioral neuroscience,” 2015.
- [2] EMOTIV, “Behavioural Neuroscience,” 2020.
- [3] W. Vanzella, N. Grion, D. Bertolini, A. Perissinotto, M. Gigante, and D. Zoccolan, “A passive, camera-based head-tracking system for real-time, three-dimensional estimation of head position and orientation in rodents,” *Journal of Neurophysiology*, vol. 122, pp. 2220–2242, dec 2019.
- [4] A. Finkelstein, D. Derdikman, A. Rubin, J. N. Foerster, L. Las, and N. Ulanovsky, “Three-dimensional head-direction coding in the bat brain,” *Nature*, vol. 517, no. 7533, pp. 159–164, 2015.
- [5] S. Venkatraman, X. Jin, R. M. Costa, and J. M. Carmena, “Investigating Neural Correlates of Behavior in Freely Behaving Rodents Using Inertial Sensors,” *Journal of Neurophysiology*, vol. 104, pp. 569–575, apr 2010.
- [6] M. O. Pasquet, M. Tihy, A. Gorgeon, M. N. Pompili, B. P. Godsil, C. Léna, and G. P. Dugué, “Wireless inertial measurement of head kinematics in freely-moving rats,” *Scientific Reports*, vol. 6, no. 1, p. 35689, 2016.
- [7] Supertech Instruments, “3D Accelerometer,” 2020.

Automatic parallelisation of structured mesh computations with SYCL

Gábor Dániel BALOGH

(Supervisors: István Zoltán REGULY, Péter SZOLGAY)

Pázmány Péter Catholic University, Faculty of Information Technology and Bionics

50/a Práter street, 1083 Budapest, Hungary

balogh.gabor.daniel@itk.ppke.hu

Abstract—Structured meshes are widely used for scientific computations such as Computational Fluid Dynamics (CFD) applications or finance. Modern applications often have grid points in the millions. To perform such computations parallelisation is crucial. However it is unfeasible to port each application every time a new architecture arrives, hence in recent years the demand for automatic parallelisation and optimisation for the used hardware is increasing. The OPS (Oxford Parallel library for Structured mesh solvers)[1] has shown good performance and scaling on a wide range of HPC architectures. In 2021 two new exascale supercomputers will launch with new AMD (Frontier) and Intel GPUs (Aurora) and the official support for the new Intel GPUs will be through SYCL which is a high level programming framework. This paper sketches our plans and progress so far to extend the OPS framework with a SYCL backend to extend the range of architectures that OPS can support and further increase Performance Portability of OPS applications and shows preliminary performance results on CPU nodes.

Keywords—HPC; SYCL; automatic parallelisation

I. INTRODUCTION

The computational cost of modern scientific simulations are continuously increasing, and only highly efficient parallel implementations can achieve the required performance. However it is not clear which hardware is the perfect fit for given applications, since in some cases the different available hardware require significantly different programming models and techniques, it is unfeasible to port the application to each of them. The huge difference in programming models and the uncertainty in the performance of future hardware leads to increased interest in domain-specific languages and other similar high level abstractions which separate the application code written by the developer and the low-level optimised parallel implementations.

Our goal is to extend the OPS domain-specific language. OPS is a domain specific language embedded in C++. OPS is an open source framework for automatic parallelisation of structured mesh applications. The goal of OPS is to separate the low-level optimised implementation for the high level description of the application. The developer should write their application on terms of high level steps such as datasets and operations on the datasets. From this description OPS will generate the platform specific implementations for different hardware. In structured mesh applications the data is defined on a regular grid where neighbouring grid points is determined by the position of cell in the grid. In such simulations the computational steps are loops over the grid performing the same operations on each grid point and their neighbourhood. To achieve the goal of OPS it is necessary to support new modern hardware, such as the new Intel GPUs. The SYCL programming framework aims to support multiple

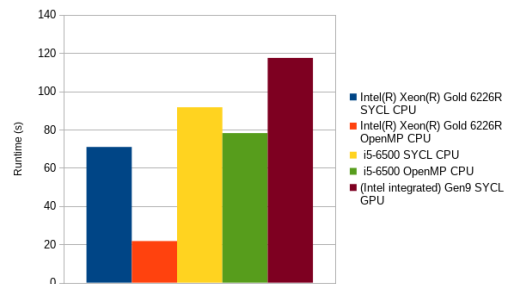


Fig. 1: Runtime of CloverLeaf3D application with meshsize 150^3 on three different architectures.

hardware from the same source using OpenCL. They provide a set of standard C++ function templates for common computational tasks. One of the great advantage of SYCL is the fact that the official support for programming Intel's new GPU series uses SYCL.

II. RESULTS

We implemented a new SYCL back-end for OPS with handling of data movement between the host and accelerator memory environment and the corresponding source-to-source translator to generate the parallel SYCL implementations of the loops. We used the SYCL implementation from Intel OneAPI, since this will be the official implementation supporting Intel GPUs in the future. The current implementation only supports single node applications. On Figure 1 we see that the SYCL implementation has similar performance on CloverLeaf3D [2] as the reference OpenMP application on Intel® Core™ i5-6500 and it's corresponding integrated GPU. We currently searching for the reason behind the difference in performance on the Intel® Xeon® Gold 6226R processor. Currently we are working on the MPI support for multi-node applications.

ACKNOWLEDGEMENTS

This research was supported by the ÚNKP-20-3-II New National Excellence Program of the Ministry for Innovation and Technology From the source of the National Research,

Development and Innovation Fund.

REFERENCES

- [1] I. Z. Reguly, G. R. Mudalige, M. B. Giles, D. Curran, and S. McIntosh-Smith, "The ops domain specific abstraction for multi-block structured grid computations," in *2014 Fourth International Workshop on Domain-Specific Languages and High-Level Frameworks for High Performance Computing*, pp. 58–67, IEEE, 2014.
- [2] A. Mallinson, D. A. Beckingsale, W. Gaudin, J. Herdman, J. Levesque, and S. A. Jarvis, "Cloverleaf: Preparing hydrodynamics codes for exascale," *The Cray User Group*, vol. 2013, 2013.

Progress report on estimation and control of COVID19 epidemics in Hungary using the theory of nonlinear dynamic systems

Balázs CSUTAK

(Supervisor: Gábor SZEDERKÉNYI)

Pázmány Péter Catholic University, Faculty of Information Technology and Bionics

50/a Práter street, 1083 Budapest, Hungary

csutak.balazs@itk.ppke.hu

Abstract—In this progress report, I present an overview of our recent works concerning the estimation and optimal control of epidemic processes, using the mathematical toolbox of nonlinear dynamic systems. A previously published compartmental model is used to capture the dynamics of COVID-19, with parameters characteristic to Hungary. A method for estimation of state variables based on linear subsystem inversion presented for a more proper epidemic analysis, giving valuable insight beside the official data. Moreover, a model predictive control based system is presented, capable of computing optimal restrictive measures in function of the goals and bounds of the management aims.

Keywords—COVID-19; Epidemic model; State estimation; System inversion; Model predictive control; Temporal logic

I. SUMMARY

COVID-19 has been part of our lives for one and a half year, representing a significant challenge for all nations around the globe. Vaccine and proper medication not being available in the early stage, governments opted for a number of restrictive measures to slow down the epidemic process. While these turned out to be effective in terms of epidemic control, they had a devastating economical impact, and balancing between the harmful effects gained high importance.

Now, even in countries that have recently managed to suppress the epidemic, the management of COVID-19 appears to be a long-term challenge. As with the appearance of mutant versions of the disease, as well as numerous possible methods to deal with the pandemic, a decision-support system capable of state estimation and optimal control of an epidemic process might prove to be crucial.

In this report, based on [1] and [2] the building blocks of such a system are presented. First, a model predictive approach for the control of a nonlinear compartmental model (shown in figure 1) capturing the key dynamical properties of COVID-19 is discussed, using signal temporal logic to enforce complex constraints and logical relations between model variables. Different policy aims lead to control sequences similar to different real-life governmental responses, corresponding to strategies like mitigation and suppression.

As officially available data is often insufficient in itself for a proper analysis, we also proposed a method for estimation of latent infections using linear subsystem inversion of the aforementioned model, based solely on published hospitalization data. Complemented by a linear state observer or an unknown-input observer, state variables of the model can be reliably computed. The estimated trajectory of COVID-19 in Hungary can be seen in figure 2.

B. CSUTAK, “Progress report on estimation and control of COVID-19 epidemics in Hungary using the theory of nonlinear dynamic systems” in *PhD Proceedings – Annual Issues of the Doctoral School, Faculty of Information Technology and Bionics, Pázmány Péter Catholic University – 2021*. G. Prószéky, G. Szederkényi Eds. Budapest: Pázmány University ePress, 2021, p. 43. This research has been partially supported by the European Union, co-financed by the European Social Fund (EFOP-3.6.3-VEKOP-16-2017-00002).

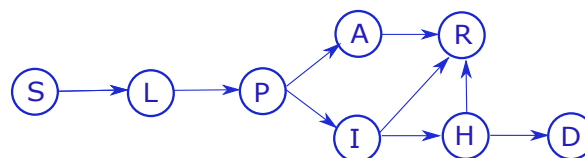


Fig. 1. Transition diagram of the disease spreading model. Characters represent compartments, arrows show direction of possible transitions. The abbreviations stand for susceptible (S), latent (L), presymptomatic (P), infected (I), asymptomatic (A), hospitalized (H), recovered (R) and deceased (D).

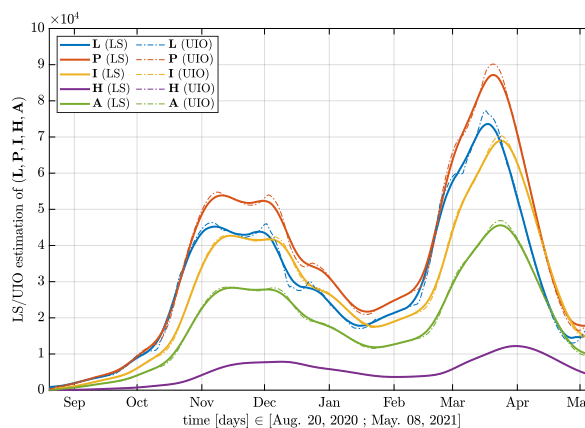


Fig. 2. Estimated trajectory for all state variables of the compartmental epidemic model. The two peaks of the epidemic in Hungary can be clearly observed. The model incorporates asymptomatic individuals, whose infection was never confirmed by a test.

ACKNOWLEDGEMENTS

I would like to gracefully acknowledge the continuous support and work of Dr. Tamás Péni, senior research fellow of ELKH-SZTAKI, Dr. Gergely Röst, professor of the University of Szeged, and Péter Polcz from Pázmány Péter Catholic University.

REFERENCES

- [1] T. Péni, B. Csutak, G. Szederkényi, and G. Röst, “Nonlinear model predictive control with logic constraints for COVID-19 management,” *Nonlinear Dynamics*, vol. 102, pp. 1965–1986, Dec. 2020.
- [2] B. Csutak, P. Polcz, and G. Szederkényi, “Computation of COVID-19 epidemiological data in Hungary using dynamic model inversion,” *IEEE 15th International Symposium on Applied Computational Intelligence and Informatics*, 2021.

Heterogenous architecture for visual servoing a prosthetic arm

Attila FEJÉR

(Supervisors: Péter SZOLGAY, Jenny BENOIS-PINEAU)

Pázmány Péter Catholic University, Faculty of Information Technology and Bionics

50/a Práter street, 1083 Budapest, Hungary

fejér.attila@itk.ppke.hu

Abstract—We propose a hardware-software system implementation for controlling a hybrid vision-guided prosthetic arm. This system contains of object selection, object matching and depth map computation blocks. Scale Invariant Feature Transform (SIFT) is used for object selection and object matching. It is the most time-consuming part of the system, so acceleration is required. The FPGA acceleration has been chosen because the small energy consumption is suitable for a wearable device. Results show that real-time processing speed (more than 100 fps) is achievable on ZCU102 FPGA board.

Keywords—FPGA, computer vision, SIFT

I. INTRODUCTION

The aim of the system is to control an upper-limb prosthesis with a hybrid EMG - visual guidance. The whole processing chain is illustrated in Figure 1. It has two different acquisition devices, the Tobii glass camera and eye-tracker, and a GoPro Dual camera system, which are mounted to the subject shoulder[2]. The task of the object selection module is to recognize the object type and locate the object in the glass frame by a Convolutional Neural Network (CNN)[3]. The next step is to find the recognized object in the GoPro Dual camera system frames by the object matching module. After the location of the object has been found in GoPro Dual system camera frames the depth map can be estimated and the prosthetic arm could be controlled to reach the object.

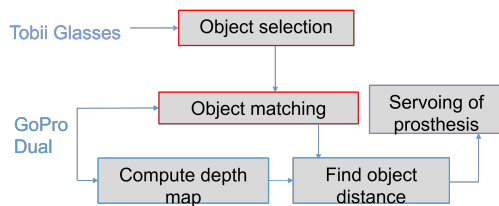


Fig. 1. The prosthetic arm vision-guided system

II. OBJECT DETECTION

The glass-frame is analysed around a gaze fixation of the subject. Before the CNN recognizes the object categories and location in the glass camera frames, some data preprocessing is necessary to get more precise gaze fixations. The geometric alignment of gaze fixation can reduce the egomotion noise. The goal of the module is to translate every gaze fixation to the reference frame plane. It uses SIFT[4], FLANN matcher, RANSAC, and homography estimation. The aim of the noise reduction module is to reduce the gaze fixations error in the reference frame. The position of the gaze fixation \hat{g}_n is estimated by kernel density estimator (KDE). The gaze-driven object recognition CNN uses the estimated gaze fixation \hat{g}_n

and the frame of the glass camera, as well as the possible bounding boxes around \hat{g}_n . The CNN predicts the location of the object and the type of the object. The last layer of CNN needs to be updated by the weight updater to be more accurate for the next video frame based on the move-to-data approach[5] which is our current work.

III. OBJECT MATCHING

Once the object detection module has detected the location and type of the object in the glass frame, the object matching module uses this information to find the location of the object in the frames of the shoulder camera system. The method is the same as described in Section II, i.e. a geometric alignment with an estimated homograph, between glass view and GoPro views.

IV. ACCELERATION ON FPGA

Real-time processing is needed to control the prosthetic arm. The measurements show that the most time-critical part of our system is the SIFT algorithm. The FPGA acceleration has been chosen over other hardware acceleration because it has lower energy consumption and the same or higher processing speed.

V. RESULTS AND CONCLUSIONS

The results show that a lightweight device can be developed by using FPGA with more than 100 images per second processing rate. In that case the input image resolution is $480\text{px} \times 480\text{px}$. The developed SIFT keypoint extractor is running on Xilinx ZCU102 FPGA board.

VI. ACKNOWLEDGEMENT

The contribution of Mr Zoltán Nagy and Mr Aymar de Ruyg is kindly acknowledged.

REFERENCES

- [1] Fejér, A., Nagy, Z., Benois-Pineau, J., Szolgay, P., de Ruyg, A., Domenger, J.-Ph. *Implementation of Scale Invariant Feature Transform detector on FPGA for low-power wearable devices for prostheses control*. Int J Circ Theor Appl. 2021; 1– 19. <https://doi.org/10.1002/cta.3025>
- [2] Fejér, A., Nagy, Z., Benois-Pineau, J., Szolgay, P., de Ruyg, A., Domenger, J.-Ph. *FPGA-based SIFT implementation for wearable computing*, 2019 IEEE 22nd International Symposium on Design and Diagnostics of Electronic Circuits and Systems (DDECS), ISSN 978-1-7281-0072-2
- [3] González-Díaz, I., Benois-Pineau, J., Domenger, J.-Ph., Cattaert, D., de Ruyg, A. *Perceptually-guided deep neural networks for ego-action prediction: Object grasping*, Pattern Recognition, Volume 88, 2019, Pages 223-235, ISSN 0031-3203, <https://doi.org/10.1016/j.patcog.2018.11.013>.
- [4] Lowe, D.G. *Distinctive Image Features from Scale-Invariant Keypoints*. International Journal of Computer Vision 60, 91–110 (2004).
- [5] Poursanidis, M., Benois-Pineau, J., Zemmari, A., Mansencal, B., de Ruyg, A. *Move-to-Data: A new Continual Learning approach with Deep CNNs, Application for image-class recognition*, arXiv preprint arXiv:2006.07152

Cognitive complexity of data manipulation languages

Árpád GORETITY

(Supervisor: István Zoltán REGULY)

Pázmány Péter Catholic University, Faculty of Information Technology and Bionics

50/a Práter street, 1083 Budapest, Hungary

goretity.arpad@itk.ppke.hu

Abstract—Cognitive complexity of different DMLs is evaluated quantitatively, according to industry-standard metrics. It is concluded that general-purpose metrics do not always reflect the experience of programmers using such specialized languages. We propose that language-specific metrics be developed in the future. Desirable properties for such metrics are defined.

Keywords—database; data manipulation language; cognitive complexity

I. INTRODUCTION

Software metrics are an easy and widely-used approach for objectively evaluating code quality. De facto standard measures for mainstream programming languages have been developed and shown to correlate with human opinions on how hard it is to understand a given piece of code. However, metrics such as cyclomatic complexity or Halstead’s difficulty almost universally assume a procedural or object-oriented programming language with eg. control flow and function calls. This sometimes makes them hard or impossible to adapt for data manipulation languages in data storage and analysis systems. We identify some of their issues by evaluating metrics on corpora of Structured Query Language [1], the MongoDB language, LINQ, and Core Data. We then propose a set of criteria for designing new metrics that better describe the cognitive complexity of such declarative languages.

II. COMPLEXITY METRICS

Our metrics of choice were the ones developed by Halstead [2]. These are based on the notion of operators and operands. We define the following variables:

η_1 = the number of unique operators;
 η_2 = the number of unique operands;
 N_1 = the number of operators;
 N_2 = the number of operands.

Halstead’s difficulty metric is then defined in Equation 1 as:

$$D = \frac{\eta_1}{2} \cdot \frac{N_2}{\eta_2} \quad (1)$$

while the Halstead effort metric is defined in Equation 2 as:

$$E = D \cdot (N_1 + N_2) \cdot \log_2(\eta_1 + \eta_2) \quad (2)$$

We automatically evaluated these metrics by lexing and parsing the involved languages (SQL, BSON, C#/LINQ, and Swift), then counting and classifying tokens and syntax nodes as operands or operators (or neither, if not applicable). The example corpora were composed of 11, increasingly more complex queries against a realistic-looking schema. The queries were also evaluated against randomly-generated data and it was ensured that they are indeed equivalent.

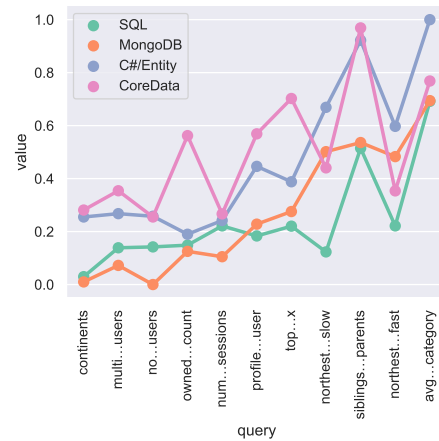


Fig. 1. Halstead difficulty for different data manipulation languages and queries of different complexity.

III. RESULTS AND CONCLUSIONS

These metrics correlate moderately with expert opinion of cognitive complexity [3]. Figure 1 shows metric values across corpora, normalized to the unit interval. It is evident that they exhibit an increasing tendency, but neither is monotonic. With the exception of MongoDB, values vary wildly even between adjacent queries of similar subjective difficulty. We thus conclude that the development of new metrics is needed [4], which are tailored to the properties of special-purpose, declarative languages. Namely: they should not assume the presence of control flow, they should not be primarily based on a measure of program length, and they should account for the semantics and cognitive complexity of different language features.

REFERENCES

- [1] Huib van den Brink, Rob van der Leek and Joost Visser, *Quality assessment for embedded SQL*, Seventh IEEE International Working Conference on Source Code Analysis and Manipulation, Paris, France, 163–170, 2007. DOI: 10.1109/SCAM.2007.23
- [2] Maurice Howard Halstead, *Elements of software science*, Elsevier North-Holland, Inc., Amsterdam, 1977. ISBN: 0-444-00205-7
- [3] Bernhard Katzmarzki and Rainer Koschke, *Program complexity metrics and programmer opinions*, Proceedings of the 20th IEEE International Conference on Program Comprehension, 17–26, 2012. DOI: 10.1109/ICPC.2012.6240486
- [4] Sheng Yu and Shijie Zhou, *A survey on metric of software complexity*, 2nd IEEE International Conference on Information Management and Engineering, 352–356, 2010. DOI: 10.1109/ICIME.2010.5477581

A theater presentation model to test the different interaction methods for light field displays

Mary GUINDY

(Supervisors: Vamsi Kiran ADHIKARLA, Péter SZOLGAY)

Pázmány Péter Catholic University, Faculty of Information Technology and Bionics

50/a Práter street, 1083 Budapest, Hungary

guindy.mary.mohsen.messak@itk.ppke.hu

Abstract—Light field displays (LFDs) is an evolving technology that provides immersive visual experiences to users without the need of additional glasses. Although many interaction techniques have been investigated and devised for the different 2D/ 3D environments and applications, applying the same interaction methods to LFDs is very difficult since sharp rendering is only done on the screen. Basic user interfaces such as FOX (Focus Sliding surface) have been designed for LFDs. In this paper, we discuss possible interaction techniques for LFDs and test them by means of a theater presentation model.

Keywords—user interface, light field visualization, 3D rendering.

I. 3D PRESENTATION MODELS

Any presentation model can be divided into three main interaction methods: (i) navigation, (ii) selection and manipulation and (iii) application/system control. Presentation models are responsible for the arrangement of objects within the scene, as well as including a set of methods for manipulating and interacting with the items in the scene.

A. Overview of 3D presentation models

As expected, 3D presentation models for 3D environments is far more challenging than those designed for 2D. Presentation models include lining-up of objects then focusing light on the object under selection. Also, changing focus can be deployed, as well as animating/ freezing selected objects. Moreover, presentation models can include decals, 3D text, overlays, 3D carousels and others.

B. Presentation models for light field displays

Unlike 2D and 3D environments, interaction methods for LFDs are still being investigated. Considering navigation, it is always preferable to use a static camera to avoid moving the objects between the sharp and blurry regions of the LFDs. Moreover, usage of free cameras is also possible. As for the selection and manipulation part, rendering to overlays on LFDs is difficult since rendering to the observer's closest plane will be blurry. A proposed solution is to render on predefined 2D area(s) on the screen plane while culling or setting the transparency of the objects in-between those areas and the observers. As for rendering to 3D regions, this could be done by means of different techniques that are used to select and manipulate objects on LFDs including bounding box outlines, color change, decals, selection tube/halo/circle/arrow, animations, hiding/revealing, change of object arrangement/spatial position. Finally, the application/ system control within the LFDs can be done by separating the main scene and the 3D controls while providing feedback from the main scene. An alternative solution is to render the interface unto reserved 2D

area(s) on the screen, similar to the technique used in selection and manipulation.

II. THEATER MODEL FOR LIGHT FIELD VISUALIZATION

The choice of the theater model was backed up by many reasons, among which is the similarity between the LFDs and the theater model in providing the same viewing experience to various spectators in an angularly-dependant manner. Moreover, a lot of interactions is possible via the theater's presentation elements (curtain, flying/ rigging system, etc.) in a side-to-side motion or up and down motion. Accordingly, movement back and forth is avoided, hence avoiding going out an into the blurry region of the LFD [1].

A. Technical considerations

Testing the different interaction methods was done on the HoloVizio C80 LFD [5] where a theater and a monitor room were modelled using MAYA [6]. Unlike conventional 2D displays, 3D LFDs have certain portion of areas that are rendered sharply (those close to the screen), where the objects under selection/ manipulation should be rendered.

B. Results and evaluation

In the theater model, the monitor control room represents the application/system control phase, where transition between the theater model and the control room is done via pressing buttons and the corresponding animation is carried out while displaying an image from the current theater state on the control room as a feedback. Once the animation is done, the view switches back to the theater scene. For navigation, a static camera was used. As for the selection and manipulation, multiple ideas were implemented including a rotating stage while moving up and down, hiding/revealing elements by means of curtains, utilizing the sharp and blurry region for LFDs along with defining a path for the objects or using carousels [1].

ACKNOWLEDGMENTS

Funding from the EU Horizon 2020 programme under the Marie Skłodowska-Curie grant No 813170 and from grants 2018-2.1.3-EUREKA-2018-00007 and KFI 16-1-2017-0015 of NRDI Fund, Hungary are gratefully acknowledged.

REFERENCES

- [1] Guindy, Mary, et al. "Interaction methods for light field displays by means of a theater model environment." *Holography: Advances and Modern Trends VII*. Vol. 11774. International Society for Optics and Photonics, 2021.
- [2] Holografika, "HoloVizio C80 glasses-free 3D cinema system." <https://holografika.com/c80-glasses-free-3d-cinema/>.
- [3] Autodesk, INC., "MAYA" <https://autodesk.com/maya>.

Developing a measurement environment for the Memristor Cellular Neural Network architecture

Dániel HAJTÓ

(Supervisor: György CSEREY)

Pázmány Péter Catholic University, Faculty of Information Technology and Bionics

50/a Práter street, 1083 Budapest, Hungary

hajto.daniel@itk.ppke.hu

Abstract—Several memristor based computational unit has been introduced in the last few decade. One of these is the Memristor Cellular Neural Network (MCNN), which is a regular CNN expanded with the capabilities of a memristor device. It has a much more complex dynamics than a CNN and much more sensitive to environmental noise. This work introduce some of the solvable problems regarding the MCNN hardware implementation and its measurement. The possible solutions for these problems and MCNN applications are also discussed briefly.

Keywords-memristor; neuromorphic computing; circuit design

I. INTRODUCTION

Memristors and memristive devices are subject of interest in the field of neuromorphic computation [1], because of their unique properties, namely their statefulness and nano-scale size. The mainstream approach in the field is stacking a large number of memristors in 2 or 3 dimensional arrays to implement constant-time matrix-vector multipliers [2], which is a very important operation in many scientific computation application [3].

II. MCNN

The theory of MCNN has been introduced recently [4] along with the basic templates [5] necessary to control the more complex dynamics compared to the CNN machine. The main difference is the replacement of the resistor of the RC unit to a MC (memristor-capacitor) unit in the state equation. This changes the single variable differential equation into a two variable differential equation system with the memristance change equation. This also changes the state into a two dimensional vector. The two independent state variable is able to store more information locally, which is advantageous for high computational efficiency.

III. MEASUREMENT ENVIRONMENT DESIGN

A simplified MCNN circuit was designed to minimize environmental noise (Fig. 1.). For the same reason several MCNN functionality that is programmable from software in regular implementations were hardwired and fine-tuned to work with the used memristor implementation. The used memristor is a previously presented [1], robust, emulated device using 16 Ge_2Se_3 based memristors. The modified properties of such construction is beneficial for the application in MCNN. One of the properties is the higher writing threshold voltage.

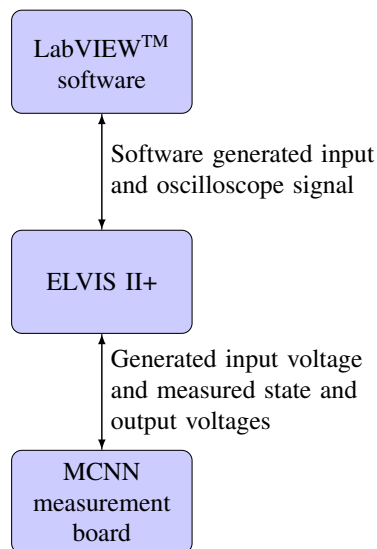


Fig. 1: Block diagram of the proposed MCNN measurement environment.

REFERENCES

- [1] Hajtó, Dániel, Adam Rak, and Gyorgy Cserey, *Robust Memristor Networks for Neuromorphic Computation Applications.*, MDPI Materials 12, 3573., 2019.
- [2] Hu, Miao et al., *Dot-product engine for neuromorphic computing: Programming 1T1M crossbar to accelerate matrix-vector multiplication*, 53rd ACM/EDAC/IEEE Design Automation Conference (DAC), pp. 1-6, 2016.
- [3] Reguly, István and Mike Giles, *Efficient sparse matrix-vector multiplication on cache-based GPUs*, 2012 Innovative Parallel Computing (InPar), pp. 1-12, 2012.
- [4] Tetzlaff, Ronald, Alon Ascoli, Ioannis Messaris, and Leon O. Chua. *Theoretical foundations of memristor cellular nonlinear networks: Memcomputing with bistable-like memristors.*, IEEE Transactions on Circuits and Systems I: Regular Papers 67, no. 2, pp. 502-515, 2019.
- [5] Ascoli, Alon, Ronald Tetzlaff Ioannis Messaris, and Leon O. Chua. *Theoretical foundations of memristor cellular nonlinear networks: A DRM2-Based Method to Design Memcomputers With Dynamic Memristors.*, IEEE Transactions on Circuits and Systems I: Regular Papers 67, no. 8, pp. 2753-2766, 2020.

Study the effect of the risk factors in the estimation of the breast cancer risk score using machine learning

Sam KHOZAMA

(Supervisors: Zoltán NAGY, Zoltán GÁSPÁRI)

Pázmány Péter Catholic University, Faculty of Information Technology and Bionics
50/a Práter street, 1083 Budapest, Hungary
khozama.sam@itk.ppke.hu

Abstract—In the current research, we introduce a novel machine learning tool for the early prediction of breast cancer. Three basic resources are used to identify the most essential risk factors; including the BCSC dataset, a medical questionnaire, and multiple international breast cancer reports. The BCSC dataset has been normalized and balanced; consequently, the questionnaire and the medical reports are analyzed in order to define the degree of importance and a potential weight factor of each risk factor. These weights are used to scale risk factors and then the optimizable tree-based ML model is trained using the balanced weighted risk factors datasets.

Keywords—Breast cancer; Cancer Prediction; Machine Learning; Risk factors.

I. INTRODUCTION

Nowadays, data analysis is one of the most developing fields of computer science, due to the fact that the size of datasets is exponentially increasing day after day. Cancer prediction is one of those fields, using data analysis and Machine Learning (ML) algorithms for the estimation of cancer [1]. ML techniques can improve the performance of cancer prediction, the estimation accuracy of which has increased significantly (15%-20%) due to using the ML algorithm during the last years [2]. Breast cancer prediction itself can be used to define those potentially high-risk women and guide them to improve their lifestyle, avoiding future therapy and costs [3].

II. MATERIALS AND METHODS

In the current research, we suggested using the BCSC dataset including 280660 records and 12 risk factors, which are described in Table 1. Besides these risk factors, the dataset includes a variable called “count”, which holds the frequency of each record within the dataset, as mentioned in the BCSC dataset (2021). The proposed risk-estimation model of breast cancer is described in Figure 1. All risk factors are used. First, the dataset is normalized to make sure that all risk factors initially have the same effect on the final risk estimation.

III. PREDICTION TOOL DESIGN

After getting the final optimizable decision tree classifier, we build the tool based on the trained model. The tool is designed using MATLAB App designer. Figure 2 shows the designed tool. After entering the values of all factors except “count”, the tool searches into the BCSC dataset to find the match between the entered risk values and all records of

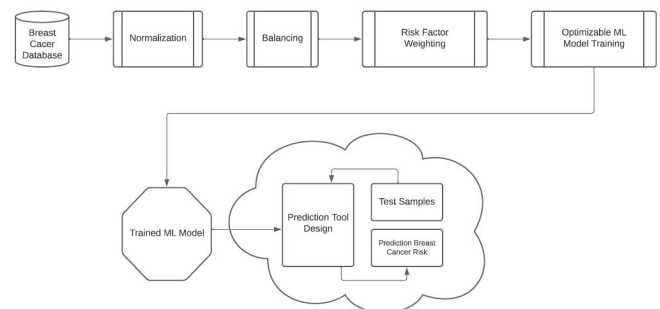


Fig. 1. Proposed system methodology

the dataset. If a match is found, the corresponding count is considered as the count of the test sample. Otherwise, the count will be 1.

IV. CONCLUSION

Weighting the risk factors of the BCSC dataset improves the performance by increasing the accuracy and reducing the false rejection and false discovery rates for all versions of balanced datasets. The weighting approach can also be used to improve the estimation score of breast cancer by scaling the individual scores of risk factors.

ACKNOWLEDGEMENTS

Data collection and sharing was supported by the National Cancer Institute-funded Breast Cancer Surveillance Consortium (HHSN261201100031C), available at: <http://www.bcsc-research.org/>.

This work is done under full supervision by Dr Ali Mayya, a teacher from the Department of Computer Engineering, Tishreen University, Lattakia, Syria.

REFERENCES

- [1] Ahmad AS, Mayya, AM (2020). A new tool to predict lung cancer based on risk factors. *Heliyon*, 6, e03402.
- [2] American Cancer Society (2019). *Breast Cancer Facts & Figures 2019-2020*. Atlanta: American Cancer Society.
- [3] Apté C, Weiss S (1997). Data mining with decision trees and decision rules. *Future Gener. Comput. Syst.*, 13, 197-210.

Non-contact monitoring of adults' respiration by computer vision algorithms

Ádám NAGY

(Supervisor: Ákos ZARÁNDY)

Pázmány Péter Catholic University, Faculty of Information Technology and Bionics

50/a Práter street, 1083 Budapest, Hungary

nagy.adam@itk.ppke.hu

Abstract—The accelerating development of technology helped significantly the spreading of different sensors in all fields of life. [1] The cameras and IoT devices appear in more and more places around us and they will provide more and more data about us and about our health. [1] Our sensors measure several kinds of vital signals that can help improve our lifestyle and our health. One of the most essential vital parameter is the respiration rate (RR). This can reveal much about the subject's medical condition and is very frequently used for example in the field of sleep analysis [3]. The current trend in medical developments points to the non-contact measurement of respiration [2]. This motivated me to develop Computer-Vision-based non-contact algorithms for monitoring the respiration of adults. In this work, I will introduce a proof-of-concept solution for the respiration monitoring of adults where I intend to demonstrate how we would be able to measure the respiration of adults using simple algorithms with low computational costs.

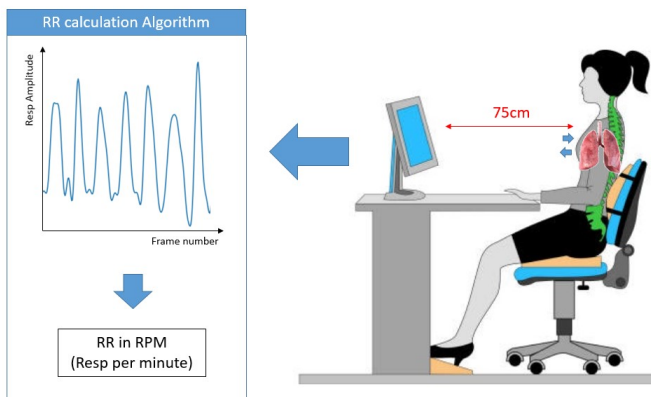


Fig. 1. The experimental setup: The subject is sitting in front of the computer roughly 75 cm from the camera. The camera captures video frames from the subject. After the RR calculation algorithm computes the respiration curve and the RR.

I. INTRODUCTION

In our previous publications we overviewed the problem of respiration monitoring of newborn babies [4]. We also showed how to optimize the monitoring algorithms for Raspberry Pi or other embedded systems [5]. However, we did not touch upon the usage of these algorithms for monitoring of adults despite the fact that it is a heavily researched topic. The reduction in the price of cameras and the spreading of IoT devices can open a new door in the field of respiration monitoring. In the future tiny cameras can measure our respiration and other vital signals in front of the mirror or in front of our computer in our workplace or when we are in bed sleeping. In this article, I want to confine its scope to merely presenting the respiration monitoring technique that I designed, which is only one of

the several solutions to this problem. I tried to keep down the computational costs of my algorithm to make it possible to run real time in an embedded system or on a mobile phone. My technique can be divided into 3 parts:

- Detection of region of interest (ROI)
- Extraction of respiration signal
- Determination of RR

For ROI detection, we used a HaarFeature detection based solution. This method can find the subject's face first and after the subject's chest which can be found at a given distance from the face if we assume that the subject is sitting or standing at a given distance from the camera. As we know, the chest is one of the places where the motion maps (provided by optical flow algorithms for example) correlate best with the respiration of the subject.

In respiration signal extraction, we use a simple optical flow algorithm in the ROI to give us motion maps. After that, the mean of these motion maps can give us a one-dimensional signal.

Finally, the respiration rate is given by detecting the respiration peaks and calculating the mean of the time differences between our detected peaks.

This algorithm was implemented for a RaspberryPi 4 system to demonstrate the feasibility of the concept, I elaborated above. We did not have time to perform parallel measurements with ECG. Therefore, the results I will demonstrate are just performed by comparing the calculated RR values to the ones we counted on the video manually. However, they can suggest us that a non-contact respiration monitoring is feasible for such a system with low computational power and it is worth to continue the research in this area.

REFERENCES

- [1] M. O. Ojo, S. Giordano, G. Prociassi and I. N. Seitanidis, *emphA Review of Low-End, Middle-End, and High-End Iot Devices in IEEE Access*, vol. 6, pp. 70528-70554, 2018, doi: 10.1109/ACCESS.2018.2879615.
- [2] Villarreal M, Chaichulee S, Jorge J, Davis S, Green G, Arteta C, Zisserman A, McCormick K, Watkinson P, Tarassenko L. *Non-contact physiological monitoring of preterm infants in the Neonatal Intensive Care Unit*. NPJ Digit Med. 2019 Dec 12;2:128. doi: 10.1038/s41746-019-0199-5. PMID: 31872068; PMCID: PMC6908711.
- [3] Douglas NJ, White DP, Pickett CK, et al. *Respiration during sleep in normal man*. Thorax 1982;37:840-844.
- [4] Ádám Nagy, D. Csetverikov, and Ákos Zarándy. *Novel methods for video-based respiration monitoring of newborn babies*, in KEPAF 2019. Képfeldolgozók és Alakfelismerők Társaságának 12. országos konferenciája, Debrecen, 2019, pp. 1–10. [Online]. Available: <http://eprints.sztaki.hu/9699/>
- [5] Ákos Zarándy, P. Földessy, Ádám Nagy, I. Jánoki, D. Terbe, M. Siket, M. Szabó and J. Varga *Multi-level optimization for enabling life-critical visual inspections of infants in resource-limited environment*, in IEEE International Symposium on Circuits and Systems, 2020

Bitwise reproducible execution of unstructured mesh applications

Bálint SIKLÓSI

(Supervisors: István Zoltán REGULY, Péter SZOLGAY)

Pázmány Péter Catholic University, Faculty of Information Technology and Bionics

50/a Práter street, 1083 Budapest, Hungary

siklosi.balint@itk.ppke.hu

I. INTRODUCTION

The IEEE-754 standard defines the behaviour of floating point representation. It is correct, but comes with roundings which cause non-associativity of the operations. The order of calculations, usually relaxed in a parallel environment, affects the results. There are some other approaches to solve this issue. One of these is the ReproBLAS project's binned representations [1]. Their method causes a $5n$ to $9n$ floating point operations overhead. An other solution can be found in Lulesh [2], although it is applicable only for boundary or halo values. In this paper we present a reproducible ordering for the indirect increments, combined with reproducible reductions. As a result, this method can guarantee full reproducibility, even if it is run on different number of MPI processes.

II. THE OP2 DOMAIN SPECIFIC LANGUAGE

The OP2 (Oxford Parallel library for Unstructured mesh solvers) project is developing an open-source framework for the execution of unstructured grid applications on clusters of GPUs or multi-core CPUs. Although OP2 is designed to look like a conventional library, the implementation uses source-source translation to generate the appropriate back-end code for the different target platforms.

Our solution is implemented in this library. Further details at [3].

III. REPRODUCIBLE INDIRECT INCREMENTS

On Figure 1 two example incrementing orders can be seen on a single cell, by executing through the edges set by using an `edge_to_cells` mapping. Since the associative laws of algebra do not necessarily hold for floating-point numbers, $cell0 = e0 + e1 + e2 + e3 \neq cell0 = e1 + e3 + e0 + e2$. This situation might happen over MPI, when OP2's partition algorithm produces different local IDs for every elements. Thus we had to implement a fixed execution order into OP2, to solve this issue. Previously we presented a work, where we stored the local increments and then applied them later in a fixed order. This method works well, but there are some cases where postponing the increment is not possible, it must be applied immediately. To solve that, we use regular coloring schemes. In this work we present three options:

- **Trivial coloring** - Assign the global ID as a color to each elements. \rightarrow no parallelization
- **Greedy coloring** - We first run the application on one process, we apply a simple greedy first fit coloring, we save it and next time on more processes we load it and distribute it the same way like the full mesh.
- **Distributed coloring** - We compute a hash value to each element, and assign a color to it if it is a local

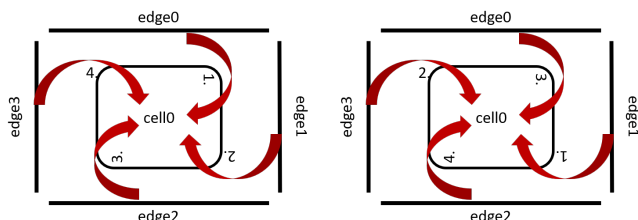


Fig. 1. Example orders of incrementing a cell in airfoil.

maximum or minimum. We repeat this, until all elements are colored.

Obviously in implementation, this produces some overheads in computational time and memory usage. Overall runtime rapidly changes with the number of used colors because of the terrible memory patterns introduced by them.

This method works with other type of mappings, not just with `edges_to_cells`.

An other difficulty of combining reproducibility with MPI is reducing into a single variable. To solve this issue, we introduce again a temporary storage for all local increments, and then we use ReproBLAS's `double_binned` structure which can apply all increments reproducibly.

RESULTS

Our results are tested on an Intel Xeon machine with 64 threads and on 2 NVIDIA V100 GPUs. We used 3 mini-applications: (1) Airfoil, a standard finite volume CFD benchmark code, (2) Aero, a finite element 2D nonlinear steady potential flow simulation and (3) MG-CFD, a multi-layer CFD code.

On CPUs we can see an acceptable slowdown effect. None of the methods reaches the $3\times$ overhead and all of them perform really well on the conjugate-gradient solver application. As it was expected, reproducibility comes with a significant slowdown effect due to the extra memory movement involved, although if the application is computationally more intensive, then the runtime difference decreases.

The slowdown on GPUs is still not optimal due to the increased irregularity in memory accesses. GPUs are much more sensitive to the data access patterns. One main side of our future work is optimizing memory usage, mainly in GPUs.

REFERENCES

- [1] J. Demmel, P. Ahrens, and H. D. Nguyen, "Efficient reproducible floating point summation and BLAS," Tech. Rep. UCB/EECS-2016-121, EECS Department, University of California, Berkeley, Jun 2016.
- [2] "Hydrodynamics Challenge Problem, Lawrence Livermore National Laboratory," Tech. Rep. LLNL-TR-490254.
- [3] "OP-DSL: The Oxford Parallel Domain Specific Languages," 2015. <https://op-dsl.github.io>.

Investigation of cell motility

Gergely SZABÓ

(Supervisor: András HORVÁTH)

Pázmány Péter Catholic University, Faculty of Information Technology and Bionics

50/a Práter street, 1083 Budapest, Hungary

szabo.gergely@itk.ppke.hu

Abstract—In this paper we present the theoretical background of automated cell detection, tracking and the detection of cell inheritance as well as measurement of cell motility based on the tracking results. We also present multiple deep learning based solution for the detection of yeast cells on phase-contrast microscopy images as well as three cell inheritance detection algorithms. For now these methods are solely trained and evaluated on images of yeast cell colonies, but in the future we are planning to investigate similar solutions on human cancer cell colonies, on which the measurement of cell motility would be much more significant.

I. INTRODUCTION

The tracking of cells on cell colonies is a rather frequently used method amongst biologists. The individual or the overall motility of the tracked cells can be a great indicator for the efficacy of certain drugs and other treatments, thus the measurement of cell motility can not only be a research opportunity, but a validation tool as well. [1]

However the tracking of cells is still frequently performed manually due to the unreliability of the available tracking algorithms amongst other reasons. Manual tracking does not only require large amounts of time and manpower but it can lead to biased decisions, thus any algorithm capable of substituting or at least helping the manual work could be useful.

Our short-term goal is to create a pipeline capable of detecting yeast cells on phase-contrast microscopy recordings via segmentation, connecting the individual detections so that any number of cells could be traced, and handling the cell divisions, which results in the appearance of new cells. In case of yeast cells the segmentation and the calculation of inheritance at the instance of cell divisions are the more difficult tasks, and after a proper segmentation the tracking of the cells is easy due to their almost stationary behavior. However cancer cells frequently exhibit much larger motility, and they can be also capable of rapid shape changes, thus our long-term goal of cancer cell tracking might be a far more difficult challenge.

II. EXPERIMENTAL METHODS

Due to not having quantitative measurement results on the developed pipeline yet, we do not propose any of our experimental methods to be a proven solution to the previously described task. However some parts of the pipeline do show promising partial results.

For the segmentation of yeast cells we developed a U-net [2] and a Detectron2 [3] based solution, and for the latter one we already have some baseline measurement results. The tracking of the detected cells is based on the generation of single representative points for each cell, and then the distance of these potentially multidimensional points can be measured

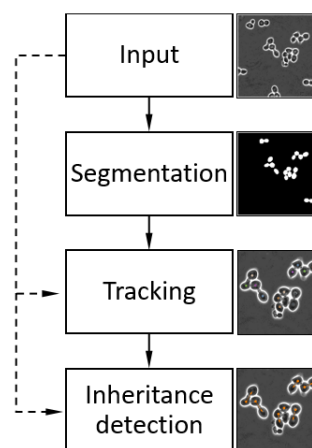


Fig. 1. A simplified data flow diagram of the designed pipeline. According to our plans, this pipeline will be complemented with at least a motility calculation stage, and possibly several other stages.

between adjacent frames. To improve the tracking of certain cells we also implemented a simple interpolation step to make the trace continuous in time.

For the detection of inheritance during cell division we implemented a simple L^2 distance based solution to serve as a baseline, and we also implemented two other methods which take into consideration the possible flow of fluids between the two cells to a certain degree.

We also described three possible metrics for the measurement of cell motility, however these measurement would not make much sense on yeast cell as they have very low motility. On the other hand we are planning to do similar measurements on cancer cell recordings on which the accurate measurement of cell motility could be a tool for the validation of anti-metastatic drugs and other treatments.

REFERENCES

- [1] Palmer, Trenis D., et al. "Targeting tumor cell motility to prevent metastasis." *Advanced drug delivery reviews* 63.8 (2011): 568-581.
- [2] Ronneberger, Olaf, Philipp Fischer, and Thomas Brox. "U-net: Convolutional networks for biomedical image segmentation." *International Conference on Medical image computing and computer-assisted intervention*. Springer, Cham, 2015.
- [3] Wu, Yuxin, et al. "Detectron2." (2019).

Computing different realizations of linear dynamical systems with embedding Eigenvalue assignment

Gergely SZLOBODNYIK

(Supervisor: Gábor SZEDERKÉNYI)

Pázmány Péter Catholic University, Faculty of Information Technology and Bionics

50/a Práter street, 1083 Budapest, Hungary

szlobodnyik.gergely@itk.ppke.hu

Abstract—In this paper we investigate realizability of discrete time linear dynamical systems (LDSs) in fixed state space dimension. We examine whether there exist different $\Theta = (A, B, C, D)$ state space realizations of a given Markov parameter sequence Y with fixed B, C and D state space realization matrices. Full observation is assumed in terms of the invertibility of output mapping matrix C . We prove that the set of feasible state transition matrices associated to a Markov parameter sequence Y is convex, provided that the state space realization matrices B, C and D are known and fixed. Under the same conditions we also show that the set of feasible Metzler-type state transition matrices forms a convex subset. Regarding the set of Metzler-type state transition matrices we prove the existence of a structurally unique realization having maximal number of non-zero off-diagonal entries. Using an eigenvalue assignment procedure we propose linear programming based algorithms capable of computing different state space realizations. By using the convexity of the feasible set of Metzler-type state transition matrices and results from the theory of non-negative polynomial systems, we provide algorithms to determine structurally different realization. Computational examples are provided to illustrate structural non-uniqueness of network-based LDSs.

This brief paper is from the paper: G. Szlobodnyik, G. Szederkényi, "Computing Different Realizations of Linear Dynamical Systems with Embedding Eigenvalue Assignment", submitted to *Acta Cybernetica*

Keywords—Linear Dynamical Systems, Parameter Identification, Structured Systems, Networks, Convex Optimization

I. SUMMARY

Many problems in computer science and engineering involve sequences of real-valued multi-variate observations. It is often assumed that observed quantities are correlated with some underlying latent (state) variables that are evolving over time. Considering linear dependencies among the latent states and the observed variables leads us to linear dynamical systems. The application of linear systems is ubiquitous, ranging from dynamical systems modeling to time series analysis, including econometrics, meteorology, telecommunication, biomedical signal processing, or social network dynamics.

In this paper we investigate realizability and structural properties of discrete time linear time invariant dynamical systems. We examine structural implications of non-unique realizability on the interaction pattern of the state variables as they are encoded in the state transition matrix. We examine the non-uniqueness of state transition matrix of LDSs. Assuming fixed input matrix B and invertible observation matrix C we prove that the feasible set of system matrices formulate a convex set. We devote particular attention to LDSs of state transition matrices that are constrained to be of Metzler property. We prove the convexity of the feasible set of state transition matrices provided that the Metzler constraint is posed. Using the eigenvalue assignment procedure we formulate a convex

optimization based procedure that can be efficiently employed to find different realizations of LDSs. Assuming 2Computing LDS Realizations with Embedding Eigenvalue Assignment the Metzler property and making use of the convexity of the feasible set of system matrices we provide algorithms capable of determining structurally different dynamically equivalent state space realizations.

REFERENCES

- [1] J. Hamilton, "Time Series Analysis", Princeton University Press, 1994.
- [2] L. Ljung, T. Glad, "Modeling dynamical systems", PTR Prentice-Hall, 1994.
- [3] Y. Sun, Z. Ji, K. Liu, "Event-Based Consensus for General Linear Multiagent Systems under Switching Topologies", *Complexity*, 2020.
- [4] Jijun QU, et al. "Fast consensus seeking on networks with antagonistic interactions", *Complexity*, 2018.

PROGRAM 3
FEASIBILITY OF ELECTRONIC AND OPTICAL
DEVICES, MOLECULAR AND
NANOTECHNOLOGIES,
NANO-ARCHITECTURES, NANOBIONIC
DIAGNOSTIC AND THERAPEUTIC TOOLS

Head: Árpád CSURGAY

Optimal design of a Van Atta array for reflector applications

András ESZES

(Supervisor: Zsolt SZABÓ)

Pázmány Péter Catholic University, Faculty of Information Technology and Bionics

50/a Práter street, 1083 Budapest, Hungary

esz.es.andras@itk.ppke.hu

Abstract—The Van Atta arrays have the exceptional property that the angle of the incident wave and the angle of the back reflected wave are identical, hence the Van Atta arrays could be considered as retrodirective surfaces. This exceptional property can be used in many areas, e.g.: sensor applications, self-driving vehicles.

In this paper after the initial considerations the full wave simulation results were detailed in accordance with the design steps of the optimal Van Atta array. The sizing of the interconnection lines were also introduced in their deep details as they are the key components of the designed array.

After the initial considerations of the group delays, several different type of delay lines were first considered (straight, meandered, Hilbert, a novel truncated Hilbert), then their numerical calculations were carried out with full-wave modeler (HFSS).

The designed array is constituting of 8 aperture coupled patch element [9] per row, and the array is operating at 10 GHz. The main purpose of the optimal design is to increase the array's operation range, to increase the monostatic RCS and to synchronize the group delays. The number of the rows could be choose freely, because there is no significant coupling between the rows.

In the future this Van Atta array will have an important role in comparison measurements, particularly in the validation of phase gradient metasurface (PGMS) and phase gradient metamaterial (PGM) based retrodirective surfaces.

Keywords—Reflector, Retrodirective array, Van Atta array, Meandered delay line, Hilbert delay line, Aperture coupled microstrip antenna

I. RESULTS

The finite element solver (FEM) was used for modeling the overall structure, the integral equation (IE) solver was used for modeling the individual components efficiently (radiator elements, interconnections).

The components of the designed array were modeled and optimized separately. For optimization purposes sequential non-linear programming (SNLP) method was applied as the main optimization method.

For the interconnection sizing, a simple parametric sweep was carried out. Finally, the overall structure that is constitute of the previously sized elements was modeled with FEM, the electrical parameters (Monostatic RCS, Bistatic RCS) then represented in the paper.

II. CONCLUSION

The designed Van Atta array is not yet optimal, due to the difficulty in the interconnection sizing (relatively small the microstrip-line size to the wavelength, initial problems with microstrip-lines near the edges). It could be a good solution

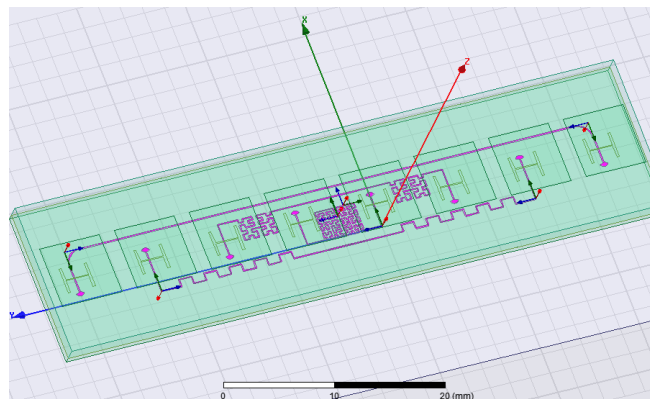


Fig. 1. Van Atta array

to improve a numerical algorithm which is fitted well to model extremely small components compared to the wavelength.

ACKNOWLEDGMENT

The authors would like to thank to the Grante Antenna Development and Production Corporation (Esztergom-Kertvaros) for providing the ANSYS-HFSS 15 full-wave modeler for the numerical calculations.

REFERENCES

- [1] Atta, L. C. V., "Electromagnetic reflector," U.S. Patent, Vol. 2908, 1959."
- [2] M. Kalaagi and D. Seetharamdoo, "Retrodirective metasurface operating simultaneously at multiple incident angles," 12th European Conference on Antennas and Propagation (EuCAP 2018), London, 2018, pp. 1-5, doi: 10.1049/cp.2018.0545.
- [3] Alharbi, M.; Alyahya, M.A.; Ramalingam, S.; Modi, A.Y.; Balanis, C.A.; Birtcher, C.R. Metasurfaces for Reconfiguration of Multi-Polarization Antennas and Van Atta Reflector Arrays. *Electronics* 2020, 9, 1262. <https://doi.org/10.3390/electronics908126>
- [4] Nanfang Yu et. al. "Light Propagation with Phase Discontinuities: Generalized Laws of Reflection and Refraction" *Science* 21 Oct 2011: Vol. 334, Issue 6054, pp. 333-337 DOI: 10.1126/science.1210713

Optimizations in Neural Network Architectures

András FÜLÖP

(Supervisors: András HORVÁTH, György CSABA)

Pázmány Péter Catholic University, Faculty of Information Technology and Bionics

50/a Práter street, 1083 Budapest, Hungary

fulop.andras@itk.ppke.hu

Abstract—Nowadays, various neural networks are used very successfully in solving many practical problems such as medical image processing or self-driving cars. One of the neural networks is the convolutional neural network, which performs particularly well in image processing tasks. The main computation of convolutional neural networks is convolution. In this paper, we introduce a method, which can optimise this operation.

Keywords—neural network; convolution; optimisation

I. INTRODUCTION

Nowadays the computers are powerful in several tasks, in special cases, the human brain is better than computers and the biological systems boast many intelligent solutions for problem-solving, like vision or face recognition and motor control.

The basis of commonly used deep learning methods are similar. The architectures apply a nonlinear transformation on inputs and use what they learn to create statistical models as outputs and the iterations continue until the outputs have reached an acceptable level of accuracy. One of the most commonly used deep learning methods is the convolutional neural network. [1] [2] [3] [4]

II. CONVOLUTIONAL NEURAL NETWORKS

There are four main operations in convolutional neural network:

- 1) convolution
- 2) non-linearity
- 3) pooling
- 4) classification

III. CONVOLUTION

In the case of convolution, we compute an element-wise multiplication between two matrices and add the multiplication outputs to get the final integer which forms a single element of the output matrix.

IV. EXPONENTIAL LINEAR UNIT IN FREQUENCY DOMAIN

In [5], an accurate frequency domain training architecture is proposed for training CNN in the Fourier domain.

The output of the Fourier domain exponential linear unit function is saturated at equiangular sampling points along the spiral on the Z plane. [5]

ACKNOWLEDGEMENTS

I would like to thank my supervisors András Horváth and György Csaba for the continuous support of my work and for their expert advice. Without their precious support it would not be possible to conduct this research.

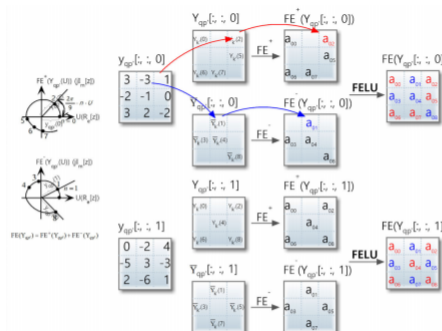


Fig. 1. Fourier domain exponential linear unit. [5]

REFERENCES

- [1] Y. Bengio, A. C. Courville, and P. Vincent, “Unsupervised feature learning and deep learning: A review and new perspectives,” *CoRR, abs/1206.5538*, vol. 1, p. 2012, 2012.
- [2] Y. LeCun, Y. Bengio, and G. Hinton, “Deep learning,” *nature*, vol. 521, no. 7553, p. 436, 2015.
- [3] A. Krizhevsky, I. Sutskever, and G. E. Hinton, “Imagenet classification with deep convolutional neural networks,” pp. 1097–1105, 2012.
- [4] Y. LeCun, B. E. Boser, J. S. Denker, D. Henderson, R. E. Howard, W. E. Hubbard, and L. D. Jackel, “Handwritten digit recognition with a back-propagation network;” in *Advances in neural information processing systems*, pp. 396–404, 1990.
- [5] J. Lin, L. Ma, and Y. Yao, “A fourier domain training framework for convolutional neural networks based on the fourier domain pyramid pooling method and fourier domain exponential linear unit,” *IEEE Access*, vol. 7, pp. 116612–116631, 2019.

Review of style transfer methods on ultrasound images

Péter MAROSÁN-VILIMSZKY

(Supervisor: Miklós GYÖNGY)

Pázmány Péter Catholic University, Faculty of Information Technology and Bionics

50/a Práter street, 1083 Budapest, Hungary

marosan.peter@itk.ppke.hu

Abstract—In the last decades, numerous ultrasound-based computer-aided diagnosis (CAD) tools were developed to support doctors and experts. While these algorithms often perform well during the segmentation or classification of a single data set, it is still challenging to achieve similarly high performance for recordings from more than one image data set. Neural style transfer, a novel technique of deep learning can ensure the linkage between different image sets by detaching style information from the image content. The possibility of style transfer between medical images increases the robustness of CAD tools.¹

Keywords-neural style transfer; computer aided diagnosis; ultrasound imaging; skin lesion

I. INTRODUCTION

Computer aided diagnosis (CAD) tools gave promising solution for object segmentation and tissue differentiation.

Appearance of ultrasound images is highly dependent on the ultrasound imager tool, so the major part of CAD tools finds it challenging to achieve high performance on recordings from different data sets.

To handle this issue and increase robustness and efficiency of CAD tools, neural style transfer (NST) methods [1] [2] [3] [4] were applied, since they are able to extract the style and content information of a given image.

II. NEURAL STYLE TRANSFER TECHNIQUES

NST is a deep learning-based optimization technique, working with two inputs, such as a content (I) and a style (J) image.

The content and style images are fed through a certain convolutional neural network (CNN) and the net activations are sampled at given layers of the architecture. Early and middle convolutional layers represents the style of the input image, while late ones store information about its content. The aim of NST techniques is to construct an image (K) with the content of I and the style of J represented by a Gramian matrix, using an iterative optimization method.

Main application fields of NST algorithms are data augmentation, image reconstruction, segmentation and classification. Latter algorithms can also be used as evaluation methods to measure the effectiveness of the NST techniques and quantify their performance.

III. A POTENTIAL ULTRASOUND-BASED APPLICATION

NST algorithms make images more similar to each other in appearance, while keeping the original structure of the image. It is the key of a robust automated segmentation algorithm. Two images (Harcsa and Hitachi) were selected to examine the efficiency of the operation of NST. Figure 1 presents how the

NST algorithm combines the two images and constructs a new one. Although quantitative evaluation was not applied on the output image yet, it possesses the resolution of a Hitachi image in aspect of speckle size, while the content of the original Harcsa image is also preserved.

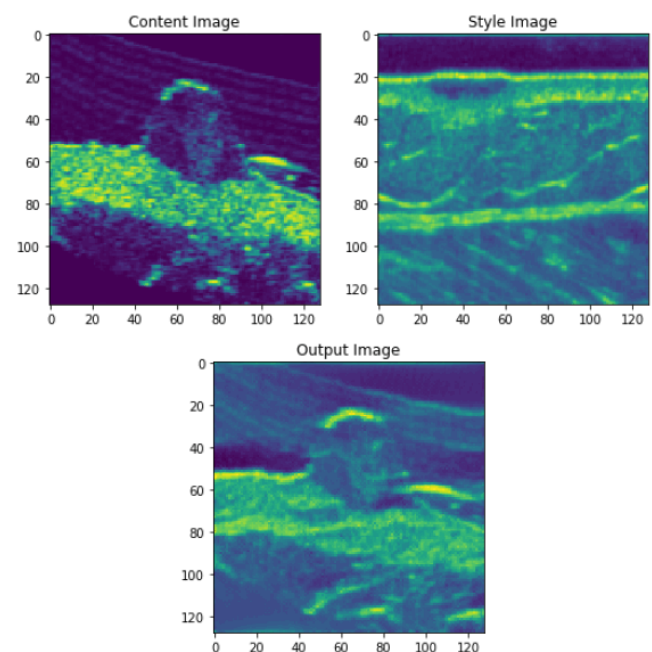


Fig. 1. Operation of neural style transfer (NST) on ultrasound skin lesion images. The content image was collected by a low-cost portable tool (Harcsa), while the style image was recorded by a commercial Hitachi imager. The output image shows the lesion recorded by Harcsa, but with the appearance parameters of a Hitachi image.

REFERENCES

- [1] L. A. Gatys, A. S. Ecker, and M. Bethge, “A neural algorithm of artistic style,” *arXiv preprint arXiv:1508.06576*, 2015.
- [2] Y. Jing, Y. Yang, Z. Feng, J. Ye, Y. Yu, and M. Song, “Neural style transfer: A review,” *IEEE transactions on visualization and computer graphics*, vol. 26, no. 11, pp. 3365–3385, 2019.
- [3] A. Semmo, T. Isenberg, and J. Döllner, “Neural style transfer: A paradigm shift for image-based artistic rendering?,” in *Proceedings of the symposium on non-photorealistic animation and rendering*, pp. 1–13, 2017.
- [4] Y. Li, N. Wang, J. Liu, and X. Hou, “Demystifying neural style transfer,” *arXiv preprint arXiv:1701.01036*, 2017.

¹The collaboration with Jedlik Innováció Kft under the GINOP-2.1.7-15-2016-02201 programme is gratefully acknowledged.

Stochastic micromagnetic simulations of invertible logic gates

Tamás RUDNER

(Supervisor: György CSABA)

Pázmány Péter Catholic University, Faculty of Information Technology and Bionics

50/a Práter street, 1083 Budapest, Hungary

rudner.tamas@itk.ppke.hu

Abstract—Nanomagnetic logic (NML) devices are shown to have low power consumption. The information throughout a NML device is stored and processed through magnetic interactions between magnetic dots. The motivation behind building two-way logic gates is coming from a different computational phenomena, called self-organising logic gates, which is a memcomputing-based architecture. By leveraging thermal fluctuations as stochastic ferromagnetism we can build such invertible logic gates to tackle some interesting computational challenges.

Keywords—two-way logic functions, nanomagnetic logic devices, majority voting, stochastic ferromagnetism

I. INTRODUCTION

In the recent years, a new paradigm, called memcomputing has risen[1], which puts the memory inside the computational unit to bypass the bottleneck of moving the data between the processing and memory units. Two way logic gates are theoretically capable of solving computationally hard (NP) problems using polynomial scaling resources and time.

II. TWO-WAY NANOMAGNETIC MAJORITY LOGIC GATES

Nanomagnetic logic gates utilise majority voting to calculate the magnetisation of the computing dot, based on the magnetisation vector of the computing cell's neighbours. At $0K$ the solution to these systems is deterministic, but for complex circuits, stochastic gradient descent algorithm is needed, introducing thermal fluctuations. They have no set input/output terminals and the data can flow through them in both direction.

III. RESULTS

To test the majority gates, I have carried out two different experiments. One for a single NAND gate, and one for a linked NAND gate which together form an AND gate. After statistical analysis, the probabilistic machine which is the result of the thermal fluctuation actually spends the majority if its simulation time in the logically coherent states.

IV. CONCLUSION

The implemented gates worked within their limitations, but other experiments will be performed, such as traversing the whole energy landscape to establish a greater understand of the stable states of the system. Another interesting challenge with the nanomagnetic two-way gates is that building more complex circuits might not work properly and they might stuck in metastable states.

T. RUDNER, "Stochastic micromagnetic simulations of invertible logic gates" in *PhD Proceedings – Annual Issues of the Doctoral School, Faculty of Information Technology and Bionics, Pázmány Péter Catholic University – 2021*. G. Prószéky, G. Szederkényi Eds. Budapest: Pázmány University ePress, 2021, p. 57. This research has been partially supported by the European Union, co-financed by the European Social Fund (EFOP-3.6.3-VEKOP-16-2017-00002).

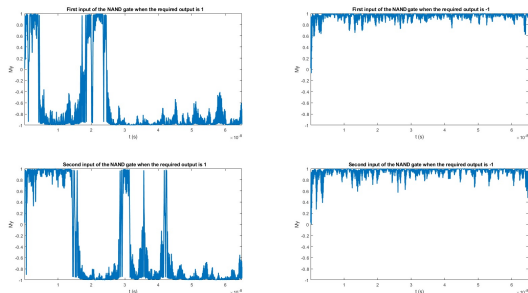


Fig. 1. This figure sums up the simulation of a backwards-operating NAND gate. Here it can be seen that in case if the required output is -1 since there is only one possible solution (both inputs should be 1), the two inputs are close to 1 on the left two figures. If the required output is 1 , then we have three possible solutions and we can see that the two input dots are fluctuating between -1 and 1 .

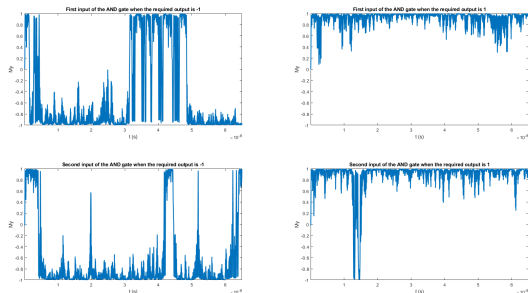


Fig. 2. In case of the AND gate, somewhat similarly to the single NAND gate, when there was only a single possible logically consistent state the dynamic of the model is strictly better. However in case if we set the desired output of the AND gate -1 , we can get three possible consistent states, so we can see the fluctuation in the M_y magnetic component. Evidently the system does not spend too much time in the states when both of the inputs were 1 which is a logically inconsistent state.

REFERENCES

- [1] F. L. Traversa and M. Di Ventra, "Universal memcomputing machines," *IEEE Transactions on Neural Networks and Learning Systems*, vol. 26, no. 11, pp. 2702–2715, 11 2015.
- [2] F. Traversa and M. Di Ventra, "Polynomial-time solution of prime factorization and np-complete problems with digital memcomputing machines," *Chaos: An Interdisciplinary Journal of Nonlinear Science*, vol. 27, p. 023107, 02 2017.
- [3] G. Csaba, M. Becherer, and W. Porod, "Development of cad tools for nanomagnetic logic devices," *International Journal of Circuit Theory and Applications*, vol. 41, no. 6, pp. 634–645, 2013. [Online]. Available: <https://onlinelibrary.wiley.com/doi/abs/10.1002/cta.1811>
- [4] G. Csaba, A. Imre, G. H. Bernstein, W. Porod, and V. Metlushko, "Nanocomputing by field-coupled nanomagnets," *IEEE Transactions on Nanotechnology*, vol. 1, no. 4, pp. 209–213, 2002.

PROGRAM 4

HUMAN LANGUAGE TECHNOLOGIES, ARTIFICIAL UNDERSTANDING, TELEPRESENCE, COMMUNICATION

Head: Gábor PRÓSZÉKY

Improving the effectiveness of open-set recognition with generated negative inputs

András Pál HALÁSZ

(Supervisors: Kálmán TORNAI, Péter Norbert SZOLGAY)

Pázmány Péter Catholic University, Faculty of Information Technology and Bionics

50/a Práter street, 1083 Budapest, Hungary

halasz.andras@itk.ppke.hu

Nowadays, various machine learning methods provide excellent results in different classification and recognition tasks, reaching or even exceeding the human level in numerous cases. The experiments yielding these results were conducted in a closed-set scenario, i.e., the assumption that all classes are known during training. A more realistic situation is the open-set case when new classes can appear during testing, and our model has to reject them, which is a great challenge. The problem of Open Set Recognition was formalized by Scheirer et al. **Scheirer2013TowardOS**

I have implemented a distance-based method to give another solution to this problem. The goal was to train a function that transforms the inputs into a feature space, in which space the features of the same class. The assumption was that in this setup, the unknown samples - as these were not trained to occupy any specific place - will "land" randomly in this space; thus these will be distinguishable from the positive samples with very high probability. In practice, however, the trained function contracted the whole input space into the small blobs of the classes. This way all the unknown samples became close to the samples of one known class.

To prevent this, I propose to use generated negative inputs. This way, we can train the model so that it will put the generated samples far away from every positive sample. As a result, during the test, the actual unknown samples will also be distinguishable from every class, thus recognized as unknown.

Generative Adversarial Networks **gan** are the most common and successful ways to generate such data. There are many variants of it, which can be used, mainly these are in the focus of my experiments.

During training the network, calculating the loss function based on the distances of individual instances does not seem to be as good as using fixed class means like in **ca**; however, this needs further investigation.

The model, after training, can very well separate the real known and generated samples (also the known classes from each other), which were not used during training; however, exhaustive testing in real environments (real unknown samples) are yet to be made, as well as the comparison of the different generative models.

Applying Deep Learning Algorithms for Azerbaijani Named Entity Recognition Dataset

Kamran IBIYEV

(Supervisor: Gábor PRÓSZÉKY)

Pázmány Péter Catholic University, Faculty of Information Technology and Bionics

50/a Práter street, 1083 Budapest, Hungary

ibiyev.kamran@itk.ppke.hu

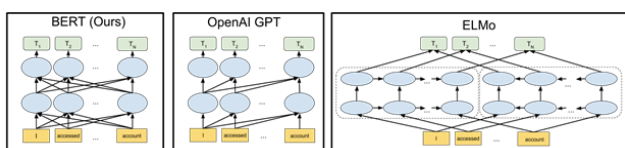
Abstract—Abstract — Named Entity Recognition is among the key areas of Natural Language Processing, specialized on detecting the entities in texts. Our purpose is to do a cross-platform knowledge transfer between the languages and compare the results. For that, we apply the multilingual BERT and XLM-RoBERTa based language models to the NER task using the FLAIR interface. WikiANN, a ‘silver standard’ NER dataset platform which generates the entities from Wikipedia. It contains entities for various languages as well as Azerbaijani language. In this research we focus on Azerbaijani language.

Keywords—Named Entity Recognition; BERT; FLAIR; WikiANN

I. INTRODUCTION

Named Entity Recognition is a one of the primary fields of the Information Extraction that can determine the entities in the given text. It is the basic part of many NLP tasks and is used in various applications like information extraction [1], question answering, document de-identification, machine translation, conversational models and so on. The task of Named Entity Recognition is to detect and group the entities in the text based on the categories like organizations, dates, times, persons, locations, etc.

There are context-free and contextual pre-trained representations, while contextual representations can be unidirectional or bidirectional. BERT, is a contextual and bidirectional language representation model as it is obvious from its abbreviation [2]. The Figure indicates BERT’s neural network structure and compares it with previous state-of-the-art contextual pre-training methods. The arrows show the information flow from one layer to the next. The green section displays the eventual contextualized representation of the input token.



Source: Adapted from [3]

Fig. 1: Comparison of BERT, OpenAI GPT and ELMo

The main difference between BERT and the other two models is that BERT model is collectively conditioned on both left and right context in all layers. In this research, we trained models based on M-BERT (Multilingual BERT) and XLM-RoBERTa.

II. EXISTING SOLUTIONS

FLAIR framework procure a simple UI with the possibilities of training and distribution of state-of-the-art sequence labelling, language models, text classification and so on.

Wikipedia is a huge multi-lingual portal with 295 languages, 35 million articles which contains 3 billion words, and it includes inherently annotated markups and plenty of information. Therefore, we use WikiAnn datasets, which were automatically created by extracting and classifying anchor links on Wikipedia for 282 languages,

Overall, regardless of some mistagging and other minor issues, WikiAnn is very useful and only existing NER dataset that contains a huge amount of language.

Although FLAIR interface provides some datasets that make possible to load with one line of code, we will use the WikiAnn datasets to train our model. We can train your model with more than one language, MultiCorpus object. After creating the (multi)corpus we should split our dataset to dev, test and train parts. Then we can start the learning process with the help of FLAIR’s LanguageModelTrainer class. Subsequently, it is possible to do a finetuning on our language model in place of starting a new one without changing any other code.

EVALUATION

Based on the evaluation results of the trained models we can state that in terms of the recall XLM-RoBERTa based model achieved a better result. In contrast with it, the M-BERT based model is better in terms of precision.

ACKNOWLEDGEMENTS

This research is supported by the European Union, co-financed by the European Social Fund (EFOP research studentship).

I express appreciation to my supervisors, Gábor Prószéky and Attila Novák, for their continuous guidance and professional advice.

REFERENCES

- [1] J. Raiman and O. Raiman, “Deeptype: Multilingual entity linking by neural type system evolution,” in *Proceedings of the Thirty-Second AAAI Conference on Artificial Intelligence, New Orleans, Louisiana, USA, February 2-7, 2018* (S. A. McIlraith and K. Q. Weinberger, eds.), pp. 5406–5413, AAAI Press, 2018.
- [2] M. E. Peters, M. Neumann, M. Iyyer, M. G. 0001, C. Clark, K. Lee, and L. Zettlemoyer, “Deep contextualized word representations,” in *Proceedings of the 2018 Conference of the North American Chapter of the Association for Computational Linguistics: Human Language Technologies, NAACL-HLT 2018, New Orleans, Louisiana, USA, June 1-6, 2018, Volume 1 (Long Papers)* (M. A. Walker, H. Ji, and A. Stent, eds.), pp. 2227–2237, Association for Computational Linguistics, 2018.
- [3] J. Devlin, M.-W. Chang, K. Lee, and K. Toutanova, “Bert: Pre-training of deep bidirectional transformers for language understanding,” in *Proceedings of the 2019 Conference of the North American Chapter of the Association for Computational Linguistics: Human Language Technologies, NAACL-HLT 2019, Minneapolis, MN, USA, June 2-7, 2019, Volume 1 (Long and Short Papers)* (J. Burstein, C. Doran, and T. Solorio, eds.), pp. 4171–4186, Association for Computational Linguistics, 2019.

Using linguistic transfer to improve abstractive Arabic text summarization

Mram KAHLA

(Supervisor: Gábor PRÓSZÉKY)

Pázmány Péter Catholic University, Faculty of Information Technology and Bionics

50/a Práter street, 1083 Budapest, Hungary

kahla.mahmoud.mram@itk.ppke.hu

Abstract—While abstractive summarization in certain languages, like English, has already reached fairly good results, progress in Arabic is still in baby shoes. This is unfortunate because with its huge amount of users and a massive amount of texts on one hand, and with its linguistic peculiarities capable to greatly improve NLP research on the other, Arabic might prove immensely important in this field. And that is why research is now being conducted on abstractive Arabic text summarization. In this research, we show how finetuning BERT can be applied to the Arabic language for abstractive text summarization. Since there are no major text corpora to work with, initially, we build a novel dataset of Arabic articles and their abstractive summaries, we managed to reach for far corpus reaching up to more than 21 thousand items each consisting of an article and its corresponding lead. Using our own corpus, we finetuned multilingual BERT[1] (which amongst the many supported languages has an Arabic feature as well) for abstractive Arabic text summarization. We also fine-tuned AraBERT[2] (which is pre-trained BERT specifically for the Arabic language) for abstractive Arabic text summarization using our own corpus. After that, we propose a transfer lingual approach that allows knowledge transfer. This approach is built to improve, fine-tune the already fine-tuned M-BERT for Hungarian to Arabic, and do the same fine-tuning for English to Arabic. The results of the ROUGE metric and manual evaluation showed that the proposed transfer lingual approach achieved state-of-the-art results.

I. RESULTS

Measuring the performance of a summarization system can be done through either automatic or manual evaluation. We evaluated our experiments using the ROUGE automatic metric and compared them to other abstractive Arabic summarization results as shown in Table I,II. Obtained results indicate that the advantage we got from our proposed method achieves new state-of-the-art results compared to previous scoring systems.

| Model | ROUGE-1 | ROUGE-2 | ROUGE-L |
|------------------|---------------|--------------|---------------|
| AraBERT | 6.121 | 0.117 | 6.121 |
| mBERT | 5.134 | 0.186 | 5.134 |
| mBERT+HUN | 6.466 | 0.261 | 6.462 |
| mBERT+ENG | 16.363 | 2.524 | 16.363 |

TABLE I
ROUGE RECALL RESULTS OF ABSTRACTIVE SUMMARIZATION

Since the reliability of automatic metrics is often perceived as insufficient, we conducted a human evaluation. Based on the annotators, the already fine-tuned multilingual BERT for English to Arabic usually comes very close to the original lead. Clarity and language proficiency is rarely a problem. The already fine-tuned multilingual BERT for Hungarian to Arabic has an almost equally good result, however, usually in a very different way. These two models are very promising.

M. KAHLA, "Using linguistic transfer to improve abstractive Arabic text summarization" in *PhD Proceedings – Annual Issues of the Doctoral School, Faculty of Information Technology and Bionics, Pázmány Péter Catholic University – 2021*. G. Prószéky, G. Szederkényi Eds. Budapest: Pázmány University ePress, 2021, p. 61. This research has been partially supported by the European Union, co-financed by the European Social Fund (EFOP-3.6.3-VEKOP-16-2017-00002).

| Model | ROUGE-1 | ROUGE-2 | ROUGE-L |
|------------------|--------------|-------------|--------------|
| TRANS.ABS* | 6.93 | 1.78 | 6.88 |
| mBERT+ENG | 12.61 | 2.11 | 12.61 |

TABLE II
COMPARISON OF ROUGE F1 SCORES BETWEEN EXISTING ABSTRACTIVE ARABIC SUMMARIZATION MODELS. RESULT WITH * MARK IS TAKEN FROM THE CORRESPONDING PAPER.

Especially that some of the summaries cannot be determined whether they are written by human or machine. The multilingual BERT shows grammatical and contextual errors. Sometimes the meaning became the opposite of the article, sometimes the syntax falls apart. The AraBERT model is by far the weakest and clearly insufficient for usage. There is a high tendency to turn the meaning of the text around. (See Figure 1)

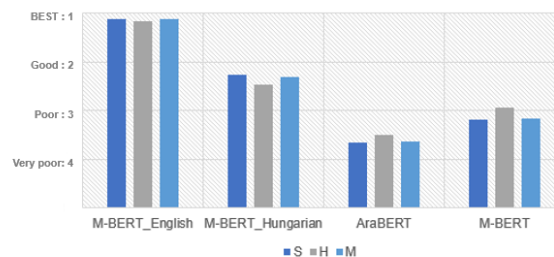


Fig. 1. Ranking results

ACKNOWLEDGEMENTS

The research is supported by the European Union and co-financed by the European Social Fund EFOP-3.6.3-VEKOP16-2017-00002. I would like to express the deepest gratitude to Professor Gábor Prószéky, main supervisor, Zizian Győző Yang, and Attila Novák for their unrelenting support. I would also like to thank Dániel Sógor and Youssef Messaoudi for their great work in the manual evaluation process.

REFERENCES

- [1] J. Devlin, M.-W. Chang, K. Lee, and K. Toutanova, "Bert: Pre-training of deep bidirectional transformers for language understanding," *arXiv preprint arXiv:1810.04805*, 2018.
- [2] W. Antoun, F. Baly, and H. Hajj, "AraBERT: Transformer-based model for Arabic language understanding," in *Proceedings of the 4th Workshop on Open-Source Arabic Corpora and Processing Tools, with a Shared Task on Offensive Language Detection*, (Marseille, France), pp. 9–15, European Language Resource Association, May 2020.

State Space Reconstruction with Generative Models

András Attila SÜLYOK

(Supervisors: Kristóf KARACS, Péter SZOLGAY)

Pázmány Péter Catholic University, Faculty of Information Technology and Bionics

50/a Práter street, 1083 Budapest, Hungary

sulyok.andras.attila@itk.ppke.hu

I. INTRODUCTION

Partially Observable Markov Decision Processes (POMDPs, [1]) represent situations when it is either impossible or too costly to collect all information about the environment that would be necessary to make a perfect decision. It has been used in medical and healthcare, educational contexts, but simple robot control and automation problems can be described using its formalism.

It is also a challenging problem, since many possible environment states have to be considered, hence straightforward planning or model-based methods cannot be used.

In this work, we focus on a special class of POMDPs inspired by Reconnaissance Blind Chess [2].

A. Reconnaissance Blind Chess

Reconnaissance Blind Chess (RBC, [2]) is a variant of chess where neither of the two players can see the other's moves. Instead, before each move, they can choose a 3×3 square that is revealed to them (neither the location, nor the contents of this square is not revealed to the opponent). There is no concept of check, the goal is simply to capture the opponent's king.

This makes it necessary to develop an effective exploration strategy: the agent has to figure out the location of opponent pieces; on the other hand, it has to move in such a way so as to minimize prediction on the opponent's part.

This has obvious applications in any artificial or natural competition where there is a limited window to observe the others' strategies.

Note that it is still a symmetric problem: both players have the same limited observation capability based on which to make moves.

Since each player has only a belief over the actual board configuration (the location of all the pieces) and it is in each player's interests to manipulate the other one's belief, the state space effectively consists of not only the board configuration, but the opponent's current belief as well.

Markowitz et al. [2] estimate the number of possible opponent states in any given perceived state to be about $1.3 \cdot 10^{68}$ based on the possible observable histories: this makes RBC as complex as most of the tasks solved by model-free RL algorithms recently, while involving much larger uncertainty.

A further complication is that the board state changes with time: it changes after each sensing by two moves, only one (the player's own) is visible.

The specific class of POMDPs we are addressing in this work (and of which RBC is an example) is:

- non-Markovian, all of the observation and action history is needed for a good policy;
- the observation is a projection of the state and the agent has direct control over it;

- the probability of the current state given the history of past observations and actions is multimodal
- there is a large amount of gameplay and also a good engine available for the fully observable case.

II. PROPOSED AGENT

We propose to use a separate reconstruction module to update the belief, ie. calculate β_{t+1} from β_t , a_t and o_{t+1} .

A naïve solution is to train a feedforward neural network with cross-entropy loss, using a one-hot representation of the states. However, this assumes that the squares in a chessboard are independent: it will learn to output a marginal distribution of β_t for each square.

This representation throws away information: for example, when the opponent first moves one of their knights and the agent only observes that the knight disappeared from its original position (as in Figure 1, there are two possible targets with probabilities p_1 and p_2). But this representation in general assigns positive probability to the knight being on both ($p_1 p_2$) or neither ($(1 - (1 - p_1)(1 - p_2))$) of the two squares at the same time.

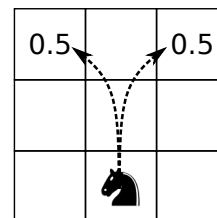


Fig. 1. Illustration of the difference between the representations of marginal and the joint distribution: the knight can move onto either of the two squares with probability 0.5. However, just storing the probabilities for each piece for each cell would imply that there is 0.25 change of the knight being at both places at the same time.

ACKNOWLEDGEMENT

This research has been supported by the European Union, co-financed by the European Social Fund through the grant EFOP-3.6.3-VEKOP-16-2017-00002.

REFERENCES

- [1] E. J. Sondik, "The optimal control of partially observable markov processes over the infinite horizon: Discounted costs," *Operations Research*, vol. 26, no. 2, pp. 282–304, 1978. [Online]. Available: <http://www.jstor.org/stable/169635>
- [2] J. Markowitz, R. W. Gardner, and A. J. Llorens, "On the complexity of reconnaissance blind chess."
- [3] R. S. Sutton and A. G. Barto, *Reinforcement learning: An introduction*, 2nd ed. MIT press, 2018. [Online]. Available: <http://incompleteideas.net/book/the-book-2nd.html>

PROGRAM 5

ON-BOARD ADVANCED DRIVER ASSISTANCE SYSTEMS

Heads: Csaba REKECZKY, Ákos ZARÁNDY

What to do after adversarial attacks detection?

Jalal ALAFANDI

(Supervisor: András HORVÁTH)

Pázmány Péter Catholic University, Faculty of Information Technology and Bionics

50/a Práter street, 1083 Budapest, Hungary

alafandi.mohammad.jalal@itk.ppke.hu

Abstract—Adversarial attacks cause a lot of harm in machine learning applications affecting the decision making processes. Adversarial attack detectors can only protect the machine learning system from an erroneous decisions but it can't assist with the decision making polices. A class retriever algorithm is needed to post-process the adversarial sample retrieving the original class in time-critical secure applications. Recovering the original class after adversarial attacks detection is a new idea which is not investigated thoroughly in the literature. We will build a retriever which relies on the premise that counter adversarial attacks can be faster taking the adversarial samples back to their original classes.

I. INTRODUCTION

The first adversarial attack algorithm was introduced by [1] where the authors posed the challenge of securing neural network parameters which can be used to create an adversarial samples. Adversarial samples exploit the high dimensionality of the input perturbing the samples slightly in many directions, which the network were not exposed to, pushing the samples outside the geometrical manifolds of the classifier.

Adversarial samples are clean samples which have been modified with unperceived perturbations altering the response of a network leading to misclassification.



Fig. 1. The figure illustrates an adversarial attack with a very low intensity perturbation entirely unperceivable to the human eyes.

Most frequently used defenses against adversarial attacks are one of the three following methods: adversarial training [2], modifying the network architecture [3] or detection based approaches [4].

The first two approaches can only be applied while training the network increasing the network resilience against adversarial attacks. The last approach, adversarial attacks detection, is more viable and secure preventing faulty decisions.

As a starting step, adversarial attacks detectors are a good solution against such attacks for real world applications as it provides the highest accuracy considering the three mentioned methods. But it is not enough on its own to secure a reliable defence which doesn't only guard the autonomous system

against adversarial attacks but also help the system to make sound and reliable decisions.

II. CLASS RECOVERY

Non-detection defences are susceptible to vulnerability against counter-counter attacks exposing the system functionality to potential dysfunction in its protective shield [5]. We can't rely solely on detection based defences in a security based decision making procedures preventing us from using the system safely. Therefore, after the detection of adversarial attacks, a class retriever algorithm has to be installed yielding a more robust and flexible system.

[6] speculated that adversarial attacks push the clean sample to the edge of the decision boundary forcing the sample outside to be on the edge of the decision boundary of a different class. They based their idea on the premise that the network will force the training samples to the edge of the decision boundary after a correct classification.

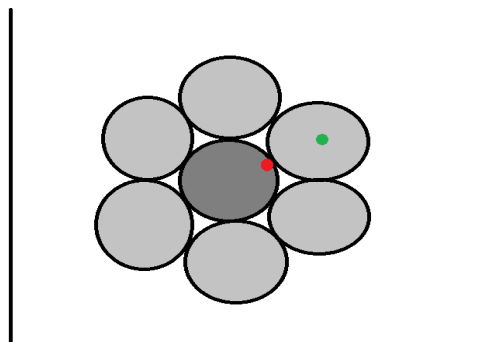


Fig. 2. A sketch of a two dimensional decision boundary of seven classes manifold. The green point is the original sample while the red point is the adversarial sample. We can see that the adversarial sample is closer to the original sample making the loss of the targeted counter attack, which is aiming to the original label, smaller.

REFERENCES

- [1] C. Szegedy, W. Zaremba, I. Sutskever, J. Bruna, D. Erhan, I. Goodfellow, and R. Fergus, "Intriguing properties of neural networks," 2013.
- [2] S. Sankaranarayanan, A. Jain, R. Chellappa, and S. N. Lim, "Regularizing deep networks using efficient layerwise adversarial training," 2018.
- [3] A. S. Ross and F. Doshi-Velez, "Improving the adversarial robustness and interpretability of deep neural networks by regularizing their input gradients," 2017.
- [4] J. Lu, T. Issaranon, and D. Forsyth, "Safetynet: Detecting and rejecting adversarial examples robustly," 2017.
- [5] N. Carlini and D. Wagner, "Adversarial examples are not easily detected: Bypassing ten detection methods," 2017.
- [6] A. Rozsa, M. Gunther, and T. E. Boult, "Towards robust deep neural networks with bang," 2018.

Deep learning for the segmentation of masonry wall images

Yahya IBRAHIM

(Supervisor: Csaba BENEDEK)

Pázmány Péter Catholic University, Faculty of Information Technology and Bionics

50/a Práter street, 1083 Budapest, Hungary

ibrahim.yahya@itk.ppke.hu

Abstract—In this paper we introduce a novel machine learning based fully automatic approach on the semantic analysis and documentation of masonry wall images, performing in parallel automatic detection and virtual completion of occluded or damaged wall regions, and brick segmentation leading to an accurate model of the wall structure. For this purpose, we propose a four-stage algorithm which comprises three interacting deep neural networks and a Watershed transform-based brick outline extraction step. At the beginning, a U-Net-based sub-network performs initial wall segmentation into brick, mortar and occluded regions, which is followed by a two-stage adversarial inpainting model. The first adversarial network predicts the schematic mortar-brick pattern of the occluded areas based on the observed wall structure, providing in itself valuable structural information for archeological and architectural applications. The second adversarial network predicts the pixels' color values yielding a realistic visual experience for the observer. Finally, using the neural network outputs as markers in a Watershed-based segmentation process, we generate the accurate contours of the individual bricks, both in the originally visible and in the artificially inpainted wall regions. Note that while the first three stages implement a sequential pipeline, they interact through dependencies of their loss functions admitting the consideration of hidden feature dependencies between the different network components. For training and testing the network a new dataset has been created, and an extensive qualitative and quantitative evaluation versus the state-of-the-art is given. The experiments confirmed that the proposed method outperforms the reference techniques both in terms of wall structure estimation and regarding the visual quality of the inpainting step, moreover it can be robustly used for various different masonry wall types.

Keywords—Masonry Wall; Inpainting; Segmentation; GAN; U-Net;

I. INTRODUCTION

Image-based analysis has recently shown a great potential in studying architectural structures, ancient artifacts, and archaeological sites: we can find several approaches on the classification of biface artifacts, architectural features, and historical items, and also on digital object reconstruction of historical monuments and materials.

By investigating masonry walls of buildings, bricks are considered as the vital components of the masonry structures. Accurate detection and separation of bricks is a crucial initial step in various applications, such as stability analysis for civil engineering, brick reconstruction, managing the damage in architectural buildings, and in the fields of heritage restoration and maintenance.

In this paper, we propose an end-to-end deep learning-based algorithm for masonry wall image analysis and virtual structure recovery. More specifically, given as input an image of a wall partially occluded by various irregular objects, our algorithm solves the following tasks in a fully automatic way:

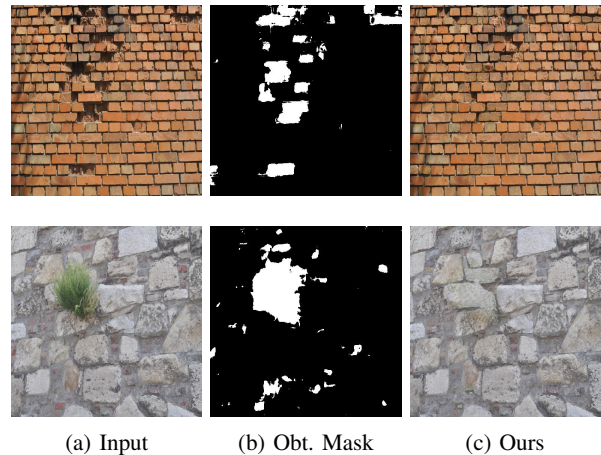


Fig. 1: Results of the proposed algorithm on real scenes (damaged wall parts in the first row, areas occluded by cement or plants in the second and third rows).

- 1) We detect the regions of the occluding objects, or other irregular wall components, such as holes, windows, damaged parts.
- 2) We predict the brick-mortar pattern and the wall color texture in the hidden regions, based on the observable global wall texture.
- 3) We extract the accurate brick contours both in the originally visible and in the artificially inpainted regions, leading to a strong structural representation of the wall.

Figure 1 shows inpainting results on walls with various damaged and occluded hidden parts (photos from Test Set (3)). The results shows the efficiency of our algorithm of detecting the occluded objects and inpainting a realistic pattern of the wall.

We have shown by various quantitative and qualitative experiments that for the selected problem the proposed approach significantly surpasses the state-of-the-art general inpainting algorithms, moreover, the segmentation process is highly general and largely robust against various artifacts appearing in real-life applications.

ACKNOWLEDGEMENTS

The authors acknowledge the support of the projects EFOP-3.6.2-16-2017-00013, EFOP-3.6.2-16-2017-00015, EFOP-3.6.3-VEKOP-16-2017-00002, NKFIA K-120233, 2018-2.1.3-EUREKA-2018-00032 and the Michelberger Master Award of the Hungarian Academy of Engineering.

Automatic selection of difficult input images for neural network based denoising algorithms

Ákos KOVÁCS^{1, 2}

(Supervisor: András HORVÁTH¹, Tamás BÜKKI²)

¹Pázmány Péter Catholic University, Faculty of Information Technology and Bionics

50/a Práter street, 1083 Budapest, Hungary

²Mediso Kft.

3 Laborc street, 1037 Budapest, Hungary

kovacs.akos@itk.ppke.hu

Abstract—The aim of my research is to create a neural network that can enhance the quality of medical images.

In this work, I would describe one approach that can be used to notice difficult, exceptional cases in a dataset. I created a neural network ensemble, which is trained as an autoencoder. The principle of the method is that the reconstruction process achieves worse results on new images that seem unfamiliar to them. These are the hard examples, so called outliers in my case.

I tested the solution on a general, not medical dataset to see if the solution was able to spot the outlier examples. After that I tested the hypothesis that a network trained on diverse data performs better than a network which trained on a homogeneous one.

The results suggest that we can achieve better performance, if we sample hard and easy samples into the training dataset, instead of simple random sampling.

Keywords—medical imaging; AI; artificial intelligence

I. INTRODUCTION

In recent years, solutions based on artificial intelligence have achieved breakthrough results in many areas. In practice, it has also shown that methods using deep learning can approximate the transformation function between data with high accuracy for large amounts of input and output data pairs. [1]

I would like to test the hypothesis that a network trained on diverse data performs better than a network which trained on a homogeneous one.

II. DETECT OUTLIERS WITH A NEURAL NETWORK ENSEMBLE

We have read in various articles [2] [3] that the autoencoders would achieve worse results on images that were new to them. These are the outliers, hard examples in my case.

However, these errors can be said to be common everyday, and if we want to create a robust noise filtering network, we don't just have to deal with the ideal cases properly. So we need to make sure that even such more complex cases are present in large numbers in the training and validation dataset.

On Fig. 1 we can see, that different subset creation strategies gives different results. The random sampled dataset gives a moderately good result. As an opposite, the hardest examples and especially the subset contained the easiest examples results really bad performance. The winner strategy was the uniformly sampled training dataset, which have about the same hard, easy and average like images.

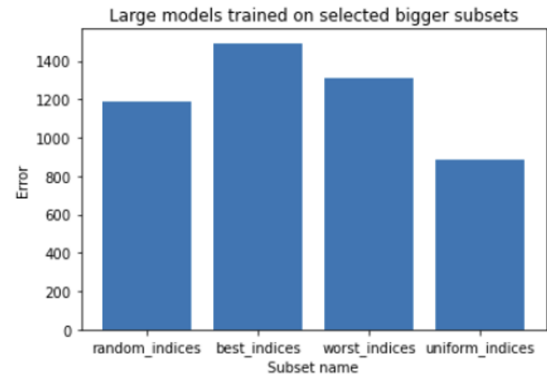


Fig. 1. The random sampled dataset gives a moderately good result. As an opposite, the hardest examples and especially the subset contained the easiest examples results really bad performance. The winner strategy was the uniformly sampled training dataset, which have about the same hard, easy and average like images.

III. CONCLUSION

The toy example, which is presented is in this article suggests, that using our software, the clinical site that works with us can automatically collect interesting recordings in advance. Thus, they need to examine a much smaller set of images to see if they are really difficult or outlier cases. With this method, we can speed up the process of data transfer and obtain more relevant training data for our neural networks.

REFERENCES

- [1] I. Goodfellow, Y. Bengio, and A. Courville, *Deep Learning*. MIT Press, 2016.
- [2] M. Sakurada and T. Yairi, "Anomaly Detection Using Autoencoders with Nonlinear Dimensionality Reduction," in *Proceedings of the MLSDA 2014 2nd Workshop on Machine Learning for Sensory Data Analysis, MLSDA'14*, (Gold Coast, Australia QLD, Australia), pp. 4–11, Association for Computing Machinery, 2014.
- [3] C. Zhou and R. C. Paffenroth, "Anomaly Detection with Robust Deep Autoencoders," in *Proceedings of the 23rd ACM SIGKDD International Conference on Knowledge Discovery and Data Mining, KDD '17*, (Halifax, NS, Canada), pp. 665–674, Association for Computing Machinery, 2017.

Change detection in unregistered 3D point clouds

Lóránt KOVÁCS

(Supervisor: Csaba BENEDEK)

Pázmány Péter Catholic University, Faculty of Information Technology and Bionics

50/a Práter street, 1083 Budapest, Hungary

kovacs.lorant@itk.ppke.hu

Abstract—This report describes briefly the change detection task for point clouds recorded in complex street-level urban environment.

INTRODUCTION

There is a growing demand for automatic public infrastructure monitoring due to the autonomous vehicle technologies and to the increasing population density. A lot of efforts are required by town management companies to analyze and compare multi-temporal recordings to find environmental differences.

This problem can be transformed to the task of change detection (CD).

Change detection is a common task in many remote sensing (RS) applications among aerial images, point clouds, or other measurement modalities [1], [2]. The rest of the existing approaches assume that the compared data frames are registered: either the sensors are stationary or the accurate location and direction parameters of the sensors are known at the time of each measurement.

RELATED WORKS

As one of the most fundamental problems in multitemporal sensor data analysis, change detection has had a vast bibliography in the last decade. Besides methods working on remote sensing images, several change detection techniques deal with *terrestrial* measurements, where the sensor is facing towards the horizon and is located on or near the ground. In these tasks optical cameras [3] and rotating multi-beam Lidars [4] are frequently used, solving problems related to surveillance, map construction, or SLAM algorithms [5].

Varghese et al. [3] defined the *ChangeNet* method for visual change detection and semantic labeling in urban image pairs. Their approach uses a parallel deep convolutional neural network architecture, capable of handling altered lighting and seasonal conditions. The *ChangeNet* extracts features using the *ResNet* architecture and combines filter outputs at different levels to localize the changes, which are identified using the same network. The output is an object-level change map. This method is also able to handle notable camera viewpoint differences.

Xiao et al. [5] introduced a method for street-side vehicle detection, classification, and change detection for car park monitoring based on mobile laser scanning data, which approach requires high accuracy point cloud registration as well.

Quin and Gruen [6] fused terrestrial images and point clouds for change detection. The use of 3D information helped them to eliminate misdetections caused by illumination changes and perspective distortions. As reported, this method is robust against small co-registration errors among images and point clouds.

CONCLUSIONS

Change detection among unregistered pointclouds can be solved by a novel, robust and quick change detection method.

REFERENCES

- [1] C. Benedek, X. Descombes, and J. Zerubia, "Building development monitoring in multitemporal remotely sensed image pairs with stochastic birth-death dynamics," *IEEE Trans. Pattern Anal. Mach. Intell.*, vol. 34, no. 1, pp. 33–50, 2012.
- [2] S. Ji, Y. Shen, M. Lu, and Y. Zhang, "Building instance change detection from large-scale aerial images using convolutional neural networks and simulated samples," *Remote Sensing*, vol. 11, no. 11, 2019.
- [3] A. Varghese, J. Gubbi, A. Ramaswamy, and P. Balamuralidhar, "Changenet: A deep learning architecture for visual change detection," in *ECCV 2018 Workshops, LNCS*, pp. 129–145, 2019.
- [4] Y. Wang, Q. Chen, Q. Zhu, L. Liu, C. Li, and D. Zheng, "A survey of mobile laser scanning applications and key techniques over urban areas," *Remote Sensing*, vol. 11, no. 13, pp. 1–20, 2019.
- [5] W. Xiao, B. Vallet, K. Schindler, and N. Paparoditis, "Street-side vehicle detection, classification and change detection using mobile laser scanning data," *ISPRS J. Photogramm. Remote Sens.*, vol. 114, pp. 166–178, 2016.
- [6] R. Qin and A. Gruen, "3D change detection at street level using mobile laser scanning point clouds and terrestrial images," *ISPRS J. Photogramm. Remote Sens.*, vol. 90, pp. 23–35, 2014.

Echocardiogram evaluation using Spatiotemporal Convolutional Neural Networks

Bálint MAGYAR

(Supervisor: András HORVÁTH)

Pázmány Péter Catholic University, Faculty of Information Technology and Bionics

50/a Práter street, 1083 Budapest, Hungary

magyar.balint@itk.ppke.hu

Abstract—Echocardiograms are widely used to assess cardiac functions. One of the most important measurement that can be extracted from echocardiogram videos is the ejection fraction (EF). The correct prediction of this measure is crucial to estimate the patient’s condition, the risk of heart failure and to choose the right treatment [1].

State-of-the-art methods use video input and spatiotemporal convolutional networks to provide an end-to-end solution. Chen et al. [2] used a custom convolutional layer to obtain bi-directional motion fields. The motion detection was combined with the segmentation results to obtain precise left ventricle segmentation. Ouyang et al. [3] presented a two stage convnet applying atrous convolution to first segment the left ventricle, and then another stage of spatiotemporal convolutions to predict the EF.

In this paper we propose an end-to-end deep learning-based method to predict the EF of the right ventricle using 3D echocardiogram videos. The applied spatiotemporal convolutional neural network - RVENet (Figure 1.) - was designed to extract image features per frame as well as the temporal movements of the heart.

Compared to existing approaches, RVENet is a single stage model that aims to predict the right ventricle EF directly from the input videos. Our hypothesis is that beside the ventricle segmentation, different regions of the input image can also contribute to the EF prediction.

Beside the prediction of the EF, the system aims to visualize the saliency of the temporal movements in order to provide interpretable results for the human experts.

Keywords-3D echocardiography; spatiotemporal convolutional networks; saliency visualization

REFERENCES

- [1] A. Kovacs, B. Lakatos, M. Tokodi, and B. Merkely, “Right ventricular mechanical pattern in health and disease: Beyond longitudinal shortening,” *Heart failure reviews*, vol. 24, no. 4, pp. 511–520, 2019.
- [2] Y. Chen, X. Zhang, C. M. Haggerty, and J. V. Stough, “Assessing the generalizability of temporally coherent echocardiography video segmentation,” in *Medical Imaging 2021: Image Processing*, International Society for Optics and Photonics, vol. 11596, 2021, 115961O.
- [3] D. Ouyang, B. He, A. Ghorbani, *et al.*, “Video-based ai for beat-to-beat assessment of cardiac function,” *Nature*, vol. 580, no. 7802, pp. 252–256, 2020.

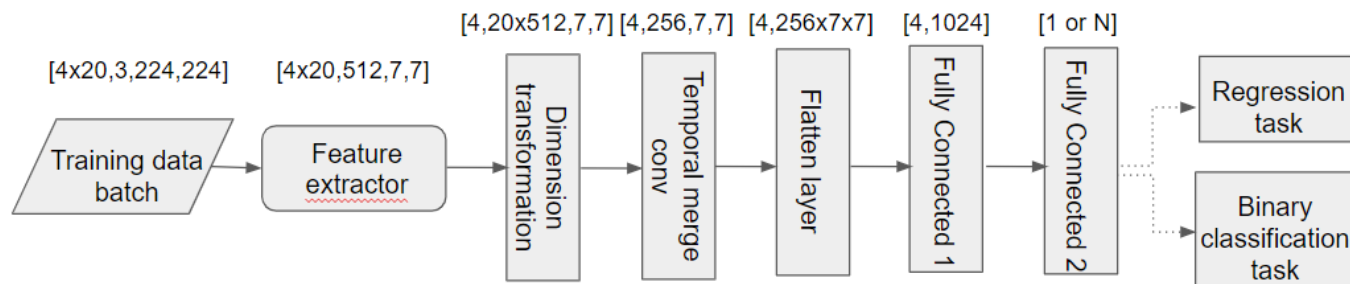


Fig. 1. The training batch contains batch size * video frames images with resolution of 224x224 px. The feature extractor is a ResNext50 model. The dimension transformation layer groups the frame features corresponding to the videos in the batch, then these group of frames are processed using the spatiotemporal convolutional layer to extract dynamic features. The final features are downscaled using fully connected layers and forwarded to either a classification or a regression head.

Application of the Mask R-CNN architecture in synaptic cleft detection

Franciska Sára RAJKI

(Supervisor: András HORVÁTH)

Pázmány Péter Catholic University, Faculty of Information Technology and Bionics

50/a Práter street, 1083 Budapest, Hungary

rajki.franciska.sara@itk.ppke.hu

Abstract—Mask R-CNN is one of the most famous neural network architecture in the field of image segmentation. It combines object detection and semantic segmentation, where the goal is to classify each pixel into a fixed set of categories. [1] There are available implementations online, including the Detectron2 [2], which is Facebook AI Research’s next generation library that provides state-of-the-art detection and segmentation algorithms. It is part of the R-CNN family. [3] However, as the architecture is very complex, it can be difficult to train the network and tune the parameters properly for your own dataset. That being said, when we received a custom dataset consisting of electron microscope images of rat brains annotated with marks of the synaptic clefts, and saw that the detectron2 implementation can handle it, I tried to use an own, much simpler implementation of Mask R-CNN, to be able to finetune it as much as we want to in the future. Our aim is to segment synaptic clefts on electron microscope images, to be able to detect the changes of the synaptic connections affected by drugs or learning.

I. SUMMARY

I wanted to implement the Mask R-CNN model myself, as that way I can tailor the network according to the task. However, there is not a lot of help online, on how to do that, as there are available famous implementations. The problem is that these are very complex and robust and hard to understand. Moreover, the one implemented in tensorflow, is not running with tensorflow 2.4., which is also a problem because of compatibility issues. Therefore building a basic Mask R-CNN, for the sake of understanding every part of it was a complicated but necessary task. Because of this, I published my way of implementing it, and the script online. [4]

With the help of this network, we are able to detect, and segment synaptic clefts on electron microscope images. This way we can monitor the changes of the synaptic connection. The synaptic cleft —also called synaptic gap— is a gap between the pre-and postsynaptic cells that is about 20 nm wide.[5]

REFERENCES

- [1] K. He, G. Gkioxari, P. Dollár, and R. Girshick, “Mask r-cnn,” 2018.
- [2] Y. Wu, A. Kirillov, F. Massa, W.-Y. Lo, and R. Girshick, “Detectron2.” <https://github.com/facebookresearch/detectron2>, 2019.
- [3] R. Girshick, J. Donahue, T. Darrell, and J. Malik, “Rich feature hierarchies for accurate object detection and semantic segmentation,” 2014.
- [4] F. Rajki, “Building a mask r-cnn from scratch in tensorflow and keras,” Mar 2021.
- [5] B. Widrow, Y. Kim, D. Park, and J. K. Perin, “Chapter 1 - nature’s learning rule: The hebbian-lms algorithm;” in *Artificial Intelligence in the Age of Neural Networks and Brain Computing* (R. Kozma, C. Alippi, Y. Choe, and F. C. Morabito, eds.), pp. 1–30, Academic Press, 2019.

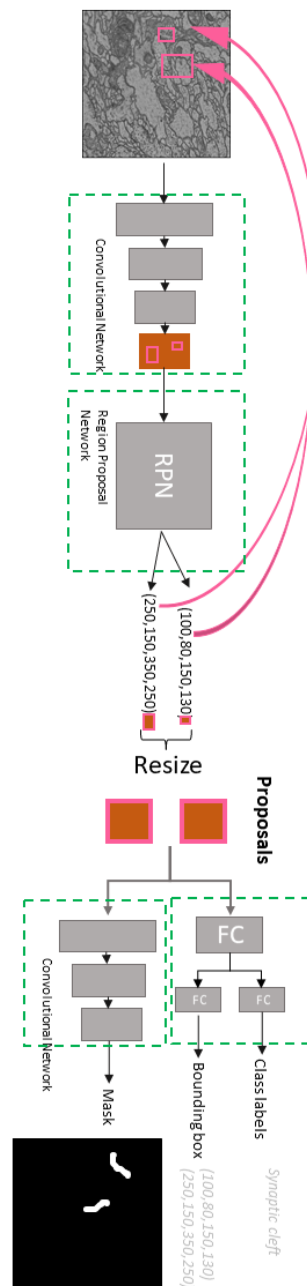


Fig. 1. The complete Mask R-CNN model, used to segment synaptic clefts.

Multimodal change detection between LiDAR point clouds

Örkény Ádám H. ZOVÁTHI
(Supervisor: Csaba BENEDEK)

Pázmány Péter Catholic University, Faculty of Information Technology and Bionics
50/a Práter street, 1083 Budapest, Hungary
h.zovathi.orkeny.adam@itk.ppke.hu

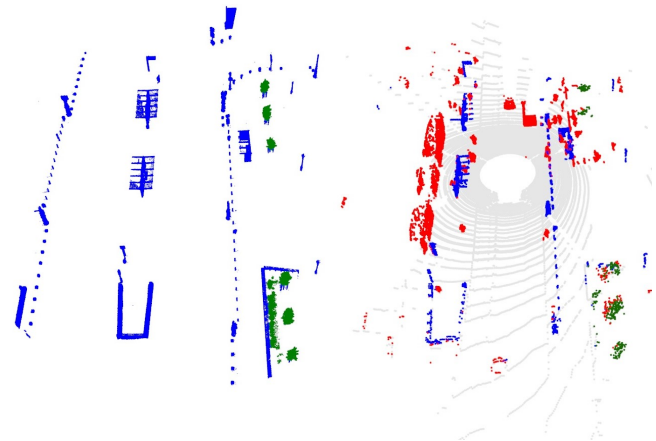
I. INTRODUCTION

Recent scientific and engineering progress in autonomous driving make us believe that cars will be able to drive without human intervention in the near future. State-of-the-art intelligent vehicles (IVs) are often equipped with real-time Lidars, such as Velodyne's rotating multi-beam (RMB) sensors, providing accurate 3D geometric information about their environment with high acquisition speed. However, their captured point cloud data is relatively sparse and inhomogeneous due to the low vertical density of sensor data, which quickly decreases as a function of distance. Thus, the analysis [1], [2] of such point clouds still remains a challenging task, especially in urban environment with many traffic participants and various occlusion effects. To overcome these limitations, Lidar based perception is often supported by detailed, prerecorded city maps that contain detailed environment and road structure information. Mobile Laser Scanning (MLS) platforms [3] may be effective candidates for this purpose, as they provide dense, accurate and feature rich point clouds precisely registered to a geo-referenced global coordinate system.

The main goal of my research is an optimal exploitation of the information stored in these MLS based 3D maps in order to improve the IVs' often imperfect onboard perception. In this context, *change detection* between the real-time captured RMB measurements and the MLS reference data appears as a crucial task. As a key challenge here, the point density of the two comparable point cloud can differ with up to 2-3 orders of magnitude, demanding novel processing techniques.

II. THE PROPOSED METHOD

As a first step of our approach, we construct a segmented environment model from the raw MLS point clouds in an offline step. During segmentation, we remove all regions which contain dynamic street parts (such as parking cars) and ghosts caused by independent object motions [3] and keep only point cloud regions belonging to *empty street* segments (Fig. 1(a)). Then, we analyse the RMB Lidar's measurement flow in real-time, performing the following two steps: First, we align the actual RMB measurement frame to the segmented MLS map, using a fast object based registration algorithm [4]. Then, we detect changes between the co-registered RMB and MLS point cloud scenes. Hereby we use a Markov Random Field based new image segmentation model, which operates in the 2D range image domain. Using compact range image representations, the proposed method is notably faster than direct 3D comparison techniques (e.g. point-to-point, point-to-triangle), meanwhile it can also robustly handle the significant point quality and density differences between the two comparable point clouds. As output of the change detection



(a) Segmented, „empty” street map (b) Change based segmentation in an extracted from the raw MLS data. RMB measurement frame

Fig. 1. Change detection results in urban environment, using the segmented MLS 3D map as reference. Dynamic changes are marked by red, vegetation parts by green, unchanged regions by blue and ground points by gray.

process, we classify the regions of the actual RMB point cloud frames into three classes (Fig. 1(b)): (i) unchanged, static environment parts, (ii) changed regions containing dynamic traffic participants or temporal renewals, and (iii) seasonal changes (tree-crowns, bushes, vegetation areas).

ACKNOWLEDGEMENTS

This work was supported by the ÚNKP-20-3 New National Excellence Program (ÚNKP-20-3-I-PPKE-59) of the Ministry for Innovation and Technology from the source of the National Research, Development and Innovation (NRDI) Fund and by the Széchenyi 2020 Program grants EFOP-3.6.3-VEKOP-16-2017-00002.

REFERENCES

- [1] Ö. Zováthi, L. Kovács, B. Nagy, and C. Benedek, “Multi-object detection in urban scenes utilizing 3D background maps and tracking,” in *2019 International Conference on Control, Artificial Intelligence, Robotics Optimization (ICCAIRO)*, pp. 231–236, 2019.
- [2] Ö. Zováthi, B. Nagy, and C. Benedek, “Exploitation of Dense MLS City Maps for 3D Object Detection,” in *International Conference on Image Analysis and Recognition (ICIAR)*, vol. 12131 of *Lecture Notes in Computer Science*, pp. 393–403, Springer, 2020.
- [3] B. Nagy and C. Benedek, “3D CNN based phantom object removing from mobile laser scanning data,” in *International Joint Conference on Neural Networks*, May 2017.
- [4] B. Nagy and C. Benedek, “Real-time point cloud alignment for vehicle localization in a high resolution 3D map,” in *Workshop on Computer Vision for Road Scene Understanding and Autonomous Driving at ECCV'18*, vol. 11129 of *LNCS*, pp. 226–239, 2019.

APPENDIX

PROGRAM 1: Bionics, Bio-inspired Wave Computers, Neuromorphic Models

| Name | Supervisor |
|----------------------------|---|
| András ADOLF | István ULBERT MD DSc |
| Zsófia BUJTÁR | Attila CSIKÁSZ-NAGY DSc |
| Suchana CHAKRAVARTY | Attila CSIKÁSZ-NAGY DSc |
| Veronika CSILLAG | Imre FARKAS MD PhD, Zsolt LIPOSITS MD DSc |
| Ward FADEL | István ULBERT MD DSc, Lucia WITTNER MD PhD |
| Bianka Vivien FARKAS | Zoltán GÁSPÁRI PhD, Tamás HEGEDŰS PhD |
| Fanni FARKAS | Zoltán GÁSPÁRI PhD |
| Anna HAJDARA | Balázs MAYER PhD, Miklós GYÖNGY PhD |
| Regina KALCSEVSZKI | Sándor PONGOR MHAS |
| Zsófia Etelka KÁLMÁN | Zoltán GÁSPÁRI PhD |
| Máté KÁLOVICS | Kristóf IVÁN PhD |
| Bence Márk KEÖMLEY-HORVÁTH | Attila CSIKÁSZ-NAGY DSc, István Zoltán REGULY PhD |
| Barnabás KOCSIS | István ULBERT MD DSc |
| Csaba Márton KÖLLŐD | István ULBERT MD DSc |
| Dániel Zoltán KOLPASZKY | Kristóf IVÁN PhD |
| Adrienn Lilla MÁRTON | Kristóf IVÁN PhD |
| Marcell MISKI | Attila CSIKÁSZ-NAGY DSc |
| Máté MOHÁCSI | Tamás FREUND MHAS, Szabolcs KÁLI PhD |
| Obada MUHAMMAD | István ULBERT MD DSc |
| Bíborka PILLÉR | Attila CSIKÁSZ-NAGY DSc |
| Anna SÁNTA | Zoltán GÁSPÁRI PhD |
| Ágnes SZABÓ | Zoltán FEKETE PhD |
| András László SZABÓ | Zoltán GÁSPÁRI PhD |
| János SZALMA | Béla WEISS PhD |
| Luca TAR | Tamás FREUND MHAS, Szabolcs KÁLI PhD |
| Bálint Áron ÜVEGES | Ferenc KOVÁCS DSc |
| Zsófia VARGA-MEDVECZKY | Franciska ERDŐ PhD |
| Moutz WAHDOW | István ULBERT MD DSc |

PROGRAM 2: Computer Technology Based on Many-core Processor Chips, Virtual Cellular Computers, Sensory and Motoric Analog Computers

| Name | Supervisor |
|-----------------------|--|
| Nawar AL-HEMEARY | Gábor SZEDERKÉNYI DSc, György CSEREY PhD |
| Boldizsár Zsolt BALOG | György CSEREY PhD, Gábor NYÍRI PhD |
| Gábor Dániel BALOGH | Péter SZOLGAY DSc, István Zoltán REGULY PhD |
| Balázs CSUTAK | Gábor SZEDERKÉNYI DSc |
| Attila FEJÉR | Péter SZOLGAY DSc |
| Árpád GORETITY | István Zoltán REGULY PhD |
| Mary GUINDY | Péter SZOLGAY DSc, Vamsi Kiran ADHIKARLA PhD |
| Dániel HAJTÓ | György CSEREY PhD |
| Sam KHOZAMA | Zoltán GÁSPÁRI PhD, Zoltán NAGY PhD |
| Ádám NAGY | Ákos ZARÁNDY DSc |
| Bálint SIKLÓSI | Péter SZOLGAY DSc, István Zoltán REGULY PhD |
| Gergely SZABÓ | András HORVÁTH PhD |
| Gergely SZLOBODNYIK | Gábor SZEDERKÉNYI DSc |

PROGRAM 3: Feasibility of Electronic and Optical Devices, Molecular and Nanotechnologies, Nano-architectures, Nanobionic Diagnostic and Therapeutic Tools

| Name | Supervisor |
|-------------------------|--------------------------------------|
| András ESZES | Zsolt SZABÓ DSc |
| András FÜLÖP | András HORVÁTH PhD, György CSABA PhD |
| Péter MAROSÁN-VILIMSZKY | Miklós GYÖNGY PhD |
| Tamás RUDNER | György CSABA PhD |

PROGRAM 4: Human Language Technologies, Artificial Understanding, Telepresence, Communication

| Name | Supervisor |
|----------------------|---------------------------------------|
| András Pál HALÁSZ | Péter SZOLGAY DSc, Kálmán TORNAI PhD |
| Kamran IBIYEV | Gábor PRÓSZÉKY DSc |
| Mram KAHLA | Gábor PRÓSZÉKY DSc |
| András Attila SÜLYÖK | Péter SZOLGAY DSc, Kristóf KARACS PhD |

PROGRAM 5: On-board Advanced Driver Assistance Systems

| Name | Supervisor |
|------------------------|-------------------------------------|
| Jalal ALAFANDI | András HORVÁTH PhD |
| Yahya IBRAHIM | Csaba BENEDEK PhD |
| Ákos KOVÁCS | András HORVÁTH PhD, Tamás BÜKKI PhD |
| Lóránt KOVÁCS | Csaba BENEDEK PhD |
| Bálint MAGYAR | András HORVÁTH PhD |
| Franciska Sára RAJKI | András HORVÁTH PhD |
| Örkény Ádám H. ZOVÁTHI | Csaba BENEDEK PhD |
